AFFDL-TR-75-102

(12)

A REVIEW OF THE ANALYSES OF HYDRODYNAMIC RAM

SURVIVABILITY BRANCH
VEHICLE EQUIPMENT DIVISION

AUGUST 1976

TECHNICAL REPORT AFFDL-TR-75-102
INTERIM REPORT FOR PERIOD AUGUST 1973 THROUGH SEPTEMBER 1974

AIR FORCE FLIGHT DYNAMICS LABORATORY
AIR FORCE WRIGHT AERONAUTICAL LABORATORIES
AIR FORCE SYSTEMS COMMAND
WRIGHT-PATTERSON AIR FORCE BASE, OHIO 45433

NOTICE

When Government drawings, specifications, or other data are used for any purpose other than in connection with a definitely related Government procurement operation, the United States Government thereby incurs no responsibility nor any obligation whatsoever; and the fact that the government may have formulated, furnished, or in any way supplied the said drawings, specifications, or other data, is not to be regarded by implication or otherwise as in any manner licensing the holder or any other person or corporation, or conveying any rights or permission to manufacture, use, or sell any patented invention that may in any way be related thereto.

This report has been reviewed by the Information Office (OI) and is releasable to the National Technical Information Service (NTIS). At NTIS, it will be available to the general public, including foreign nations.

This technical report has been reviewed and is approved for publication.

PHILIP F. FRY, JR.
Project Physicist

FOR THE COMMANDER:

DUANE A. BAKER, Lt Colonel, USAF
Act'g Chief
Vehicle Equipment Division
Air Force Flight Dynamics Laboratory

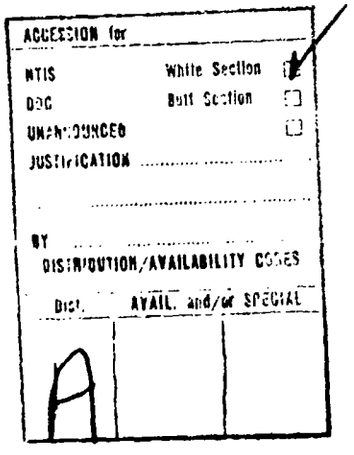

Copies of this report should not be returned unless return is required by security considerations, contractual obligations, or notice on a specific document.

UNCLASSIFIED

SECURITY CLASSIFICATION OF THIS PAGE (When Data Entered)

REPORT DOCUMENTATION PAGE

READ INSTRUCTIONS BEFORE COMPLETING FORM

1. REPORT NUMBER: AFFDL-TR-75-102	2. GOVT ACCESSION NO.
3. RECIPIENT'S CATALOG NUMBER	
4. TITLE (and Subtitle): A REVIEW OF THE ANALYSES OF HYDRODYNAMIC RAM	5. TYPE OF REPORT & PERIOD COVERED: Interim Report. Aug [illegible] 73 – Sep [illegible] 74
6. PERFORMING ORG. REPORT NUMBER	
7. AUTHOR(s): Philip F. Fry	8. CONTRACT OR GRANT NUMBER(s)
9. PERFORMING ORGANIZATION NAME AND ADDRESS: Survivability Branch, Vehicle Equipment Division, Air Force Flight Dynamics Laboratory, Wright-Patterson Air Force Base, Ohio 45433	10. PROGRAM ELEMENT, PROJECT, TASK AREA & WORK UNIT NUMBERS: 4363 01 27 / 62201F
11. CONTROLLING OFFICE NAME AND ADDRESS: Air Force Flight Dynamics Laboratory, Wright-Patterson Air Force Base, Ohio	12. REPORT DATE: Aug [illegible] 76
	13. NUMBER OF PAGES: 163 / 178p.
14. MONITORING AGENCY NAME & ADDRESS (if different from Controlling Office)	15. SECURITY CLASS. (of this report): Unclassified
	15a. DECLASSIFICATION/DOWNGRADING SCHEDULE

16. DISTRIBUTION STATEMENT (of this Report)

Approved for public release; distribution unlimited

17. DISTRIBUTION STATEMENT (of the abstract entered in Block 20, if different from Report)

18. SUPPLEMENTARY NOTES

19. KEY WORDS (Continue on reverse side if necessary and identify by block number)

Hydraulic ram
Fluid shocks
Fluid pressures
Penetration
Fuel tanks
Projectile/bullet impact into fuel tanks/liquid-filled containers

20. ABSTRACT (Continue on reverse side if necessary and identify by block number)

Analytical models applicable to hydrodynamic ram studies are reviewed. These include Stepka and Morse's observations of shock formation, Yurkovich's analysis of the shock, and Lundstrom's analysis of the fluid drag pressures. Several approaches to the wall analysis are also reviewed; these include Chou's use of the method of characteristics, and Ball's adaptation of piston theory. Finally, damage reduction methods are also discussed.

DD FORM 1 JAN 73 1473 EDITION OF 1 NOV 65 IS OBSOLETE

UNCLASSIFIED

SECURITY CLASSIFICATION OF THIS PAGE (When Data Entered)

012070

FOREWORD

This report summarizes the analysis work performed on the hydrodynamic ram effect at Air Force Flight Dynamics Laboratory under work unit 43630127 (Fuel Tank Responses to Projectile Impact and Fluid Shock Pulses). The work was performed during the period of August 1973 through September 1974. It is intended that this study will form the basis for a comprehensive test program and for the development of a refined and verified analysis method to be accomplished in the next couple of years.

In preparing this report, one purpose has been in the foreground, to create a document which will serve as a single reference for the complicated technology in this field at the current time. It should be reasonably complete in its description of all the significant contributions to hydrodynamic ram studies. All of the major works as well as selected works of lesser significance have been included. All equations needed have been incorporated in the text, with some of the details of derivation required for a full understanding placed in the appendices.

Four individuals are due an especial expression of appreciation for their generous contribution of time while the original reports and papers were being prepared; they are: Dr. Robert Ball : of the Naval Postgraduate School, Dr. Eric Lundstrom of NWC, Dr. K.S. Nagaraja of the AFFDL and Dr. Peter Torvik of the Air Force Institute of Technology. Others, whose patience and encouragement were most helpful and appreciated were Mr. Andre Holten and Lt Col Duane Baker of AFFDL. To all, the author wishes to express his thanks.

TABLE OF CONTENTS

TABLE OF CONTENTS (Contd)

TABLE OF CONTENTS (Contd)

LIST OF ILLUSTRATIONS

LIST OF ILLUSTRATIONS (Contd)

LIST OF TABLES

LIST OF SYMBOLS

Arabic Letters

A area

A_p presented area of the projectile (usually taken as a constant equal to the projectile's widest cross section normal to the major axis)

a cavity radius

a_m maximum cavity radius

a_p term defined by $a_p = a_m|_{\xi = X_p}$

C_D coefficient of drag

C sound velocity

C_1 constant, $C_1 = \gamma\alpha^-/2\omega^2\zeta^*$

C_2 constant, $C_2 = -\gamma\alpha^+/2\omega^2\zeta$

c_r release velocity

D drag force ($\frac{\rho v^2}{2} A_p C_D$); flexural rigidity

E energy; modulus of elasticity (Young's modulus)

E_c energy required to form a cavity

e specific internal energy (energy/vol)

F force; surface traction force

f arbitrary function

h plate thickness

I kinetic enthalpy

i specific enthalpy

k spring constant

k_2 shear stress resultant

M mach number (u/c); bending stress moment

LIST OF SYMBOLS (Contd)

m mass

n a factor in the Tait equation of state (taken here as constant)

P pressure

Q shear stress resultant

q an exponent defined $\bar{\rho} = \bar{\rho}_1 r^q$, $(q = 3(\bar{\rho}_1 - 1))$

R gas constant (8.32 j/(mole · °K); the distance coordinate normal to the projectile trajectory

r radial distance; radius

r_p distance to an arbitrary point in the fluid from the projectile at retarded time τ, $r_p = \sqrt{R^2 + [x - X_p(\tau)]^2}$

S specific entropy; surface

T temperature

t time

U_s shock velocity in the fluid

u particle velocity

V volume; potential energy

v velocity

W weight of TNT (lbs); work; Wronskian

w transverse displacement of the mid-plane

$\underline{X}$ trajectory length

x distance

Y energy transferred / length

Greek Letters

α slope for shock radius vs time on a log-log plot; slope for projectile penetration distance vs time on log-log plot

LIST OF SYMBOLS (Contd)

α^+ constant, $\alpha^+ = -\zeta + \zeta^*$

α^- constant, $\alpha^- = -\zeta - \zeta^*$

β a term in the nondimensional conservation equations,

$\beta = \frac{r_s \dot{u}_s}{u_s^2}$; the velocity decay coefficient

$\beta = \frac{\rho A_p C_D}{2m}$

γ arbitrary parameter, $\gamma = \frac{\dot{2}AP_i}{m}$-

Δ a difference operator, $\Delta x = x_i - x_{i-1}$

ζ source strength function, $\zeta = R\dot{R}$; a parameter,

$\zeta = \frac{\rho C A_p}{2m}$

ζ^* a parameter, $\zeta^* = \sqrt{\zeta^2 - \omega^2}$

η constant, usually chosen in the range of 20 to 30

Ⓗ coefficient of $\ln \bar{r}$, introduced in the velocity profile equation, $Ⓗ = \frac{\beta n_s}{\bar{u}_1} \frac{\partial}{\partial n_s} \ell n\, \bar{\rho}_1$

θ angle; half angle for the projectile nose cone; a coordinate in the spherical system

Λ term defined as $\Lambda = \frac{\dot{a}}{2} \cdot \frac{a_p}{R_p} \left[\frac{v_p}{\frac{x - \bar{x}_p(\tau)}{R_p} \cdot \frac{v_p}{C} - 1} \right]$

λ arbitrary constant

ν Poisson's ratio; arbitrary constant for variation of parameters

ξ dummy variable for integration over distance

ρ density

T cavity period, time for one oscillation

τ specific volume (volume/mass); retarded time, $\tau = t - r/c$

LIST OF SYMBOLS (Contd)

Φ rotation of the cross section about the tangential axis

ϕ scalar velocity potential; angle coordinate in spherical system

Ψ rotations of the cross section about the radial axis

Ω scalar force potential

ω angular frequency (rad/sec)

Mathematical Notations

$\dot{}$ time derivative

$\bar{}$ nondimensional quantity; average value

$\vec{}$ vector

$\hat{}$ unit vector

∇ the del operator, $\nabla = \frac{\partial}{\partial x}\hat{i} + \frac{\partial}{\partial y}\hat{j} + \frac{\partial}{\partial z}\hat{k}$ in rectangular coordinates

$\times$ cross product

$\cdot$ dot product

Subscripts

o in front of shock wave, ambient

1 directly behind shock front

2 shear wave

av average

c cavity

e external; equivalent

f fluid; final

g gage

h.s. hemisphere

i i^{th} segment of the bullet path; incident

imp. impulse

LIST OF SYMBOLS (Contd)

m	maximum
n	natural
P	projectile; plate
R	radial
r	release; reflected wave
s	shock; sphere
s_o	measured along the axis of symmetry
w	wall
θ	tangential

SECTION I

INTRODUCTION

Vietnam combat experience has demonstrated that aircraft can be particularly vulnerable to small arms and automatic fire. Typically, a small arms round can penetrate the skin and fuel tank of a low flying aircraft. If the fuel which escapes from this impacted area ignites, then an explosion and fire can bring the aircraft down. In addition, small arms rounds can cause excessive structural damage as their kinetic energy is given up to the fluid and then transferred to the fuel tank walls. In the past, this phenomenon has been called hydraulic ram, but this term already refers to an engineering device. It is suggested that the term, hydrodynamic ram, is both more descriptive and more appropriate.

A similar rupture phenomenon had been a problem for NASA when hypervelocity particles impacted the liquid oxygen fuel tanks of spacecraft. NASA made a series of studies to measure and explain the event, but was able to eliminate their problem without completing the research. Thin metal bumpers, placed in front of the fuel tank, break the meteorite particles into a shower of very small, light pieces. The spacecraft fuel tank walls can then withstand the distributed load.

A similarly simple solution is not possible to protect aircraft against ordnance projectiles; further, it is not reasonable to design

the structure to withstand the impact, because of the weight penalty. Thus, it became necessary, from a military standpoint, to study hydrodynamic ram more closely in order to find clues to an efficient defense mechanism. As a result, several additional studies have been completed; however, in most cases each study treats only one or two aspects of the hydrodynamic ram event in detail. Thus, a complete grasp of hydrodynamic ram can only be gained by studying more sources, and there is the real possibility that some worthy discussions or analyses might be omitted simply because they were published several years ago. A repetition of the known analyses and explanation of hydrodynamic ram in consistent notation is, therefore, necessary for both completeness and perspective, and is the subject of this report.

1. THE HYDRODYNAMIC RAM EVENT

Hydrodynamic ram is initiated by the impact of a projectile into a liquid-filled container. Detailed analyses explain the event by using different models along the trajectory. But it is obvious, even without knowledge of those models, that the projectile is going to give up some of its energy along every increment of its path. This lost projectile energy is transferred to the fluid as kinetic and thermal energy; the fluid then transfers its kinetic energy to the tank walls. Thus, hydrodynamic ram is fluid loads, especially impulsive loads, on the fuel tank walls.

In sequential order, the phases of hydrodynamic ram are impact, fluid shock, fluid drag, and exit. These phases are illustrated in Figure 1.

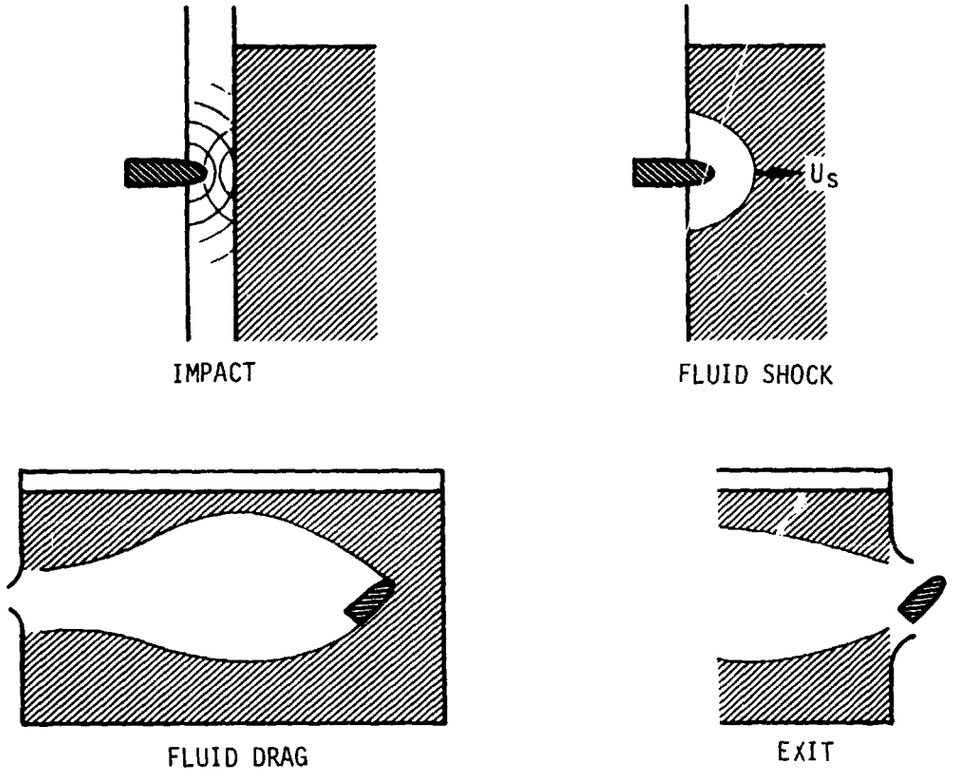

Figure 1. Four Phases of the Hydrodynamic Ram

The impact phase occurs as the projectile penetrates the tank wall, and subsequently, shock waves are induced in both the wall and the projectile. This phase is very brief, typically less than 0.1 msec. (A projectile, 60 mm in length, traveling at an average velocity of 0.85 km/sec, would be in contact with the entrance wall for 51 μsec.) Because this phase is so brief and difficult to observe, there is no analysis available which treats specifically the impact portion of the hydrodynamic ram problem. It should be presumed, however, that the stresses created by the projectile at impact will cause small cracks to form and will radically alter the load-bearing capacity at the impact region so that the ensuing high pressure will find the impact region the weakest part of the tank walls. Nevertheless, for simplicity of analysis, it is normally assumed that the projectile will simply create a hole slightly larger than the projectile impact area in the front wall, and all other impact effects are ignored.

The second phase (fluid shock phase) of the hydrodynamic ram event is characterized by a local, nearly hemispherical, shock surface in the fluid which is formed about the impact point. This second phase is also of extremely short duration, beginning at impact, and lasting less than 0.2 msec. Usually the shock radius reaches a maximum of about 20 cm. It is easily observed with shadowgraph photography, and consequently there is considerable analysis available. The shock phase is reported in detail by NASA researchers, and it is the only phase they reported since the light particles they studied spend

nearly all of their energy on impact. The significance of this phase was established by Stepka and Morse (1:13)* who observed that, for small projectiles fired through prepunched holes, fracture took place between 27 and 40 msec after impact. The model usually replaces the projectile with an impact impulse over a very brief increment of time. The analysis involves determining the location and velocity of the shock surface, and evaluating the very high pressures behind the shock surface. This initial severe loading of the impacted wall by the fluid within the shock region can be expected to produce or extend fractures in every case, and hence to further modify the material properties of the wall.

The third phase lasts for several milliseconds; it is thus relatively long, and has been very closely observed and analyzed. Although it is sometimes called the cavity phase, the term "drag phase" is preferred, because the pressure field can be accurately related to the fluid drag of the tumbling projectile. A gaseous cavity is an easily observed characteristic of this phase; it is formed as the projectile imparts an outward radial velocity to the fluid. The cavity surface continues to expand, even after the projectile has exited the tank, its shape finally becoming nearly spherical (Figure 2). The cavity collapses to some minimum volume, then rebounds on itself. This cycle can be repeated three or four times before the cavity dies.

---

* Reference 1, page 13.

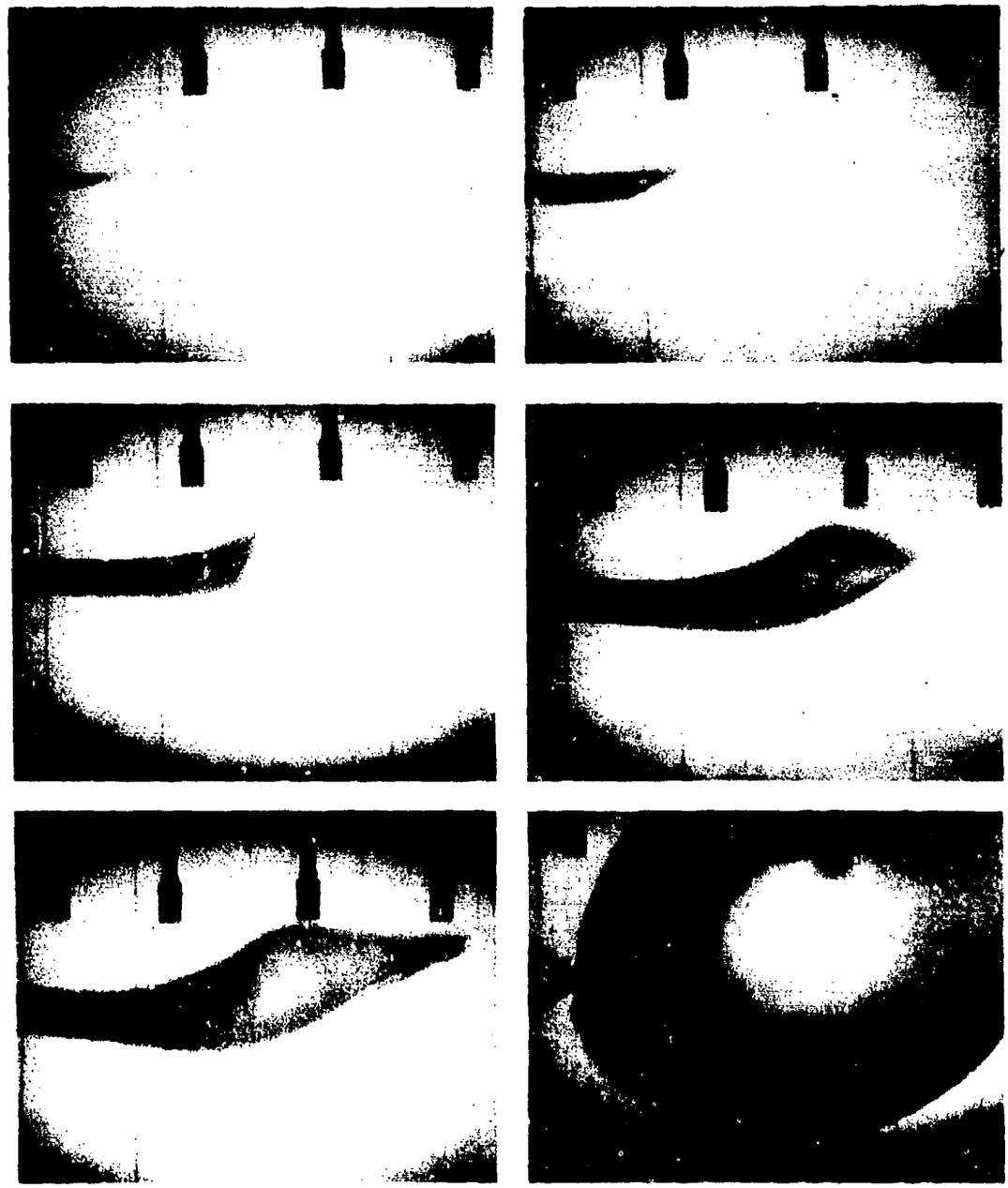

(Photos Courtesy NWC)

Figure 2. Cavity Formation

19/4 20/4 19/1 11-18-76

ADA 031976

* Military aircraft
~~HYDRODYNAMICS~~ Keep
* Hydraulic ram effect
* Projectiles
* Ammunition damage
* Bibliographies
water tanks Terminal ballistics
Vulnerability
SHOCK WAVES Theory
HYPERVELOCITY IMPACT
~~HYDRAULIC~~ RAM EFFECT
IMPACT SHOCK
DAMAGE
PENETRATION
~~PROJECTILES~~
SURVIVABILITY
BERNOULLI DISTRIBUTION
SMALL ARMS AMMUNITION
RUPTURE
FUEL TANKS
~~FLUID MECHANICS~~
PERFORATION (ENGINEERING)
~~TEST~~

(05) Piston theory

Though the pressure field is not so easily observed, it is the most important characteristic of the drag phase. Generally, a pressure transducer located where it sees no reflections will detect a single pressure pulse (2), and this pulse may have a steep enough front that, for some applications, it could be termed a shock. Most pulses are less than 0.5 msec and some are spikes of less than 0.1 msec. The pressure field is not uniform; much higher pressures are observed near the projectile when it is in a fully tumbled position. Typical peak pressures at about 15 cm from the bullet are less than 70 and are seldom over 140 bars from projectiles up to 14.7 mm API. Two pressure pulses are shown in Figure 3, where the second curve would be considered typical.

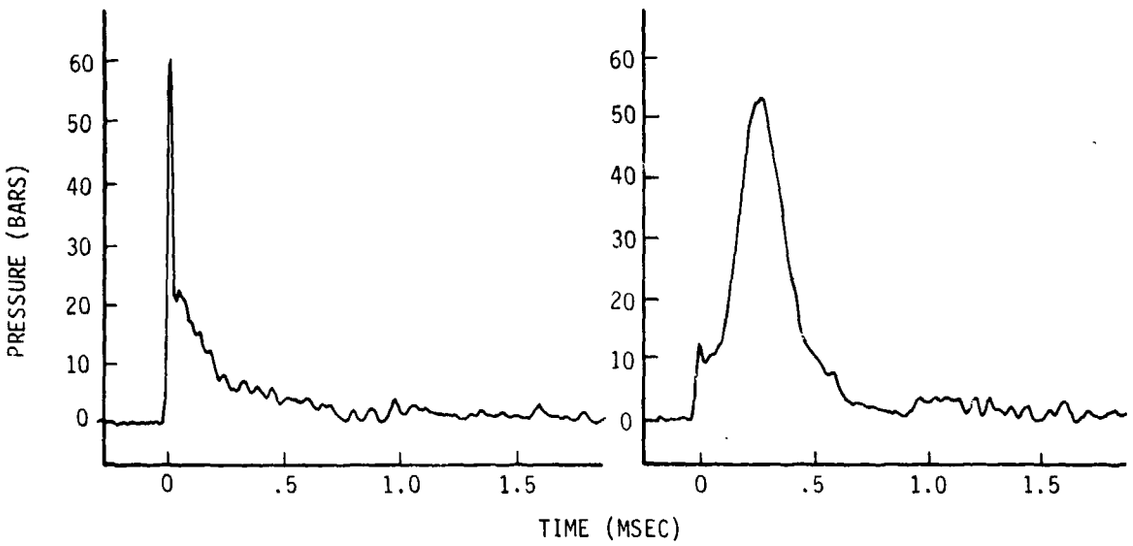

(t=0 is adjusted to beginning of pulse.)

Figure 3. Pressure History Plots

Because the exit phase, like the impact phase, is also very brief, its effects have been neglected in testing programs and by analysis. It is clear from high speed photographs that the projectile will tumble almost invariably in the fluid, and will thus exit in a tumbled condition most of the time. Further, since the tumbled projectile is preceded by a very high pressure region, it is supposed that the bullet strikes an exit wall that is already under some stress. To support this, researchers have occasionally noted that the rear wall can be seen to bulge before the projectile penetrates it. However, close examination and measurement of this event are totally lacking.

2. OBJECTIVES

There are two major objectives to this study of the hydrodynamic ram. The first is to find means of attenuation, the reduction of the damage to some minimum and acceptable level. But in spite of the great amounts of data and complicated models and analysis, no completely satisfactory solution has been forthcoming. An adequate solution to the hydrodynamic ram rupture is expected to be some combination of materials and geometry which will spread the pressure pulse out over space or time or both. This dispersion of the pulse must be to such an extent that each element of the wall experiences a sufficiently small impulse so that its yield limits are not exceeded. Of the many materials that have been suggested to reduce the damage, only foams (flexible and rigid) have shown any promise. Although some benefit from attenuation materials is anticipated, it appears now that this benefit will be quite limited. Ram attenuation is discussed in the last section.

Since ram attenuation has proved so elusive, greater importance has been placed on the other major objective, predicting the location and extent of the damage. This objective can be met by developing and verifying the analytical equations, many of which are the substance of the following pages.

SECTION II

HYDRODYNAMIC EQUATIONS

In this section, some of the equations basic to the studies of hydrodynamics are presented. Since their inclusion is intended only to refresh the reader who already has an understanding of hydrodynamics and to serve as a point of reference for later sections, the presentation contains very little explanation. The following topics are covered: conservation equations, jump conditions, thermodynamic relations, velocity potential, and Bernoulli's equation. Some of these equations are then repeated in nondimensional form following the work of Bach and Lee.

1. CONSERVATION EQUATIONS

The conservation equations can be derived by considering an arbitrary, infinitesimally small volume which is allowed to move with the fluid. Then one assumes there are no viscous stresses, that heat conduction is negligible, and that there are no discontinuities of pressure, velocity, or internal energy. Under these conditions, the mass, momentum, and energy of each elemental volume are conserved. Conservation of Mass (Continuity Equation): The change in density is related to a corresponding change in the dimensions of the small volume

$$\frac{d\rho}{dt} + \rho \nabla \cdot \vec{u} = 0 \qquad (1)$$

where ρ is the density and μ is the particle velocity.

Conservation of Momentum: Newton's second law, $F = m \frac{d\vec{v}}{dt}$, is applied to the elemental volume:

$$\frac{d\vec{u}}{dt} + \frac{1}{\rho} \nabla P = 0 \tag{2}$$

where P is the pressure.

Conservation of Energy: The work done on a small volume of constant mass is equal to the change in internal and kinetic energy of the volume

$$\rho \frac{d}{dt} \left[e + \frac{\vec{u} \cdot \vec{u}}{2} \right] = - \nabla \cdot (\rho \vec{u}) \tag{3}$$

where e is the specific internal energy (energy per unit volume). If now the mass and momentum equations are combined with the energy equation, the result is a more useful form for the conservation of energy equation:

$$\frac{de}{dt} - \frac{P}{\rho^2} \frac{d\rho}{dt} = 0 \tag{4}$$

In all these equations, it must be noted that

$$\frac{d}{dt} = \frac{\partial}{\partial t} + (\vec{u} \cdot \nabla) \tag{5}$$

since the volume has been allowed to move with the fluid. One can convert from moving to fixed elemental volume by using Equation 5.

For shock wave work, the conservation equations are most frequently written in spherical coordinates. By referring to Appendix A, these equations can be easily written out, and are listed in Lagrangian coordinates as follows:

$$\underline{\text{Conservation of Mass}} \quad \frac{\partial \rho}{\partial t} + \rho \frac{\partial u}{\partial r} + u \frac{\partial \rho}{\partial r} + 2 \frac{\rho u}{r} = 0 \qquad (6)$$

$$\underline{\text{Conservation of Momentum}} \quad \rho \frac{\partial u}{\partial t} + \rho u \frac{\partial u}{\partial r} + \frac{\partial \rho}{\partial r} = 0 \qquad (7)$$

$$\underline{\text{Conservation of Energy}} \quad \frac{\partial e}{\partial t} + u \frac{\partial e}{\partial r} - \frac{p}{\rho^2}\left(\frac{\partial \rho}{\partial t} + u \frac{\partial \rho}{\partial r}\right) \qquad (8)$$

Equations 6, 7, and 8 are valid throughout the fluid, except across a shock front. The abrupt changes across the shock surface are treated as discontinuities, and the proper equations, usually referred to as jump conditions, must be found. These relations can be derived by referring to Figure 4 and by considering what an observer situated at the shock surface would see (3:33-36). The following equations then express conservation of mass, momentum, and energy across the shock front.

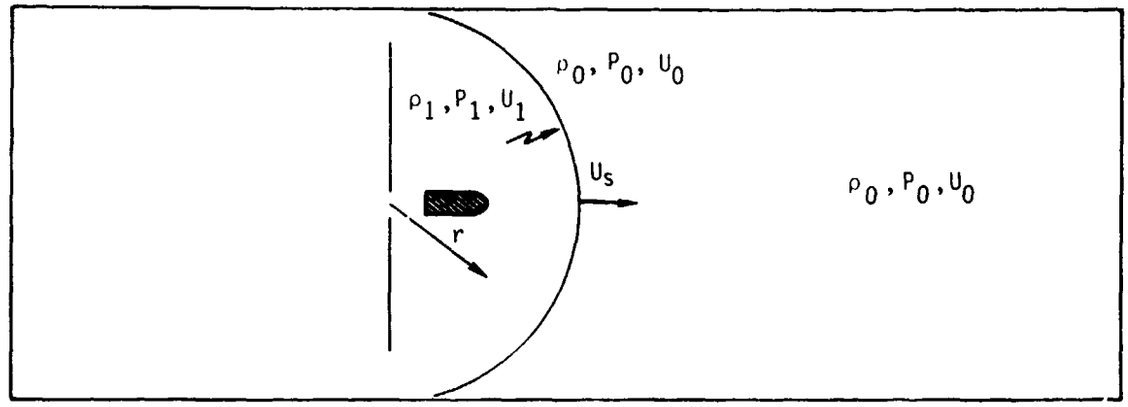

Figure 4. Jump Conditions

Mass $$\rho_0(U_s - u_0) = \rho_1 (U_s - u_1) \tag{9}$$

Momentum $$\rho_0(U_s - u_0)(u_1 - u_0) = P_1 - P_0 \tag{10}$$

Energy $$P_1u_1 - P_0u_0 = \rho_0(U_s - u_0)\left[(e_1 - e_0) + \frac{u_1^2 - u_0^2}{2}\right] \tag{11}$$

where subscripts o represent initial conditions ahead of the shock; subscripts 1 represent shock conditions immediately behind the shock surface; and U_s is the velocity of the shock surface.

Since U_0 is nearly always zero, these equations are easily simplified for most applications:

Mass $$\rho_0 U_s = \rho_1 (U_s - u_1) \tag{12}$$

Momentum $$\rho_0 U_s u_1 = P_1 - P_0 \tag{13}$$

Energy $$\rho_1 u_1 = \rho_0 U_s \left[(e_1 - e_0) + \frac{u_1^2}{2}\right] \tag{14}$$

Finally, velocity terms can be eliminated from Equations 12-14 to get the Rankine-Hugoniot relation,

$$e_1 - e_0 = \frac{1}{2} (P_0 + P_1) \left(\frac{1}{\rho_0} - \frac{1}{\rho_1}\right) \tag{15}$$

2. THERMODYNAMIC RELATIONS

Several relations from thermodynamics play a key role in the analysis of hydrodynamic shocks (3 and 4). The first relation has already been implied in the assumptions required for the conservation equations, i.e., heat conduction and viscosity can be neglected. The assumption that there is no heat exchange between neighboring volumes is the same

as assuming that the changes in the states of the infinitesimal volume are adiabatic, or that entropy is constant throughout. Constant entropy throughout the region is given by

$$\frac{dS}{dt} = 0 \tag{16}$$

where S is the specific entropy. A second important relation states that the change in specific internal energy is given by the change in the heat minus the work done on the volume:

$$de = TdS - Pd\tau \tag{17}$$

where T is the temperature and τ is the specific volume (volume per unit mass). Note that $\rho\tau = 1$.

Finally, since the conservation equations give three equations for four unknowns, a fourth equation is needed. An equation of state can be chosen that relates any three of the variables, P , T , ρ , τ , and e , because it is known from thermodynamics that only two of these are really independent. For example, for a perfect gas, the temperature can be written as a function of the pressure and volume: $PV = RT$. We will

need the Tait equation of state which can be written in the form $P=F(\rho,S)$, where F represents the equation of state. Specifically, we will use the adiabatic form of the Tait equation of state $P=F(\rho)$, given here without derivation (3:44):

$$P = \frac{\rho_o^2 C_o^2}{n}\left[\left(\frac{\rho}{\rho_o}\right)^n - 1\right] \qquad (18)$$

where C_o = sound velocity in the undisturbed fluid and n is taken to be constant.

3. VELOCITY POTENTIAL

A number of simplifications can be made for fluid flow which is radial. For this condition, the curl of the velocity $(\nabla\times\vec{u})$ is zero, and hence the velocity can be written as the gradient of the scalar velocity potential: $\vec{u}=\nabla\phi$. If, in addition, the fluid velocity is small and nearly constant, the potential ϕ satisfies the wave equation.

It is useful to define some additional terms before showing this last statement:

Specific Enthalpy: $$i = e + \tau P \qquad (19)$$

Kinetic Enthalpy: $$I = i - i_o + \frac{\vec{U}\cdot\vec{U}}{2} \qquad (20)$$

Sound Velocity: $$c^2 = \left(\frac{dP}{d\rho}\right)_s \tag{21}$$

where i_0 is the enthalpy of the undisturbed fluid and the derivative in Equation 21 is taken at constant entropy (4:84).

Finally, by combining Equation 17 with the differential form of Equation 19, we obtain

$$di = TdS + \tau\, dP \tag{22}$$

The conservation of mass equation (Equation 1) can be rewritten so that it illustrates for irrotational flow ($\nabla \times \vec{u} = 0$) the conditions for which the scalar potential ϕ satisfies the wave equation. Equation 1 can be rewritten as

$$\nabla \cdot \vec{u} = -\frac{1}{\rho}\frac{d\rho}{dt} \tag{23}$$

It is shown in Appendix B that with the assumption of constant entropy, Equation 23 can be written as

$$\nabla \cdot \vec{u} = -\frac{1}{c^2}\left[\frac{\partial I}{\partial t} - \frac{\partial}{\partial t}(\vec{u}\cdot\vec{u}) - \frac{1}{2}(\vec{u}\cdot\nabla)(\vec{u}\cdot\vec{u})\right] \tag{24}$$

Since $\vec{u}=\nabla\phi$, for irrotational motion, and $I=-\frac{\partial\phi}{\partial t}$ (see, also, Appendix B), the assumption of irrotational motion, constant entropy, and small velocities and velocity derivatives implies that ϕ satisfies the wave equation

$$\nabla^2\phi = \frac{1}{c^2}\frac{\partial^2\phi}{\partial t^2} \tag{25}$$

4. BERNOULLI'S EQUATION

Bernoulli's equation is the basic relation to be solved to find a description of the pressure field in the tank. The general form of Bernoulli's equation can be derived (3:286) by considering the conservation of momentum equation (Equation 2) when the system is exposed to some external force, $\vec{F}$:

$$\frac{d\vec{u}}{dt} + \frac{1}{\rho}\nabla P = \vec{F} \tag{26}$$

The form of Equation 26 is converted to a fixed elemental volume by using Equation 5. At the same time, only irrotational flow and conservative external forces are considered ($\vec{F}=\nabla\Omega$ where Ω is a scalar force potential); thus

$$\frac{\partial}{\partial t}\nabla\phi + (\vec{u}\cdot\nabla)\vec{u} + \frac{1}{\rho}\nabla P = \nabla\Omega \tag{27}$$

Since $\vec{u} = \nabla\phi$, $(\vec{u}\cdot\nabla)\vec{u}$ can be replaced with $\frac{1}{2}\nabla\vec{u}^2$. Interchanging space and time derivatives, and assuming ρ constant, Equation 27 can be rewritten and integrated to yield the generalized form of Bernoulli's equation

$$\frac{p}{\rho} + \frac{u^2}{2} + \frac{\partial\phi}{\partial t} = \Omega + f(t) \qquad (28)$$

where $f(t)$ is a constant of integration and hence is a function of time only. Equation 28 has been derived for irrotational, incompressible flow involving only conservative forces. Allowing $f(t)$ to be zero would further require the equation be limited to steady flow. Finally, it should be noted that the terms have units of energy per unit mass.

5. NONDIMENSIONAL FORM

One of the tools used in the analysis of shock waves formed by the point release of energy is the principle of similarity. This principle states that the properties of shock waves do not change, even though the energy released does change, provided that the time and distances by which the event is measured are scaled by the amount of energy difference. The advantages of similitude are that it allows the correlation of results from different impact conditions, and that it permits reasonable assumptions about the relative importance of terms, often permitting simplifications that might not normally be apparent.

There are two forms of similarity, the general form and the self-similar form, the latter being the simpler. The goal is to express the hydrodynamic equations in terms of scaled (nondimensionalized) functions that can be made to satisfy conditions for a self-similar solution. Thus, scaling factors must be found so that, with varying projectile impacts, the density, pressure, and particle velocity profiles will have the same form. The primary reference for this section is Bach and Lee (5).

Letting the subscript s_0 indicate quantities along the axis of symmetry (horizontal axis), e_0 be the sound velocity in the undisturbed region, M_{s_0} be the shock mach number along the axis of symmetry, and the bar above the symbol indicate that it is a nondimensional quantity, the following definitions are used to write the hydrodynamic equations in nondimensional form.

Shock Mach Number: $$M_{s_0} = \frac{U_{s_0}(t)}{C} \tag{29}$$

Position: $$\bar{r} = \frac{r}{r_{s_0}(t)} \tag{30}$$

Velocity: $$\bar{u}(\bar{r}, M_s) = \frac{u(r,t)}{U_{s_0}(t)} \tag{31}$$

Density: $$\bar{\rho}\left(\bar{r}, M_{s_0}\right) = \rho \frac{(r,t)}{\rho_0} \tag{32}$$

Pressure: $$\bar{P}\left(\bar{r}, M_{s_0}\right) = \frac{P(r,t)}{\rho_0 U_{s_0}(t)} \tag{33}$$

Specific Internal Energy: $$\bar{e}\left(\bar{r}, M_{s_0}\right) = \frac{e(r,t)}{U_{s_0}^2(t)} \tag{34}$$

For all this work, the shock wave is considered hemispherical, and therefore $U_{s_0} = U_s$, and $M_{s_0} = M_s$.

The conservation equations can now be given in spherical coordinates and in terms of the nondimensional variables just defined.

Conservation of Mass:

$$(\bar{u} - \bar{r})\ \frac{\partial \bar{\rho}}{\partial \bar{r}} + \bar{\rho}\ \frac{\partial \bar{u}}{\partial \bar{r}} + 2\ \frac{\bar{u}\bar{\rho}}{\bar{r}} = -\beta M_s\ \frac{\partial \bar{\rho}}{\partial M_s} \tag{35}$$

Conservation of Momentum:

$$(\bar{u} - \bar{r})\ \frac{\partial \bar{u}}{\partial \bar{r}} + \beta \bar{u} + \frac{1}{\bar{\rho}}\ \frac{\partial \bar{P}}{\partial \bar{r}} = -\beta M_s\ \frac{\partial \bar{u}}{\partial M_s} \tag{36}$$

Conservation of Energy:

$$(\bar{u} - \bar{r})\left[\frac{\partial \bar{e}}{\partial \bar{r}} - \frac{\bar{P}}{\bar{\rho}^2}\ \frac{\partial \bar{\rho}}{\partial \bar{r}}\right] + 2\beta \bar{e} = -\beta M_s\left[\frac{\partial \bar{e}}{\partial M_s} - \frac{\bar{P}}{\bar{\rho}^2}\ \frac{\partial \bar{\rho}}{\partial M_s}\right] \tag{37}$$

where

$$\beta = \frac{r_s \dot{U}_s}{U_s^2} \tag{38}$$

The derivation of Equations 42-44 is given in Appendix C.

The simplified jump conditions (Equations 12, 13, and 15) can also be written in nondimensional form. The subscripts 1 and o mean the same as before so that $\bar{\rho}_1 = \frac{\rho_1}{\rho_0}$, etc. Also, Equations 13 and 15 are further simplified by recognizing that ρ_0 and e_0 are small enough that $P_1 - P_0 \cong P_1$ and $e_1 \pm e_0 \cong e_1$. After these small simplifications, the nondimensional jump conditions become

Mass:
$$\bar{\rho}_1(1-\bar{u}_1) = 1 \tag{39}$$

Momentum:
$$\bar{P}_1 = \bar{u}_1 \tag{40}$$

Energy:
$$\bar{e}_1 = \frac{\bar{u}_1^2}{2} = \frac{\bar{P}_1}{2}\left(1 - \frac{1}{\bar{\rho}_1}\right) \tag{41}$$

Finally, the Tait equation of state can also be written in nondimensional form:

$$\bar{P} = \frac{1}{nM_s^2}\left[\bar{\rho}^n - 1\right] \tag{42}$$

6. SHOCK FRONT FORMATION

A point source disturbance in an infinite fluid will create a pressure pulse that moves radially away from the point of the disturbance and which decays in amplitude. The fluid characteristics within the pulsed region are not constant; the second velocity within the pulsed region varies depending on the pressure and the density. Since the sound velocity is greatest in regions of highest pressure, the disturbance will propagate more quickly through those regions. The net result is as shown in Figure 5; the high pressure disturbance tends to overtake the leading lower pressure disturbances, and thus a shock tends to form at the front of every pressure pulse. And, continuing this argument, the back part of the pulse will tend to spread out.

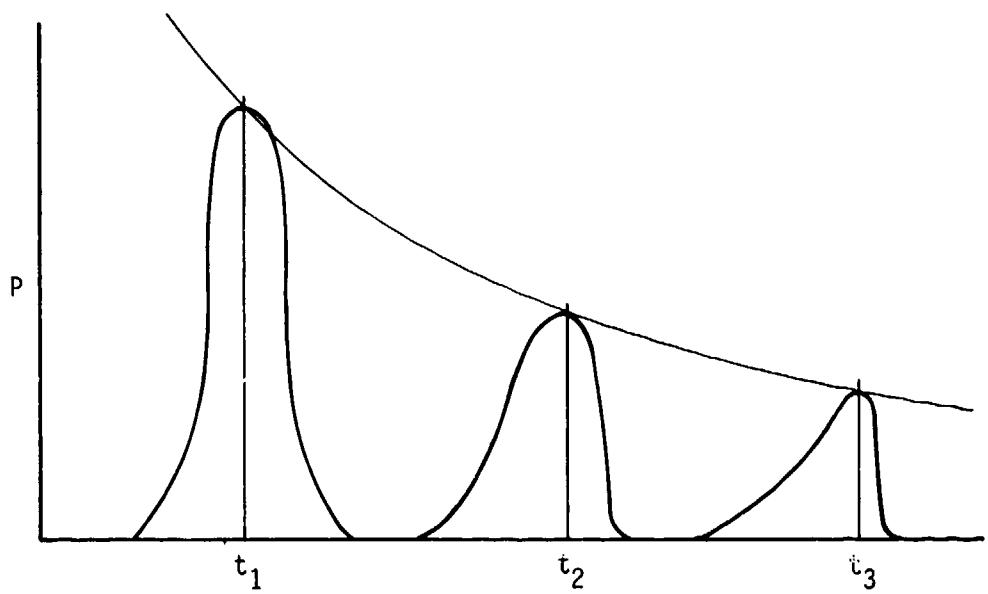

Figure 5. Shock Front Formation

SECTION III

FLUID SHOCKS

A shock front is a region of the fluid characterized by abrupt changes in fluid variables such as pressure, density, and particle velocities. Fluid shocks are invariably created at impact and are frequently observed at points adjacent to the projectile trajectory. The latter shocks dissipate quickly as the disturbed region expands radially and thus have not been carefully observed or analyzed. Fluid shocks at the impact point, however, have been extensively photographed, measured, and analyzed, and are the subject of this section.

The impact shock, formed as the projectile strikes the tank wall, creates a hemispherical shock surface which expands about the impact point. If the projectile is a very light particle, it may not penetrate the tank wall, or it may just penetrate and be essentially stopped within a few centimeters. A heavier projectile, such as a bullet, can be expected to penetrate the wall and have sufficient velocity remaining to continue through the fluid, transferring some of its kinetic energy to the fluid at every increment along its path. In the first case, the impact shock is due to a point source release of energy, and it is this phenomenon that was observed and reported by NASA. In the second case, the projectile cannot be a point source of energy except in the limiting case or as an approximation. Since accurate measurements of the variables associated with impact shock of a bullet have not been made, this section reports observations

made by NASA of light hypervelocity particles. This is followed by the shock phase analysis of Yurkovich which was intended to be used for ordnance projectiles, but has only been verified against data from light hypervelocity particles.

1. DESCRIPTION OF THE FLUID SHOCK ABOUT THE IMPACT POINT

In their preliminary investigations, Stepka and Morse (1) studied front wall fracture. They fired small spheres and cylinders (nylon, aluminum, steel, copper, and tungsten) into aluminum tank wall specimens mounted on a transparent plastic tank. Some of the projectiles were fired into specimens with pre-punched holes to eliminate the effects of the wall-projectile interaction. The shock waves were monitored by piezoelectric crystal pressure sensors near the impact point (36 6 mm and 47.5 mm) and by a high-speed continuous-writing camera throughout the fluid (up to 1.6 frames/μsec). These were comparatively low-energy experiments, the kinetic energy of most of the shots being between 100 J and 1350 J. The results most significant to hydrodynamic ram investigations are that velocities were clearly an important factor in causing fracture, and that tank volume, liquid level, and compressibility were not. Further, it was found that pressurization of the tank reduced fracturing for high velocities. It was also noted that fracture occurred between 27 and 40 μsec after impact, while the shock front was still only several centimeters in radius. Pressures of approximately 7 kilobars were calculated at about 15 mm from the impact point. Figure 6 shows the pressure sensor records. Finally, it can be seen from Figure 7 that fracture thresholds exist; for a given projectile and target, the

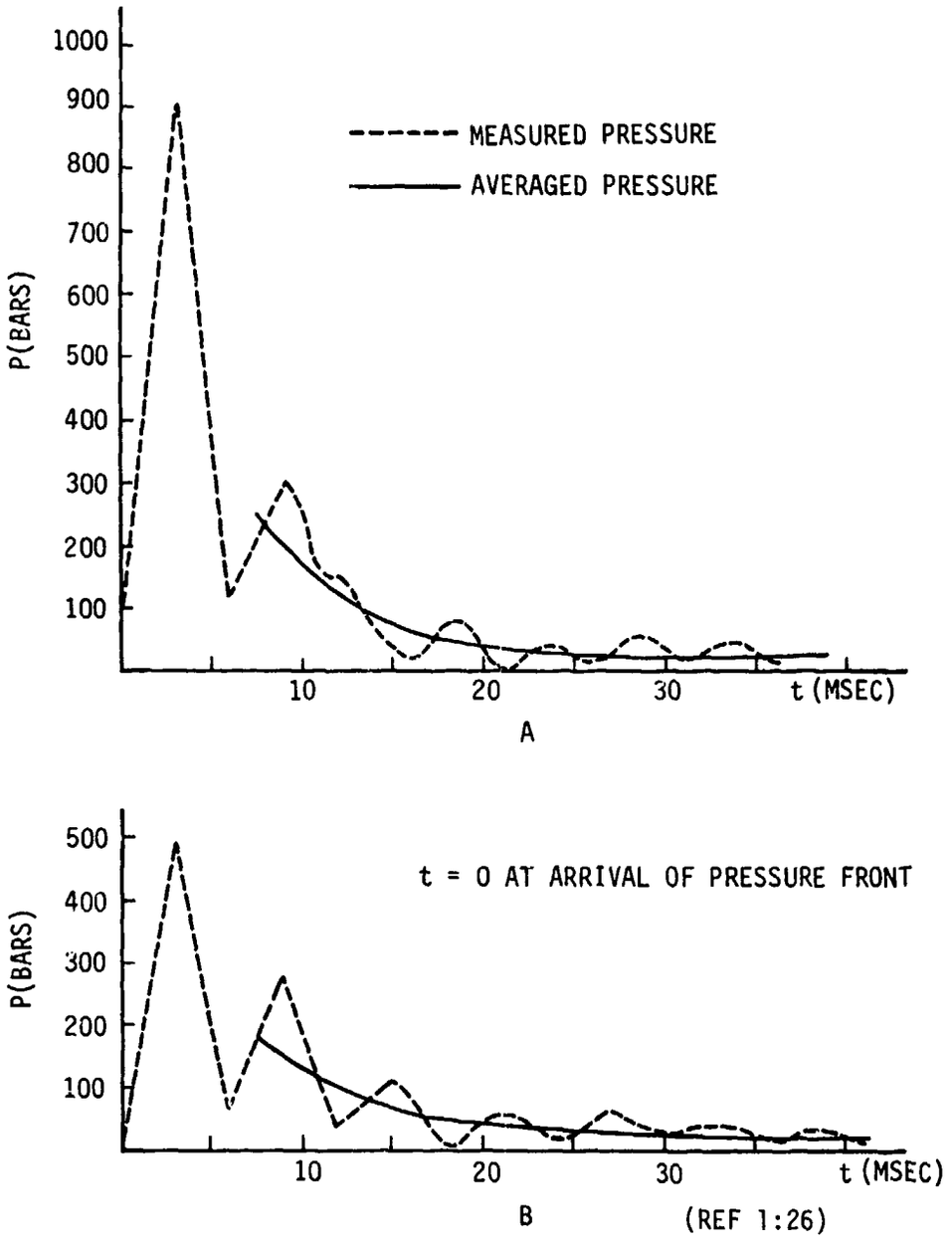

A. Pressure measured 36.6 mm from impact point

B. Pressure measured 47.5 mm from impact point

Impacting particle: aluminum sphere, 5.55 mm diameter; velocity - 2.039 mm/μsec

Figure 6. Pressure Histories Near the Region of Hypervelocity Impact

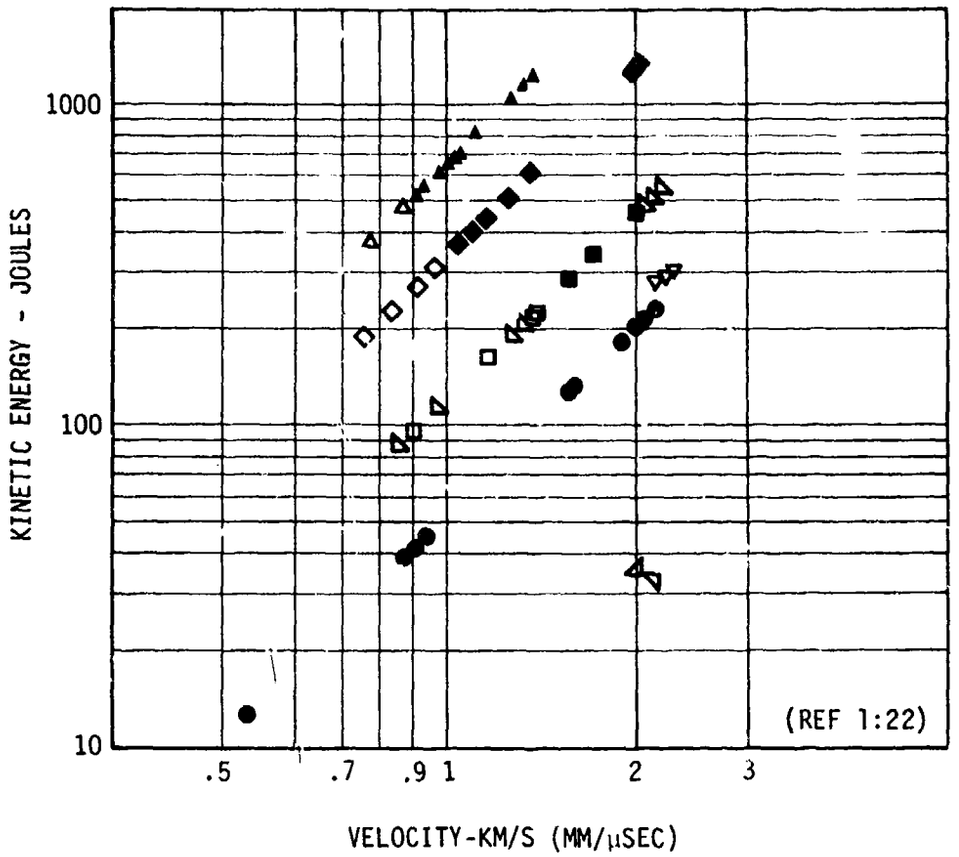

Target: 1.59 mm aluminum wall of a water-filled tank

Projectile: spheres;	Mass(gm)	Diameter(mm)	Material	Symbol
	1.34	5.55	Tungsten	△
	.699	5.55	Steel	◇
	.251	5.55	Aluminum	□
	.105	5.55	Nylon	○
	.249	3.18	Tungsten	◺
	.130	3.18	Steel	▽
	.019	2.38	Aluminum	◿
	.016	1.59	Steel	◁

Open symbols: puncture only
Solid symbols: fracture/rupture

Figure 7. Puncture vs Fracture as Functions of Projectile Kinetic Energy and Velocity

type of damage changes from puncture to fracture as the velocity of the projectile is increased.

In a follow-on report, Stepka, Morse, and Dengler (6) investigate the characteristics of the pressure waves in liquid-filled tanks. A test set-up similar to that in the preliminary investigations was used with the addition of a Kerr cell shadowgraph system and a new gun capable of velocities in the 2.7 mm/μsec to 6.4 mm/μsec range. The primary goal was to measure the shape, velocity, and the time-rate-of-change-of-magnitude of the shock wave.

The shape of the wave was determined to be hemispherical regardless of the obliquity of the impacting particle. McMillan had reported earlier (7:205) that the shock surface was actually ellipsoidal with very small eccentricity, and was with the longer axis, the one in the direction of the projectile trajectory. Velocities of the shock front can be determined from plots of the shock position as a function of time (Figure 8) and it can be seen that the slopes of these curves can be approximated by straight lines on a log-log plot. Thus

$$\frac{\Delta \log r}{\Delta \log t} = \alpha \tag{43}$$

or

$$\frac{r_2}{r_1} = \left(\frac{t_2}{t_1}\right)^{\alpha} \tag{44}$$

where α is a nearly constant slope. The exponent α is between 0.7 and 0.9; for the copper cylinder in Figure 8, α is 0.733 between 10 and 20 μsec after impact.

The projectile deceleration is indicated in Figure 9. The same relationships hold as before, but with the slope α not nearly so constant. However, for the more massive particles, as in tests 10 and 11, α is basically constant at about 0.77 and 0.91, respectively.

The maximum pressures occur just behind the shock surface, immediately after impact, and are shown in Figure 10. These measurements are not made directly, but shadowgraph photography is used to learn the velocity of the shock front. Shock front velocity is then related to pressure at the shock front through the Tait adiabatic equation of state, the specific volume, and the specific heat, as plotted in Figure 11. Note from Figure 10 that the maximum pressures behind the shock front decay vary rapidly with distance. Thus, for the highest impact energies shown here (8254 J), and presumably for considerably higher impact energies, the extremely high pressure region remains local. Thus, damage to the side and rear walls is not normally related to the fluid shock produced at front wall impact.

The energy of the projectile can be measured at impact, and if clear photographs are available, its energy after impact can be

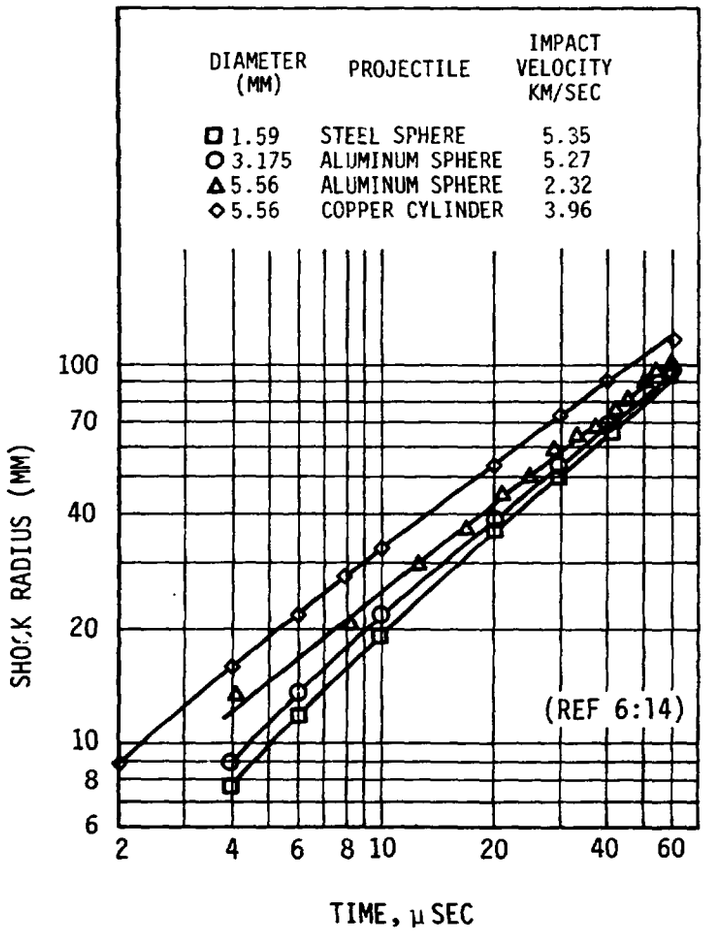

Figure 8. Shock Radius vs Time for Hypervelocity Penetration Through Prepunched Holes

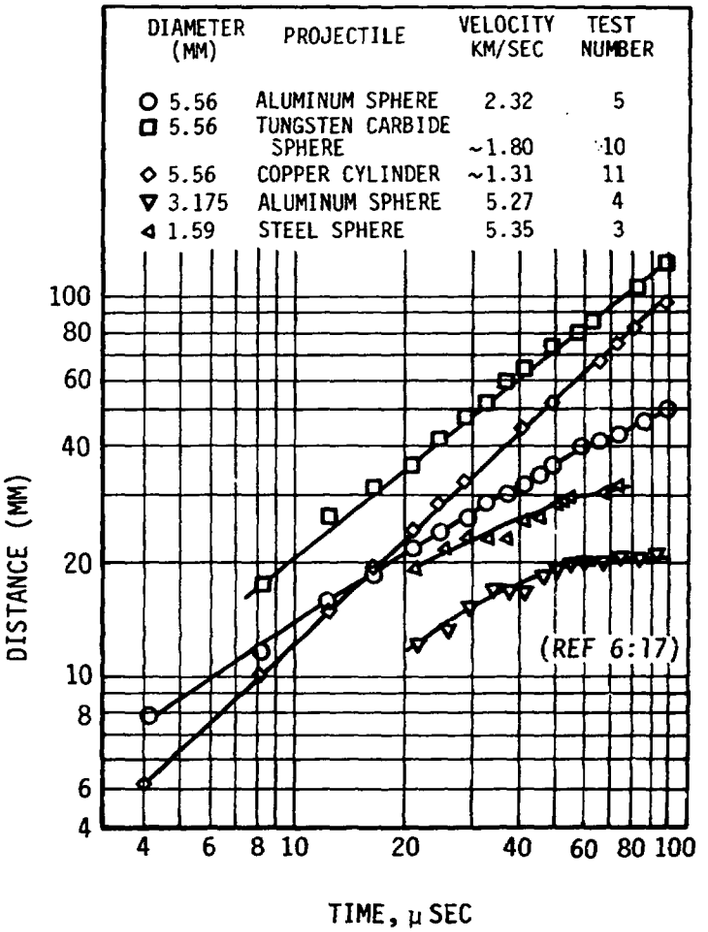

Figure 9. Projectile (Projectile Fragments) Penetration Depth vs Time Into Water Through Prepunched Hole

DIAMETER, MM	PROJECTILE MATERIAL	SHAPE	VELOCITY, KM/SEC	ENERGY, J
◿ 5.56	STEEL	CYLINDER	4.27	8254
◇ 5.56	COPPER	CYLINDER	3.96	7624
▽ 3.175	STEEL	SPHERE	4.27	1185
○ 5.56	ALUMINUM	SPHERE	2.32	672
△ 1.59	STEEL	SPHERE	5.35	232
□ 5.56	ALUMINUM	SPHERE	1.90	451

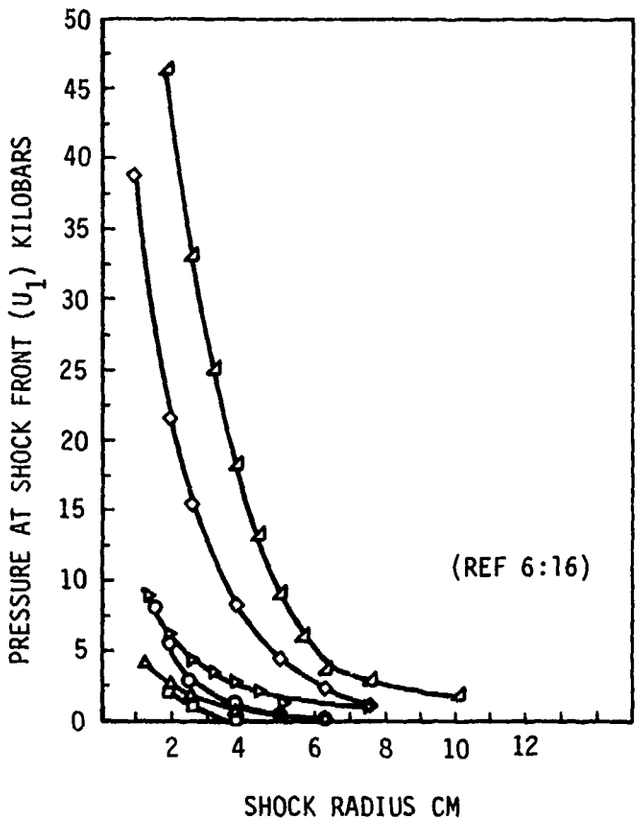

Figure 10. Shock Front Pressures in Water as a Function of Shock Radius

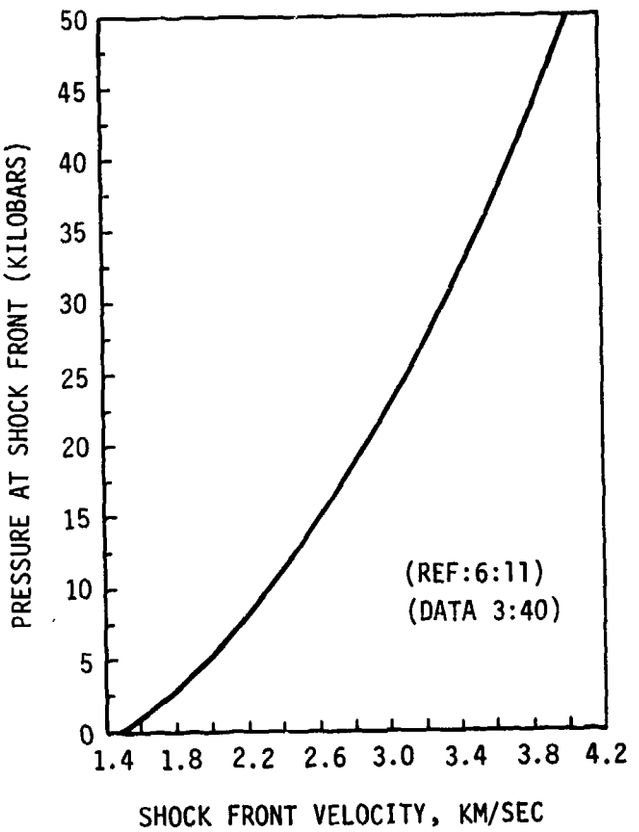

Figure 11. Shock Front Pressures in Water (20°C) as a Function of Shock Front Velocity

deduced from velocity measurements. The energy loss in the fluid due to drag can then be calculated reasonably well with the analytical equation (6:19)

$$E = \frac{E_0}{\left[1 + \frac{3C_D}{4}\left(\frac{\rho_f}{\rho_P} \cdot \frac{v_0}{2r_P}\right)\right]^2} \qquad (45)$$

where E_0 is the energy of the projectile just after impact, C_D is the coefficient of drag of the fluid on the projectile, ρ_f and ρ_P are the densities of the fluid and the projectile, respectively; v_0 is the projectile velocity just after impact, and r_P is the projectile radius. Equation 45 will be derived later in a slightly different form (Section III). The energy loss for the light particles studied here was well over 90% within the first 20 μsec. As an example, an aluminum sphere with 3.175 mm diameter and having an impact velocity of 5.27 mm/μsec was essentially stopped within 20 mm. Thus, it is natural to want to approximate the energy release that formed the shock wave as a point source for these very light projectiles. Bullets, even fragments, would not normally be expected to follow such a large energy loss percentage so quickly.

2. COMPRESSION OF THE FLUID NEAR THE IMPACT POINT

Williams (9) has presented a model of the fluid compression behind the shock front based on the fluid volume displaced by the projectile during the first couple of millimeters. The following assumptions are required: (1) the projectile penetrates the wall smoothly and

continuously, (2) the projectile and shock velocities remain constant during penetration, and (3) the tank wall, volume of the wall removed, and the tank wall displacement have no effect on the fluid behind the shock surface (even though the tank wall displacement velocity may be significant). With these assumptions, then, and reference to Figure 12, the total fuel volume displaced by the projectile is given by

$$V_p = \pi \int_0^x R^2(\xi)\, d\xi \tag{46}$$

where $R(\xi)$ is the distance the projectile protrudes into the fluid, $R(\xi)$ is the radius of the projectile, and ξ is a dummy variable which is equal to 0 at the tip of the projectile and increases to the left. The volume enclosed by the hemispherical shock surface is

$$V_0 = \frac{2\pi}{3} U_s^3 t^3 \tag{47}$$

The ratio of the volume within the shocked region at any instant and the volume originally occupied by that region is the compression

$$\frac{V_0 - V_p}{V_0} = 1 - \mu \tag{48}$$

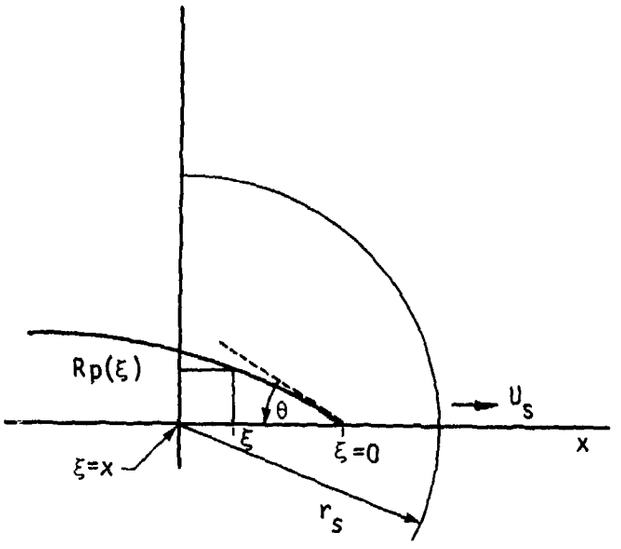

Figure 12. Projectile - Shock Front Diagram

where

$$\mu = \frac{V_p}{V_o} = \frac{3}{2} \int_0^x \frac{r^2(\xi)\, d\xi}{U_s^3\, t^3} \tag{49}$$

is the relative mean compression ratio of the fuel within the shock. In the approximation that the nose of the projectile is a cone with angle θ, then $r(\xi) = \xi \tan\theta$ and the integral is easily evaluated to give the relative mean compression ratio for this case

$$\mu = \frac{\tan^2\theta}{2} \cdot \frac{V_p^3}{U_s^3} \tag{50}$$

Thus the initial mean compression ratio, up to penetration of the shoulder of the projectile, is essentially time-independent. This model is particularly useful for the calculation of very early shock pressures.

3. DENSITY, PARTICLE VELOCITY, PRESSURE PROFILES, AND THE ENERGY EQUATION

If the projectile were to release all of its energy at a single point instead of continuously along its trajectory, one could reference the published works of the authors on blast waves. This is basically the limiting case that Yurkovich describes, drawing upon the work of Bach and Lee (5). This assumption is clearly valid for light particles, which may be essentially stopped within a few centimeters. However, this model can be criticized since a bullet will not normally lose a large percentage of its energy in such a short distance. This is especially true for normal impact, which is the case generally found in testing situations. But, it may not be a valid criticism for tumbled entry, because large percentages of the projectile energy could be lost during impact. And, tumbled entry is the condition which can be most frequently expected in a combat situation, where the bullet must first penetrate the aircraft skin at an oblique angle, and with a relative tangential velocity.

In the Yurkovich model, the projectile becomes a point source of energy immediately inside the front wall. The hemispherical shock surface that is formed is taken to be half the shock sphere formed by a blast wave in an infinite fluid. The functional form of the density behind the shock surface must be known or assumed. Then, it is possible to derive profile equations for the fluid density, the fluid particle velocity, and the fluid pressure in the shocked region. Finally, the energy in this region can be written in terms of an integral which must be evaluated numerically.

a. Density Profile. Consider the projectile tip to have just penetrated the front wall without disturbing the fluid. At this instant, the projectile deposits a significant amount of its energy, resulting in a hemispherical shock surface which expands radially from the impact point. This hemisphere will have the same characteristics as half a sphere formed by a point release of energy into an infinite fluid; i.e., all wall effects are ignored.

An expanding shock sphere in an infinite fluid would enclose a mass

$$m = 4\pi \int_0^{r_s} r^2 \rho \, dr \tag{51}$$

where $\rho = \rho(r,t)$ and r is the radius of the sphere. The mass which had originally occupied this volume was

$$m_o = \frac{4}{3} \pi r_s^3 \rho_o \tag{52}$$

But, these masses must be equal, thus

$$\int_0^{r_s} r^2 \rho \, dr = \frac{r_s^3 \rho_0}{3} \tag{53}$$

or, in nondimensional units (Equations 30 and 33),

$$\int_0^1 \bar{\rho}(\bar{r}, M_s) \, d\bar{r} = \frac{1}{3} \tag{54}$$

where the integration can be performed once the functional form of $\bar{\rho}$ is known. Yurkovich used the same form assumed by Porzel (11)

$$\bar{\rho} = \bar{\rho}_1(M_s) \bar{r}^{\,q(M_s)} \tag{55}$$

Integration of Equation 55 together with the result given in Equation 54 determine $q(M_s)$ to be

$$q(M_s) = 3(\bar{\rho}_1 - 1) \tag{56}$$

The density profile behind the shock front can now be written explicitly:

$$\bar{\rho}(\bar{r}, M_s) = \bar{\rho}_1(M_s) \bar{r}^{\,3(\rho_1 - 1)} \tag{57}$$

b. Particle Velocity Profile. Since ρ is known, it is possible to solve the Conservation of Mass equation in nondimensional coordinates for $\bar{u}$, the nondimensional particle velocity. Equation 38 is rewritten

$$(\bar{u} - \bar{r})\frac{\partial \bar{\rho}}{\partial \bar{r}} + \bar{\rho}\frac{\partial \bar{u}}{\partial \bar{r}} + 2\frac{\bar{u}\bar{\rho}}{\bar{r}} = -\beta M_s \frac{\partial \bar{\rho}}{\partial M_s} \tag{58}$$

Substituting

$$\begin{aligned} \bar{\rho} &= \bar{\rho}_1 \bar{r}^q \\ \frac{\partial \bar{\rho}}{\partial \bar{r}} &= \bar{\rho}_1 q \bar{r}^{(q-1)} \\ \frac{\partial \bar{\rho}}{\partial M_s} &= \left(\frac{\partial \bar{\rho}_1}{\partial M_s} + \bar{\rho}_1 \frac{\partial q}{\partial M_s} \ln \bar{r}\right)\bar{r}^q \end{aligned} \tag{59}$$

and rearranging terms,

$$\frac{\partial \bar{u}}{\partial \bar{r}} + \frac{q+2}{\bar{r}}\bar{u} = q - \beta M_s\left(\frac{\partial}{\partial M_s}\ln\bar{\rho}_1 + \ln\bar{r}\frac{\partial q}{\partial M_s}\right) \tag{60}$$

Once M_s is fixed, $q(M_s)$ will be constant, so that for each M_s, Equation 60 can be rewritten as a first-order linear differential equation in the standard form

$$\frac{dy}{dx} + P(x)y = Q(x) \tag{61}$$

Using the integrating factor $\bar{r}^{(q+2)}$, the integration of Equation 60 gives

$$\frac{\bar{u}}{\bar{r}} = \frac{q - \beta M_s \frac{\partial}{\partial M_s} \ln\bar{\rho}_1}{q+3} - \beta M_s \frac{\partial q}{\partial M_s}\left[\frac{\ln\bar{r}}{q+3} - \frac{1}{(q+3)^2}\right] + \frac{C}{\bar{r}^{q+3}} \tag{62}$$

where the integration constant C is found to be 0 for the boundary conditions $\bar{u} = \bar{u}_1$, and $\bar{r} = 1$. Recalling that $q+3 = 3\bar{\rho}_1$, the derivative can be written as $\frac{\partial q}{\partial M_s} = 3\frac{\partial \rho_1}{\partial M_s}$, and the particle velocity profile has the final form

$$\bar{u} = \bar{u}_1 \bar{r}\left(1 - \Theta \ln\bar{r}\right) \tag{63}$$

where

$$\Theta = \frac{\beta M_s}{\bar{u}_1} \frac{\partial}{\partial M_s} \ln\bar{\rho}_1 \tag{64}$$

Equation 63 can be simplified for strong shocks. Since $\bar{\rho}_1$ is a function of M_s alone, and, further, is nearly constant for shocks which have a constant density ratio across the shock wave, the velocity ratio for very strong shocks is

$$\bar{u} \cong \bar{u}_1 \bar{r} \tag{65}$$

c. Fluid Pressure Profile. For both density and velocity profiles, Yurkovich has followed Bach and Lee (5). However, in obtaining the pressure profile, he makes the strong shock simplification before the derivation, while Bach and Lee make the assumption after the derivation. Since the final equations are different, and since neither has been verified for bullets, both will be presented here for completeness.

The conservation of momentum is restated in nondimensional coordinates (Equation 43):

$$(\bar{u} - \bar{r}) \frac{\partial \bar{u}}{\partial \bar{r}} + \beta u + \frac{1}{\bar{\rho}} \frac{\partial \bar{P}}{\partial \bar{r}} = - \beta M_s \frac{\partial \bar{u}}{\partial M_s} \qquad (66)$$

To find the normalized pressure function $\bar{P}$, this equation is rearranged for integration with respect to $\bar{r}$:

$$\bar{P} = - \int \bar{\rho} \left[(\bar{u} - \bar{r}) \frac{\partial \bar{u}}{\partial \bar{r}} + \beta \left(\bar{u} + M_s \frac{\partial \bar{u}}{\partial M_s} \right) \right] d\bar{r} \qquad (67)$$

Noting that $\bar{\rho}$, $\bar{u}$, q, and Θ are functions of M_s alone, the following substitutions are made

$$\begin{aligned} \bar{\rho} &= \bar{\rho}_1 \bar{r}^q \\ \bar{u} &= \bar{u}_1 \bar{r} \left(1 - \Theta \ln \bar{r} \right) \\ \frac{\partial \bar{u}}{\partial \bar{r}} &= \bar{u}_1 \left(1 - \Theta - \Theta \ln r \right) \\ \frac{\partial \bar{u}}{\partial M_s} &= \bar{r} \left(\frac{\partial \bar{u}_1}{\partial M_s} - \ln \bar{r} \frac{\partial}{\partial M_s} u_1 \Theta \right) \end{aligned} \qquad (68)$$

Rearranging and identifying similar terms, gives

$$\bar{P} = -\bar{\rho}_1 \int \left[\bar{P}_2 \bar{r}^{q+1} + \bar{P}_3 \bar{r}^{q+1} \ln \bar{r} + \bar{P}_4 \bar{r}^{q+1} \ln^2 \bar{r} \right] d\bar{r} \qquad (69)$$

where the following functions have been defined:

$$\begin{aligned} \bar{P}_2 &= \bar{u}_1 (\bar{u}_1 - 1)(1 - \Theta) + \beta \left(\bar{u}_1 + M_s \frac{\partial \bar{u}_1}{\partial M_s} \right) \\ \bar{P}_3 &= \bar{u}_1 \Theta \left[1 + \bar{u}_1 (\Theta - 2) - \beta \right] - \beta M_s \frac{\partial}{\partial M_s} \bar{u}_1 \Theta \\ \bar{P}_4 &= \bar{u}_1^2 \Theta^2 \end{aligned} \qquad (70)$$

and $\bar{P}_1$ will be defined later. Equation 69 is then integrated to give

$$\begin{aligned} \bar{P} = -\bar{\rho}_1 \Bigg\{ & \frac{\bar{P}_2}{q+2} \bar{r}^{(q+2)} + \frac{\bar{P}_3}{(q+2)^2} \bar{r}^{(q+2)} \left[(q+2) \ln \bar{r} - 1 \right] \\ & + \frac{\bar{P}_4}{(q+3)^3} \bar{r}^{(q+2)} \left(\left[(q+2) \ln \bar{r} - 1 \right]^2 + 1 \right) \Bigg\} + K \end{aligned} \qquad (71)$$

and the constant of integration K, is determined from the boundary condition that $\bar{P} = \bar{P}_1$ at $\bar{r} = 1$:

$$K = \bar{P}_1 - \bar{\rho}_1 \left\{ \frac{\bar{P}_2}{q+2} - \frac{\bar{P}_3}{(q+2)^2} + \frac{2\bar{P}_4}{(q+2)^3} \right\} \qquad (72)$$

Finally, the pressure profile can be written as

$$\bar{P} = \bar{P}_1 + \frac{\bar{\rho}_1}{q+2}\bar{P}_2\left\{1-\bar{r}^{(q+2)}\right\} - \frac{\bar{\rho}_1}{(q+2)^2}\bar{P}_3\left\{1+\bar{r}^{(q+2)}\left[(q+2)\ln\bar{r}-1\right]\right\} + \frac{\bar{\rho}_1}{(q+2)^3}\bar{P}_4\left\{2-\bar{r}^{(q+2)}\left(\left[(q+2)\ln\bar{r}-1\right]^2+1\right)\right\} \tag{73}$$

For strong shock waves, $\rho_1 = \frac{\rho_1}{\rho_0}$ is very large and thus $\bar{u}_1 = 1-\frac{1}{\rho_1}$ is just slightly less than 1. The third and fourth terms of Equation 73, which are modified by terms $\frac{1}{(q+2)^n} = \frac{1}{(3\beta_1-1)^n}$ with $n = 2$, and 3, respectively, can be eliminated, and $\bar{P}_2$ simplifies. Thus, for strong shocks, Bach and Lee write

$$\bar{P} = \bar{P}_1 + \frac{\bar{u}_1\bar{\rho}_1}{q+2}\left(1-\bar{r}^{(q+2)}\right)\left(\bar{u}_1+\beta-1\right) \tag{74}$$

As mentioned earlier, Yurkovich makes the simplifying assumption of a strong shock wave before deriving the pressure profile, i.e.,

$$\begin{aligned} \bar{\rho} &= \bar{\rho}_i\,\bar{r}^q \\ \bar{u} &\cong \bar{u}_1\bar{r} \\ \frac{\partial\bar{u}}{\partial\bar{r}} &\cong \bar{u}_1 \\ \frac{\partial\bar{u}}{\partial M_s} &\cong \bar{r}\,\frac{\partial\bar{u}_1}{\partial M_s} \end{aligned} \tag{75}$$

Putting these substitutions into Equation 67, $\bar{P}$ can be written as

$$\bar{P} = \bar{P}_1 + \frac{\bar{\rho}_1}{q+2} \bar{P}_2^* (1 - \bar{r}^{(q+2)}) \tag{76}$$

where $\bar{P}_2^*$ is just $\bar{P}_2$ as in Equation 70 when Ⓜ is near 0:

$$\bar{P}_2^* \cong \bar{u}_1 (\bar{u}_1 + \beta - 1) + \beta m_s \frac{\partial \bar{u}_1}{\partial m_s} \tag{77}$$

To compare Yurkovich's results with those of Bach and Lee (Equation 74), Equation 76 is written out as

$$\bar{P} = \bar{P}_1 + \frac{\bar{u}_1 \bar{\rho}_1}{q+2} \left(1 - \bar{r}^{(q+2)}\right)\left(\bar{u}_1 + \beta - 1\right) + \left(1 - \bar{r}^{(q+2)}\right) \frac{\beta M_s}{\bar{\rho}_1 (q+2)} \frac{\partial \bar{\rho}_1}{\partial M_s} \tag{78}$$

The last term in Equation 78 is an extra term for Yurkovich's results; no study of its significance was made for this report.

d. Energy Equation. A final relationship that is available for describing the properties within the shocked region is the energy equation. Since the total energy deposited into the fluid is conserved, the energy deposited in the hemisphere is the sum of the change in the internal energy and the change in the kinetic energy. For a sphere,

$$E_s = 2\pi \int_0^{r_s} \left[(e - e_0)\rho + \frac{u^2 - u_0^2}{2} \rho \right] r^2 \, dr \tag{79}$$

or, for a hemisphere in nondimensional coordinates with $u_0 = 0$,

$$E_{h.s.} = \pi \rho_0 C_0^2 M_s^2 r_s^2 \int_0^1 \left[(\bar{e} - \bar{e}_0) + \frac{\bar{u}^2}{2} \right] \bar{\rho}\, \bar{r}^2\, d\bar{r} \qquad (80)$$

where the only quantity not known within the integral is the specific internal energy $\bar{e}$. This work is tremendously simplified for the strong shock assumption; $\bar{e}_0$ is small and can be neglected. Further, for a strong shock, the fluid variables will remain relatively constant for some distance behind the shock surface, thus permitting $\bar{e}$ to be replaced by $\bar{e}_1$. Combining appropriate relationships, Equation 41 $(\bar{e}_1 = \frac{\bar{u}_1^2}{2})$, Equation 55 $(\bar{\rho} = \bar{\rho}_1 \bar{r}^q)$, and Equation 65 $(\bar{u} = \bar{u}_1 \bar{r})$, to rewrite Equation 80, gives

$$E_{h.s} = \frac{\pi}{2} \rho_0 C_0^2 M_s^2 r_s^3 \bar{u}_1^2 \bar{\rho}_1 \int_0^1 (1 + \bar{r}^2)\, \bar{r}^{(q+2)} d\bar{r} \qquad (81)$$

Integrating over the hemisphere, and replacing q with $3(\bar{\rho}_1 - 1)$, finally yields

$$E_{h.s.} = \frac{\pi}{3} C_0^2 M_s^2 r_s^3 \rho_0 \bar{u}_1^2 \left(\frac{3\bar{\rho}_1 + 1}{3\bar{\rho}_1 + 2} \right) \qquad (82)$$

e. Discussion. In summary, profiles have been developed for the density, particle velocity, pressure, and energy of the fluid, the

pressure and energy relationships being the ones which will be applied most often. But, $\bar{P}_1$, $\bar{\rho}_1$, $\bar{u}_1$, and β, have not yet been evaluated.

Yurkovich has used the Tait equation of state, Equation 42; so that the value of $\bar{P}_1$ just behind the shock surface can be found from

$$\bar{P}_1 = \frac{1}{n M_s^2} \left[\bar{\rho}_1^n - 1 \right] \tag{83}$$

which from Equation 40 must also be the expression for $\bar{u}_1$. Now Equation 39 can be used to get a relationship for $\bar{\rho}_1$:

$$\bar{\rho}_1 = \frac{1}{1 - \frac{\bar{\rho}_1^n - 1}{n M_s}} \tag{84}$$

A direct solution of Equation 84 for $\bar{\rho}_1$ in terms of n and M_s is not possible, however, a table of values of $\bar{\rho}_1$ vs M_s for a given value of n can be computed from a rearrangement of Equation 84. The relation

$$M_s^2 = \frac{1}{n} \frac{\bar{\rho}_1^{(n+1)} - \bar{\rho}_1}{\bar{\rho}_1 - 1} \tag{85}$$

was used to plot Figure 13. Then, from Equation 39, $\bar{P}_1$ and $\bar{u}_1$ are easily found also as functions of n and M_s from

$$\bar{P}_1 = \bar{u}_1 = 1 - \frac{1}{\bar{\rho}_1} \tag{86}$$

Equation 86 is plotted in Figure 14.

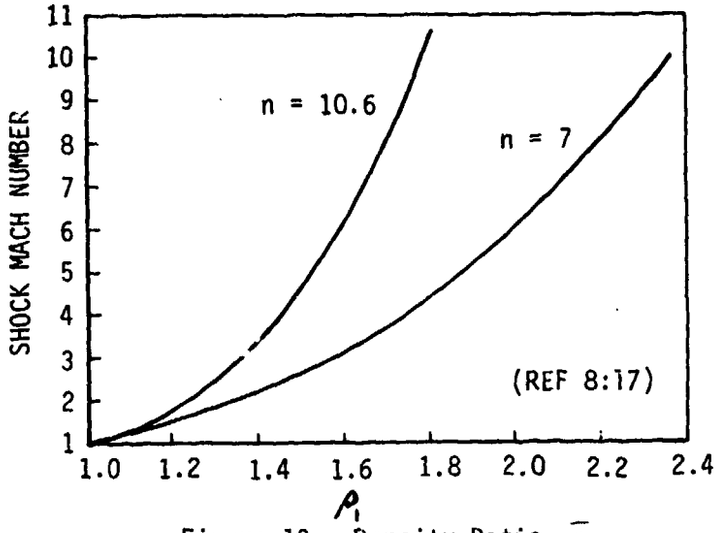

Figure 13. Density Ratio, $\bar{\rho}_1$, vs Shock Mach Number

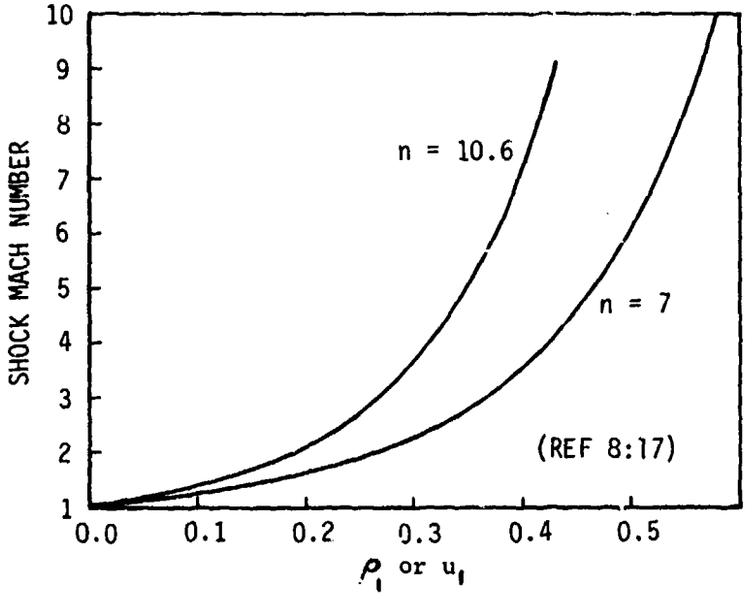

Figure 14. Nondimensional Pressure ($\bar{P}_1$) or Nondimensional Velocity ($\bar{u}_1$) as Function of the Shock Mach Number, M_s

With $\bar{P}_1$ known, Equation 33 can be used to find the pressures just behind the shock front from

$$P_1 = \bar{P}_1 \rho_0 u_s^2 \tag{87}$$

This information is plotted in Figure 15.

To solve for the pressure profile, $\bar{P}$, it is necessary to find

$$\frac{\partial \bar{\rho}_1}{\partial M_s} = \frac{2 n M_s (\bar{\rho}_1 - 1)^2}{n \bar{\rho}_1^{n+1} - (n+1) \bar{\rho}_1^{n} + 1} \tag{88}$$

and

$$\frac{\partial \mathcal{H}}{\partial M_s} = \frac{\beta M_s}{\rho_1} \frac{\partial^2 \rho_1}{\partial M_s^2} + \mathcal{H} \left[\frac{1}{M_s} + \frac{1}{\beta} \frac{\partial \beta}{\partial M_s} - \frac{1}{\rho_1} \frac{\partial \rho_1}{\partial M_s} \right] \tag{89}$$

The term β is taken as constant by Yurkovich, and with this assumption, the term involving $\frac{\partial \beta}{\partial m_s}$ is zero in Equation 89.

Finally, a value for β can be estimated from Equation 38. Based on Figure 8, the shock radius has already been assumed proportional to time to some power α, which has been approximated by 0.8 for light hypervelocity particles. Thus, by assuming $r_s = h t^{\alpha}$, Equation 38 gives

$$\beta = 1 - \frac{1}{\alpha} \tag{90}$$

and, for meteorite work at least, β = -0.25.

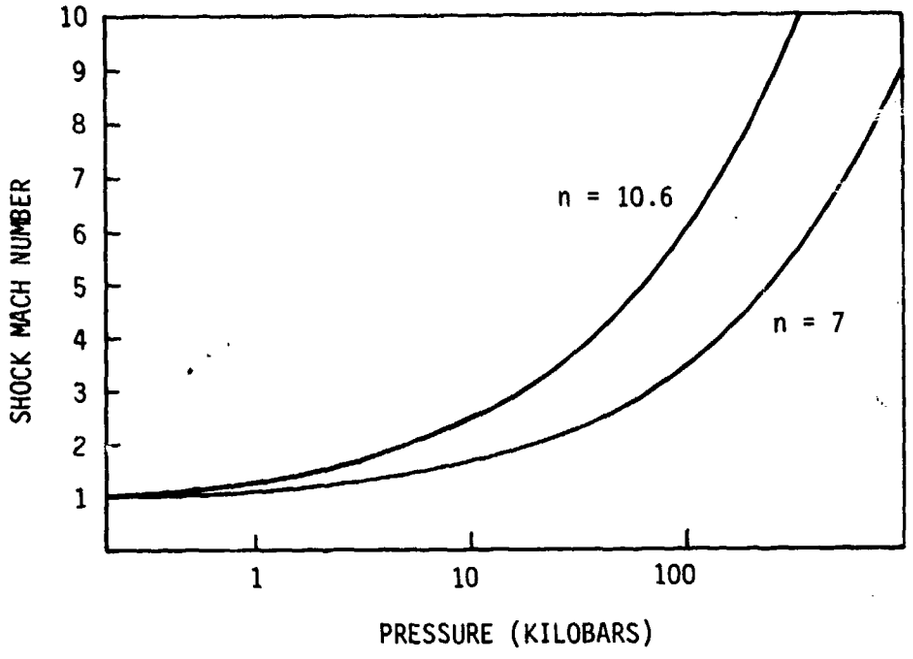

Figure 15. Pressure, P_1 at Shock Front as a Function of the Shock Mach Number, M_s

The pressure function $\bar{P}$ can now be evaluated from Equation 76 and plotted as in Figure 16. These curves show the pressure profiles based on the strong shock assumption as implemented by Yurkovich. Two other pressure profiles are available from the work of Bach and Lee: a complete solution (Equation 73) and another solution based on a strong shock assumption (Equation 74). These three solutions are plotted in Figure 17 for $n = 7$, $\beta = -0.25$, and $M_s = 1.5$. The curves for the other mach numbers between 1 and 2 have also been plotted, though they are not pictured here. They all show the same forms as in Figure 17, and with lower pressures for lower shock mach numbers. Only the Bach and Lee strong shock curve does not become negative for weaker shocks, indicating that an adjustment is required before these relations are applied, especially to cases of weaker shocks, as with projectiles.

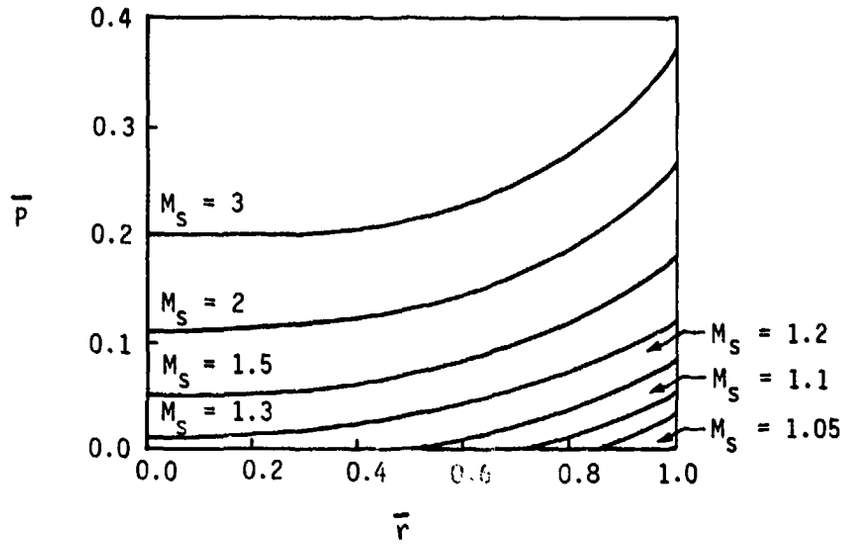

Figure 16. The Nondimensional Pressure, $\bar{P}$ (M_s, $\bar{r}$), as a Function of Nondimensional Distance for Several Values of M_s and for n = 7

One possible critical assumption was in the evaluation of the term β. The term β was treated as a constant; and the measurements of the shock front radius (Figure 8) do indicate that α (hence β) is a constant. But these curves were obtained for light hypervelocity projectiles for a very short time interval and there is no reason to assume that these curves will be so nearly straight for either the lower shock front velocities of bullets or for the longer time intervals that may be important for fragments. The solution suggested by Yurkovich did not present the method for dealing with a varying β, and so is not discussed in this report. But β is a function of M_s and the technique for finding $\beta(M_s)$ is available in Bach and Lee (Reference 5). It must be recommended therefore, that before applying this analysis to the shock portion of the hydrodynamic ram effect, either α should be measured to determine its value, or preferably that this analysis should be extended to include the method used by Bach and Lee to find the functional form of β.

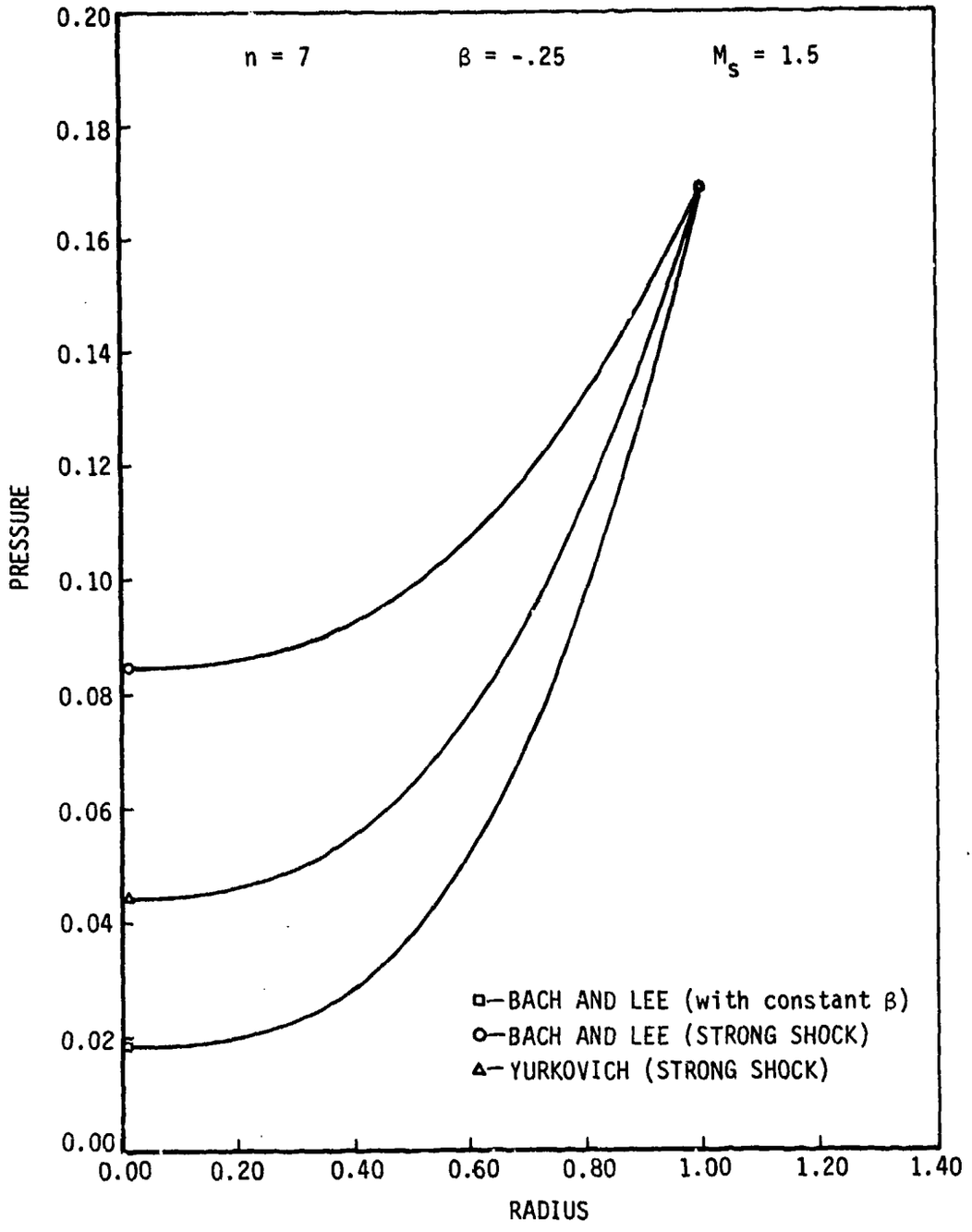

Figure 17. A Comparison of Nondimensional Pressure vs Nondimensional Shock Front Radius

Another result of Yurkovich's analysis of the shock phase is the energy density equation which is gained by dividing $E_{h.s}$ in Equation 81 by the volume of the hemisphere enclosed by the shock.

$$\frac{E_{h.s}}{\frac{2\pi}{3} r_s^3} \cong \frac{\rho_0}{2} C_0^2 M_s^2 \bar{u}_1^2 \left(\frac{3\rho_1 + 1}{3\rho_1 + 2} \right) \tag{91}$$

Equation 90 is plotted in Figure 18 for the condition n = 7 (water) and gives the energy density at the shock front. Since the derivation of Equation 87 was based on the strong shock assumption, the dependence of $\bar{r}$ is lost from the relationship, and hence there is no energy profile.

SECTION IV

CAVITY DESCRIPTION AND FLUID DRAG ANALYSIS

No aspect of the hydrodynamic ram phenomenon has received more attention than the cavity phase. The motion of the fluid has been monitored inside the tank during thousands of tests by high speed cameras (seldom over 7000 fps) peering through plexiglass windows, and by pressure transducers recording high pressures and sometimes shocks at half a dozen or more points throughout the tank. Strain gages, witness sheets, and even cavity gages have been used to monitor the violent fluid and tank motions for up to a tenth of a second.

As the projectile penetrates the tank, the bullet displaces the fluid by imparting velocities to the fluid particles in the direction of the normal to the bullet surface at every point. The observed net result is that the fluid is forced to move radially away from the bullet's path, leaving a cavity in the fluid and creating high pressure in the vicinity of the bullet of 35 to 140 bar (400-2000 psi) at about 10-20 cm from the bullet.

Occasionally, the projectile will remain stable throughout its trajectory and the cavity that is produced is just a cylinder about the path. When this happens, there is little visible motion of the fluid and the projectile loses a minimum amount of velocity before it exits the tank.

Normally, however, the bullet will tumble within 20 to 30 cm. The larger the drag the fluid exerts on the bullet, the more projectile kinetic energy is transferred to fluid kinetic energy. Thus a tumbling 0.50 caliber bullet can be stopped by a 3-foot tank, while a stable projectile may not. As the tumbling projectile gives up varying amounts of its energy, the diameter of the cavity it creates changes proportionally; a smoothly tumbling projectile will create a series of connected cavities with regularly varying cross sections, with the location of the smallest cross sections corresponding to the points in the trajectory where the bullet is traveling nose first, and the largest cross sections corresponding to those parts of the trajectory where the bullet is traveling with its length facing forward. The cavity grows into a sphere as the smaller cross sections begin to collapse while the wider cross sections, whose fluid particles have more kinetic energy, are still expanding. At its maximum radius, the cavity is most nearly spherical and remains spherical as it collapses to some minimum radius. If the cavity is fairly large and nearly spherical, it will rebound to a second maximum radius which is about 2/3 the diameter of the first cavity. This cycle can be repeated two, three, or more times before the cavity dies. Typically, a 0.50 caliber bullet can be expected to have about a 50 cm first maximum radius and about a 5 cm first minimum radius. The first minimum can be expected at about 30 msec after impact, and a second minimum about 30 msec after the first.

In this section of the report, methods are described for estimating the pressures in the fluid from a knowledge of either the cavity radius or the cavity period. Equations which relate the fluid energy to the projectile energy are developed, and equations which describe the pressures in the fuel tank as functions of time and position due to projectile drag are derived. Following these are some brief remarks on the pressures associated with cavity collapse and then a concluding discussion.

1. PRESSURE ESTIMATION TECHNIQUE

Cardea and Torvik (Reference 12) present a method of estimating the pressure in the tank as a function of the distance from the center of the cavity if either the maximum diameter of the cavity a_m or the cavity period is known. Much of their work is based on Cole (3:364), who gives the maximum recorded pressure gage reading in terms of the weight of TNT exploded by

$$P_{gm} = \frac{2590}{r} W^{1/3} \tag{92}$$

where W is the weight of the TNT in pounds, r is the distance from the detonation in feet, and $P_{gm} = P_m - P_o$ in psi. While Cardea and Torvik note that the energy in one pound of TNT is 1.514×10^6 ft-lbs, Cole observes that about half this energy goes into the formation of the cavity. This leads to

$$P_{gm} = \frac{28.5}{r} E_c^{1/3} \tag{93}$$

where E_c is the energy required to form the cavity.

There are two methods to estimate E_c. By assuming that the cavity behind the projectile is sufficiently like that produced by an underwater explosion of TNT, Cole's results can be used. Thus, for a cavity in an incompressible fluid sufficiently distant from the tank wall to ignore reflection the energy required to form the cavity is a function of the maximum cavity radius a_m, and is given by

$$E_c = \frac{4\pi}{3} P_0 a_m^3 \tag{94}$$

where P_0 is the ambient pressure. For use in Equation 92, Equation 93 is rewritten as

$$E_c^{1/3} = 1.612\, a_m\, P_0^{1/3} \tag{95}$$

A second method for estimating the cavity energy is given also by Cole (3:276) as the Willis formula

$$E_c^{1/3} = \frac{P_0^{5/6}}{1.14 \rho_0^{1/2}}\, T \tag{96}$$

where T is the time for one cavity oscillation, and ρ_0 is the ambient density. This second method is preferable because the cavity period is measured more easily than the maximum cavity radius.

2. PROJECTILE/FLUID ENERGY BALANCE

As the projectile moves through the tank, its motion is opposed by fluid particles; the total force opposing the projectile is the fluid drag. It is assumed that all of the energy that is given up by the bullet is either absorbed by the fluid particles as fluid kinetic energy or lost as work done on the fluid in displacing the particles and creating the cavity. Thus, the equation to solve is

$$dE_p = dE_f + dW \tag{97}$$

where the work done against external pressure P_e to change the volume is

$$dW = P_e\, dV \tag{98}$$

Considering the volume expansion along each increment of length dx to be always perpendicular to x,

$$dW = (P_0 - P_c)\, \pi a^2\, dv \tag{99}$$

Both Yurkovich (8) and Lundstrom (13) have completed the solution of Equation 96 in detail. There are fundamental differences to their approaches, but their basic schemes are parallel, and they both derive similar incidental information in the process. To illustrate the similarities of their approaches and to facilitate a comparison of the results, their solutions for each of the major steps of the energy balance equation will be given sequentially. Thus, both solutions of dE_p are given, and then both solutions of dE_f are given. Preceding the calculation of dE_f, it is necessary to show the derivation of the source potential ϕ.

a. Calculations of dE_p. The kinetic energy lost by the projectile is given by

$$dE_p = -mv\,dv \tag{100}$$

where m and v are the projectile mass and velocity, respectively. Then the energy loss along the trajectory is

$$\frac{dE_p}{dx} = -mv\frac{dv}{dx} = -m\frac{dv}{dt} \tag{101}$$

But the last term is the force opposing the projectile, i.e., the fluid drag

$$-m\frac{dv}{dt} = D = \frac{\rho v^2}{2} A_p(x)\, C_D(x) \tag{102}$$

where ρ is the fluid density, $C_D(x)$ is the coefficient of drag, and $A_p(x)$ is the area that the projectile presents to the fluid as it moves along its trajectory. Both the presented area and the coefficient of drag change as the projectile moves through the fluid; however, the problem is normally simplified by fixing the presented area of the projectile and considering only the coefficient of drag as a variable. The presented area, $A_p(x)$, of the projectile is taken to be the area of its widest cross section, A_p .

Lundstrom combines Equation 101 and Equation 102 to get

$$\frac{dv}{v} = -\beta dx \tag{103}$$

where the velocity decay coefficient is defined as

$$\beta = \frac{\rho A_p C_D}{2m} \tag{104}$$

Equation 103 is integrated to obtain v ,

$$v = v_0 e^{-\int \beta dx} \tag{105}$$

Finally, by combining Equations 101 and 104, Lundstrom's final equation for the energy deposition along the trajectory, can be written as

$$\frac{dE_p}{dx} = mv^2\beta \tag{106}$$

Equation 105 can be used to write the final equation (Equation 107) in terms of the constant v_o, which is measurable at impact, and the function β which must be determined by observation:

$$\frac{dE_p}{dx} = mv_o\,\beta e^{-2\int\beta dx} \tag{107}$$

Yurkovich combined Equations 101 and 102 differently to get

$$\frac{dv}{v^2} = -\beta dt \tag{108}$$

This equation is not integrated to find v since the functional form of β is not known. Yurkovich approximates β with $\bar{\beta}_i$, the average value of β in the ith segment of the projectile path. Then, Equation 108 is between the end points of each segment to give

$$v_{i+1} = \frac{v_i}{1 + \bar{\beta}_{i+1} v_i \Delta t} \tag{109}$$

where the subscripts i and i+1 refer to values at the beginning and end of the ith segment, and $\Delta t = t_{i+1} - t_i$. $\bar{\beta}_{i+1}$ is now an unknown constant.

Yurkovich uses Equation 109 to find two more relationships. Equation 109 is integrated to find the distance the projectile moves during each time interval, Δt,

$$\Delta x = \frac{1}{\bar{\beta}_{i+1}} \ln \left[1 + \bar{\beta}_{i+1} v_i \Delta t \right] \tag{110}$$

Also, Equation 109 can be combined with $E_P = \frac{mv^2}{2}$ to get the energy of the projectile in each segment

$$E_{P_{i+1}} = \frac{E_{P_i}}{\left[1 + \bar{\beta}_{i+1} v_i \Delta t \right]^2} \tag{111}$$

(For constant C_D, this would reduce to Equation 45, which was given without derivation.) Finally, the total energy loss due to drag is the sum of all the segments of energy

$$E_{P_o} - E_{P_f} = \sum_{i=1}^{n+1} E_{P_i} \tag{112}$$

Equation 112 can be differentiated numerically to find Y, the energy transferred per unit length of the projectile path. Then dE_P is approximated by

$$\Delta E_P = Y \Delta x \tag{113}$$

b. Velocity Potential Due to a Line of Sources. The final goal of the fluid drag section is the solution of Bernoulli's equation, Equation 28, for the pressure distribution throughout the fuel tank, and this equation requires the differentiation of the velocity potential, ϕ. Thus both authors have described the fluid energy differential, dE_f, in terms of ϕ. Yurkovich has drawn upon the known velocity potential of a spherical bubble, while Lundstrom has derived an appropriate velocity potential for the problem based on the concept of source strengths. Lundstrom's velocity potential is derived in the following paragraphs.

The potential, ϕ, can be constructed from a line of sources defined as points in the fluid from which fluid flow can be thought to emanate. These sources are imagined to exist at close intervals along the projectile trajectory as in Figure 18. While the concept is purely fictitious, it can be used effectively to describe the flow of fluid away from an explosion or from the trajectory of a projectile. The source is assigned a strength, m, which is related to the rate of fluid flow ($m = \Delta v/\Delta t$). The fluid flow associated with a point source is determined by that volume of fluid which would pass through the surface of an imaginary sphere enclosing the source (Figure 19):

$$m\,\Delta t = \frac{4\pi}{3}\left[(r+\Delta r)^3 - r^3\right] \tag{114}$$

which, after simplifying and taking the limit leaves

$$m = 4\pi r^2 \dot{r} \tag{115}$$

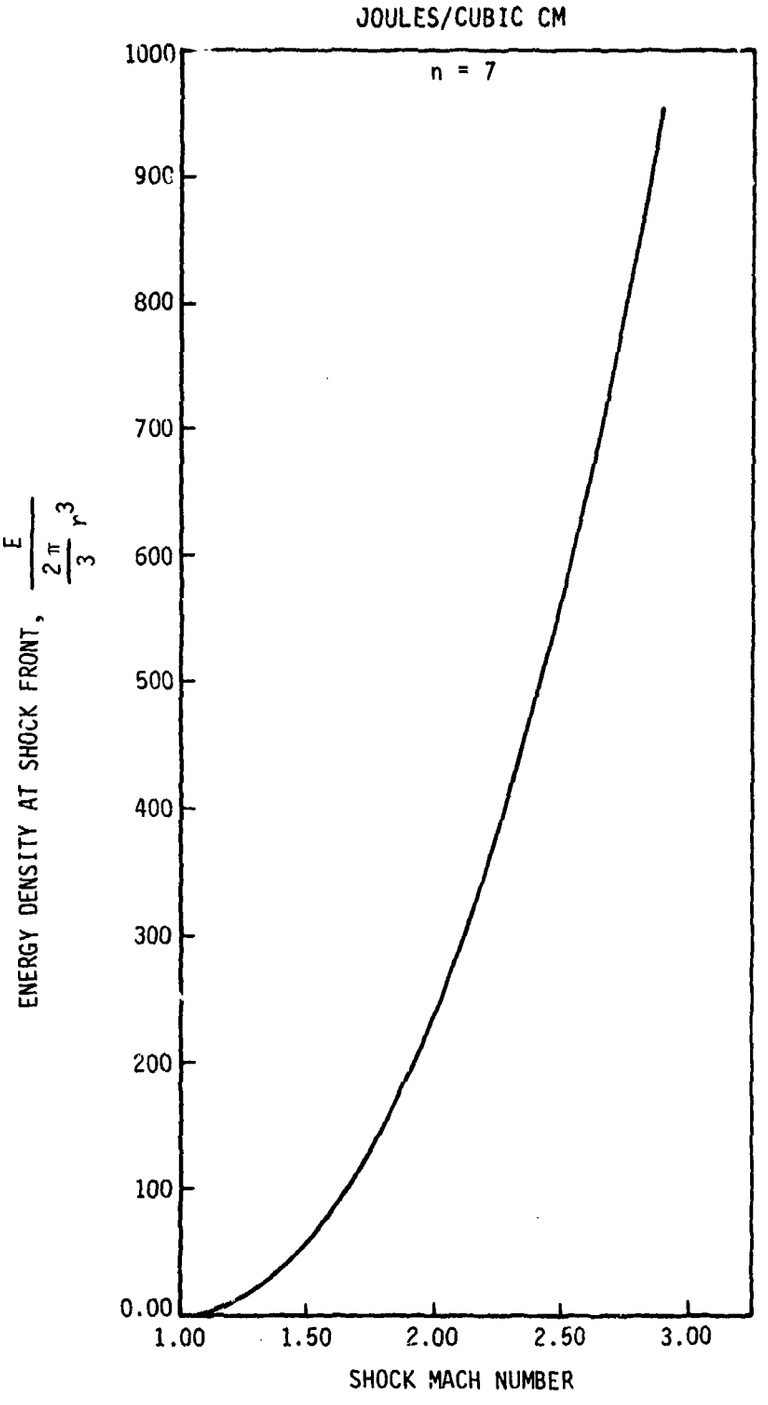

Figure 18. Energy Density at the Shock Front as a Function of Shock Mach Number

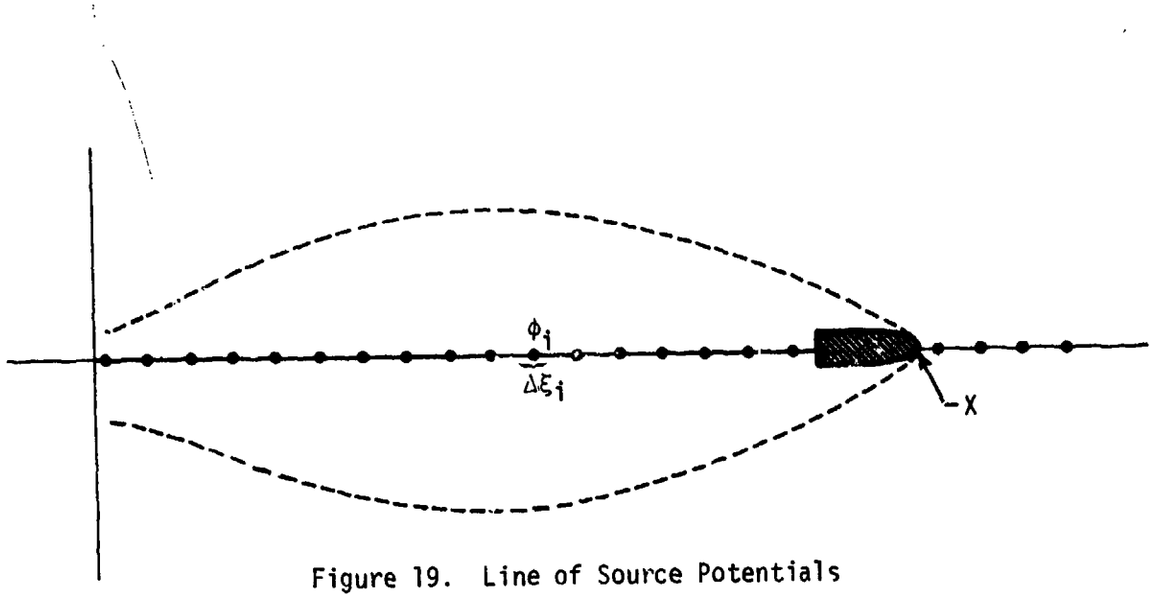

Figure 19. Line of Source Potentials

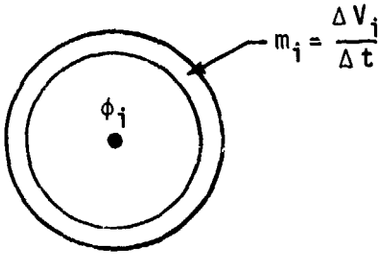

Figure 20. Imaginary Sphere Enclosing a Source

Since all the flow is radial, the velocity potential gradient must be just $\dot{r}$, so that

$$\frac{\partial \phi}{\partial r} = \frac{m}{4\pi r^2} \tag{116}$$

One integration shows that the potential function for the point source of fluid is given as

$$\phi = -\frac{m}{4\pi r} \tag{117}$$

The fluid velocity away from the trajectory of a penetrating bullet can be thought of as due to many sources along the bullet path, each having the above potential. Thus, the potential to solve in Bernoulli's equation is $\phi = \frac{1}{X}\sum \phi_i \Delta \xi_i$; for arbitrarily close sources, it is

$$\phi = -\frac{1}{4\pi X}\int_0^X \frac{m(\xi)}{r}\, d\xi \tag{118}$$

where ξ is a dummy variable of integration along the x axis and X is the interval of projectile travel.

A final simplification is made. Nearly all of the fluid velocity is observed to be radially outward from the trajectory; i.e., all of the

motion is confined to the slice $d\xi$ for each increment of the bullet trajectory. This allows the source strength to be represented by a function $m' = \frac{m}{X}$, which represents the flow rate in each cross section of the trajectory:

$$m' \Delta t = \pi \left[(R + \Delta R)^2 - R^2 \right] \tag{119}$$

In the limit, m' is simplified to

$$m' = 2\pi R \dot{R} \tag{120}$$

Equation 118 is finally reduced to

$$\phi = -\frac{1}{2} \int_0^X \frac{\zeta}{R} d\xi \tag{121}$$

where a source strength function ζ was defined by

$$\zeta = R\dot{R} \tag{122}$$

c. Calculations of dE_f. Yurkovich approximates the cavity behind the passing projectile as a set of expanding spheres, with centers fixed on the projectile path (assume the x axis for simplicity). Then the velocity potential outside this expanding gas sphere is known, and, with reference to Figure 18, the energy of the fluid can be calculated.

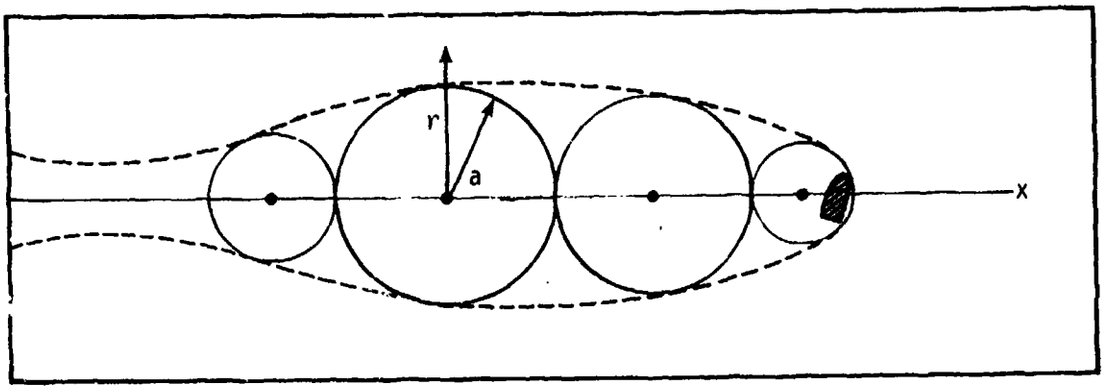

Figure 21. Approximation of the Cavity by a Series of Spheres

The kinetic energy of the fluid due to the expanding bubble follows from

$$E_f = \int_v \frac{\rho_0}{2} (\nabla \phi)^2 \, dv \tag{123}$$

where, for radial flow, the velocity has been replaced by $\nabla\phi$. Lamb (14:46) derives the relationship that

$$\int_v (\nabla \phi)^2 \, dv = -\int_s \phi \frac{\partial \phi}{\partial r} \, ds \tag{124}$$

and also gives the velocity potential (14:122) as

$$\phi = \frac{a^2 \dot{a}}{r} \tag{125}$$

for a bubble with radius a.

It is possible now to evaluate the fluid energy at the bubble surface. At $r = a$: $\left.\frac{\partial \phi}{\partial r}\right|_{r=a} = -\dot{a}$ and $dS = a \sin\theta d\theta d\phi$ Thus

$$\int_s \phi \frac{\partial \phi}{\partial r} dS = \int_0^{2\pi}\int_0^{\pi} (a\dot{a})(-\dot{a})\, a \sin\theta d\theta d\phi \qquad (126)$$

so that

$$E_f\big|_{r=a} = 2\pi\rho_0 a^3 \dot{a}^2 \qquad (127)$$

Noting that the volume of the spherical bubble is $\frac{4\pi a^3}{3}$, Equation 127 can be written as

$$E_f\big|_{r=a} = \tfrac{3}{2}\rho_0 \dot{a}^2 V \qquad (128)$$

Yurkovich assumes that this relationship will hold for volumes of arbitrary shape, i.e., for cylinders of length Δx, thus

$$\Delta E_f = \tfrac{3}{2}\rho_0 \pi (a\dot{a})^2 \Delta x \qquad (129)$$

Now, combining Equations 97, 99, 113, and 129, Yurkovich writes that

$$\Delta E_p = Y\Delta x = \tfrac{3\pi}{2}\rho_0 (a\dot{a})^2 \Delta x + (P_0 - P_c)\pi a^2 \Delta x \qquad (130)$$

where P_c is included here for comparison with Lundstrom's expressions (Yurkovich allowed P_c to be zero).

Lundstrom follows Birkhoff (15:228) in expressing the fluid kinetic energy throughout the cross section dA of the trajectory. The fluid is considered infinite and is bounded only by the cavity radius $a(\xi)$. But since all the flow has been assumed radial, and since it will be necessary to assume only noncompressible fluid, an upper limit of the integration $a\eta$, where $\eta > 1$, is established. Thus, the fluid kinetic energy in the slice dA is given by

$$dE_f = \left[\int_a^{a\eta} \frac{\rho \dot{R}^2}{2} \, dA \right] dx \tag{131}$$

Using $dA = 2\pi a \, da$ and evaluating ζ at the cavity boundary allows $\dot{R}^2 dA$ to be written as $\frac{\zeta^2 da}{a}$. But ζ is proportional to the line source strength, which in turn is constant for each value of $x = \xi$. The integral in Equation 130 can now be evaluated to give

$$dE_f = \pi \rho \, \zeta^2 \, \ln \eta \, dx \tag{132}$$

Lundstrom adds that for η in the 20 to 30 range, correct cavity shapes are predicted; thus, $\ln \eta$ is between 3.0 and 3.4 and can be considered constant.

Having evaluated the kinetic energy in each slice, it is now possible to write the energy transfer rate. Defining Υ as the energy transferred per unit distance, $\Upsilon = \frac{dE_p}{dx}$, gives

$$dE_p = \Upsilon \, dx \tag{133}$$

Then, by combining this with Equations 132 and 98, the energy balance equation can be written in the form

$$dE_p = \Upsilon dx = \pi \rho \zeta^2 \ln \eta \, dx + \left(P_o - P_c\right) \pi a^2 \, dx \tag{134}$$

Yurkovich's simplified approach has yielded a difference equation which compares very well to Lundstrom's differential equation except for the first term on the right. For $\ln \eta$ in the range 3.0 to 3.4, the term $\pi \rho \zeta^2 \ln \eta$ in Equation 134 is more than twice the term $\frac{3\pi}{2} \rho (a\dot{a})^2$ in Equation 130.

d. Additional Results. The energy balance equation serves two purposes. First, it can be rearranged and differentiated to yield expressions for the cavity expansion rate and the maximum cavity radius. Second, in Lundstrom's derivation, the energy balance equation must also yield a suitable form for the source strength function which can be integrated to give the velocity potential. Only the differential equation, Equation 134, will be used in deriving the following expressions though similar expressions could be obtained from the difference equation, Equation 130.

Equation 134 can be solved for ζ^2:

$$\zeta^2 = \frac{P_o - P_c}{\rho \ln \eta}\left[\frac{\gamma}{\pi\,(P_o - P_c)} - a^2\right] \tag{135}$$

Then, with the definitions

$$a_m^2 = \frac{\gamma}{\pi(P_o - P_c)} \tag{136}$$

and

$$\bar{\dot{a}} = \frac{P_o - P_c}{\rho \ln \eta} \tag{137}$$

the source strength function becomes

$$\zeta = \bar{\dot{a}}\sqrt{a_m^2 - a^2} \tag{138}$$

Later, $a_m(\xi)$ will be shown to be the maximum cavity radius at ξ_o, and $\bar{\dot{a}}$ can be thought of as the average cavity expansion rate, though neither term is quite constant since P_c may vary slightly. The negative solution was ignored for Equation 138 because the sources must be positive for cavity expansion; and, cavity collapse cannot be described by the velocity potential given in Equation 121.

At the cavity surface (or for R between a and $a\eta$ for incompressible flow), ζ can be written as $\zeta = a\dot{a}$ from Equation 122. Making this substitution in Equation 133 and rearranging leads to

$$a\dot{a} = \bar{\dot{a}} \sqrt{a_m^2 - a^2} \tag{139}$$

from which the cavity expansion rate can be written as

$$\dot{a} = \bar{\dot{a}} \sqrt{\left(\frac{a_m}{a}\right)^2 - 1} \tag{140}$$

Equation 139 can also be used to derive a relationship for the source strength function ζ which does not depend upon the cavity radius a. Rearrangement and integration of Equation 139 from t_p, the time the bullet arrives at x_p, to t, i.e.,

$$\int_0^a \frac{a}{\sqrt{a_m^2 - a^2}}\, da = \int_{t_p}^{t} \bar{\dot{a}}\, dt \tag{141}$$

yields

$$\sqrt{a_m^2 - a^2} = a_m - \bar{\dot{a}}\,(t - t_p) \tag{142}$$

Thus, the source strength function can be written as

$$\zeta = \bar{\dot{a}} \left[a_m - \bar{\dot{a}} \left(t - t_p \right) \right] \tag{143}$$

Since the maximum cavity radius occurred at $\dot{a} = 0$, it is apparent from Equation 139 that the maximum radius is just a_m. And, from Equation 142 the cavity reaches its first maximum $(a = a_m)$ at time t_m,

$$t_m = t_p + \frac{a_m}{\dot{a}} \tag{144}$$

Rewriting Equation 144 to get

$$a_m = \bar{\dot{a}} \left(t_m - t_p \right) \tag{145}$$

$\bar{\dot{a}}$ is seen to be just the average growth rate of the cavity during the first expansion.

3. PRESSURE DISTRIBUTION

The pressure field generated in a fuel tank by a decelerating projectile is given by Bernoulli's equation (Equation 28) for the irrotational flow of an incompressible fluid with no viscosity. The

derived expression is abbreviated by neglecting external forces, and the constant of integration is determined from the initial static condition to be $F(t)\frac{P_0}{\rho}$. The equation to solve is

$$\frac{P-P_0}{\rho} = -\frac{(\nabla\phi)^2}{2} - \frac{\partial\phi}{\partial t} \tag{146}$$

Both Yurkovich and Lundstrom solve this equation, Lundstrom uses the velocity potential derived above while Yurkovich (3:289) uses

$$\phi = -\frac{a^2\dot{a}}{r} - \frac{v_s}{2}\frac{a^3}{r^2}\cos\theta \tag{147}$$

where θ is the angle between x and r as shown in Figure 22.

In the solution of the pressure distribution, using Equation 147, the term $\nabla\phi$ is given in spherical coordinates by

$$\nabla\phi = \frac{\partial\phi}{\partial r} + \frac{1}{r}\frac{\partial\phi}{\partial\theta} \tag{148}$$

In the earlier derivation the center of the sphere was fixed, but for this portion of the problem the sphere must be allowed to move in the fixed tank. Therefore the term $\frac{\partial\phi}{\partial t}$ must be written as

$$\frac{\partial\phi}{\partial t} = \left(\frac{\partial\phi}{\partial t}\right)_m - v_s\left(\frac{\partial\phi}{\partial x}\right)_t \tag{149}$$

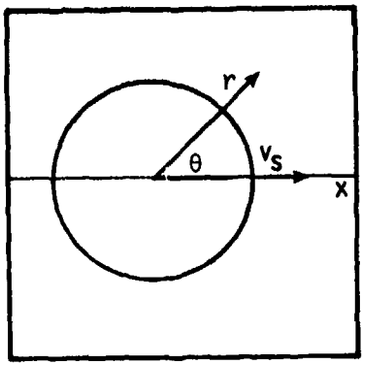

Figure 22. The Angle, θ, for a Sphere with Forward Motion

where m refers to the fixed coordinate system of the tank and v_s is the forward velocity of the sphere. Finally, it is necessary to write $\left(\frac{\partial \phi}{\partial x}\right)_f$ in spherical coordinates:

$$\left(\frac{\partial \phi}{\partial x}\right)_f = \cos \frac{\partial \phi}{\partial r} - \frac{\sin \theta}{r} \frac{\partial \phi}{\partial \theta} \tag{150}$$

The following then is Yurkovich's solution of Bernoulli's equation for an expanding sphere moving horizontally in the fluid and at some distance from the tank walls:

$$\begin{aligned} \frac{P - P_0}{\rho_0} = {} & \frac{1}{r} \frac{d}{dt} \left(a^2 \dot{a}\right) + \frac{1}{2} \left(\frac{a}{r}\right)^2 \cos\theta \left(a \dot{v}_s + 5 v_s \dot{a}\right) \\ & + \left(\frac{a}{r}\right)^3 v_s \left(\cos^2\theta - \frac{1}{2} \sin^2\theta\right) - \left(\frac{a}{r}\right)^4 \frac{\dot{a}^2}{2} \\ & - \left(\frac{a}{r}\right)^5 v_s \dot{a} \cos\theta - \left(\frac{a}{r}\right)^6 \frac{v_s^2}{a} \left(\cos^2\theta + \frac{1}{4} \sin^2\theta\right) \end{aligned} \tag{151}$$

Yurkovich notes that this equation can be used not only for cavity growth, but also for cavity collapse, provided great care is used in choosing the proper parameters for the velocity potential.

Equation 151 can be simplified for two important cases for which $\dot{v}_s$ is small. First, for distances far from the cavity, $\frac{1}{r^3}$ and higher order terms are sufficiently near zero that

$$\frac{P-P_0}{\rho_0} \cong \frac{1}{r}\frac{d}{dt}(a^2\dot{a}) + (\frac{a}{r})^2 \frac{3v_s}{2}\cos\theta \qquad (152)$$

If in addition, there is no forward velocity, $v_s = 0$, and

$$\frac{P-P_0}{\rho_0} \cong \frac{1}{r}\frac{d}{dt}(a^2\dot{a}) \qquad (153)$$

This final condition, lack of forward velocity, is characteristic of cavity collapse.

Lundstrom's solution of Bernoulli's equation is based on the velocity potential derived earlier from a line of sources, rewritten as

$$\phi(x,R,t,) = -\frac{\dot{\tau}}{2}\int_0^{X_p(\tau)} \frac{a_m(\xi)-\dot{\bar{a}}\left[t-\frac{r}{c}-t_b(\xi)\right]}{\sqrt{R^2+(x-\xi)^2}}\,d\xi \qquad (154)$$

where the terms are defined as in Figure 23. The form for the source strength function ζ is taken from Equation 143; $a_m(\xi)$ and $r(\xi)$ are func-

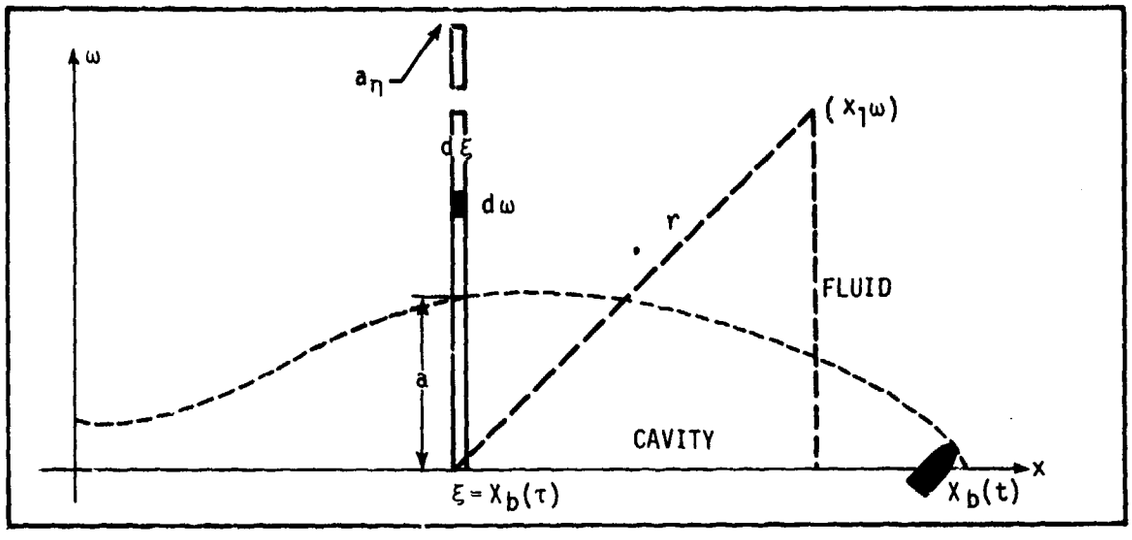

Figure 23. Flow Diagram for the Drag Phase

tions of position along the projectile path; and $X_b(\tau)$ is the position of the projectile at the retarded time $\tau = t - r/c$. The partial derivatives of ϕ can be calculated by using Liebnitz's rule (16:274) which states that if

$$F(r,t) = \int_0^{b(t)} f(\xi,t)\, d\xi \tag{155}$$

then

$$\frac{\partial F}{\partial t} = \int_0^{b(t)} \frac{\partial f}{\partial t}\, d\xi + f(b,t)\, \frac{\partial b(t)}{\partial t} \tag{156}$$

Using Liebnitz's rule on Equation 154 yields

$$\frac{\partial \phi}{\partial t} = -\frac{\bar{a}}{2}\left[\frac{a_p}{R_p}\cdot\frac{\partial X_p(\tau)}{\partial t} - \bar{a}\int_0^{X_p(\tau)}\frac{1}{\sqrt{R^2+(x-\xi)^2}}\,d\xi\right] \quad (157)$$

where $a_p = a_m|_{\xi=X_p}$ and $R_p^2 = R^2+\left[x-X_p(\tau)\right]^2$. The integral in Equation 157 can be evaluated from tables as $\ln\left[\frac{x-R_0}{x-X_p+R_p}\right]$ where R_0 is the distance from the point (x,R) to the impact point. It only remains to find a suitable expression for the term $\frac{\partial X_p}{\partial t}$. Noting that $\frac{\partial X_p}{\partial \tau} = v_p$, the bullet velocity evaluated at X_p, gives

$$\frac{\partial X_p}{\partial t} = v_p\,\frac{\partial \tau}{\partial t} \quad (158)$$

But $\tau = t - r/c$ leads to

$$\frac{\partial \tau}{\partial t} = 1 + \frac{1}{c}\left(\frac{x-x_p}{r}\right)\frac{\partial x_p}{\partial t} \quad (159)$$

Finally, taking $\frac{\partial \tau}{\partial t}\Big|_{x=X_p(\tau)}$ gives

$$\frac{\partial X_p(\tau)}{\partial t} = \frac{v_p}{1-\frac{v_p}{c}\cdot\frac{x-X_p}{R_p}} \quad (160)$$

Then the final form for $\frac{\partial \phi}{\partial t}$ is

$$\frac{\partial \phi}{\partial t} = \Lambda + \frac{(\bar{a})^2}{2} \ln \left(\frac{x - R_0}{x - X_p(\tau) + R_p} \right) \tag{161}$$

where Λ is defined as

$$\Lambda = \frac{\bar{a}}{2} \cdot \frac{a_p}{R_p} \left[\frac{v_p}{\frac{x - X_p(\tau)}{R_p} \cdot \frac{v_p}{c} - 1} \right] \tag{162}$$

The derivatives $\frac{\partial \phi}{\partial x}$ and $\frac{\partial \phi}{\partial R}$ are analogous. The results are:

$$\frac{\partial \phi}{\partial x} = \Lambda \cdot \frac{x - X_p(\tau)}{2 e R_p} + \frac{1}{2} \int_0^{X_p(\tau)} \zeta(\xi) \frac{x - \xi}{r^3} d\xi \tag{163}$$

and

$$\frac{\partial \phi}{\partial R} = \Lambda \cdot \frac{R}{2 c R_p} + \frac{R}{2} \int_0^{X_p(\tau)} \frac{\zeta(\xi)}{r^3} d\xi \tag{164}$$

where ζ is defined as in Equation 143. The integrals cannot be evaluated until the form of ζ is known, and ζ cannot be predicted unless some function is chosen for the tumble of the projectile.

Equations 161, 163, and 164 can be used to rewrite Bernoulli's equation (Equation 146):

$$\frac{P - P_0}{\rho} = -\frac{\partial \phi}{\partial t} - \frac{1}{2}\left[\left(\frac{\partial \phi}{\partial x}\right)^2 + \left(\frac{\partial \phi}{\partial R}\right)^2\right] \qquad (165)$$

4. CAVITY COLLAPSE PRESSURES

Collapse of the cavity is the final phenomenon associated with fluid drag. A 50-cal projectile will exit a one meter tank in less than 2 msec; the formation of the cavity is still taking place at this time, and collapse does not occur until about 30 msec. By the time collapse begins, the cavity normally has a nearly spherical shape and very little forward motion. Thus the fluid particles converge along radial lines to the center of the cavity, compressing whatever vapor might be entrapped. At total collapse, the cavity reaches a minimum volume, and the fluid particle motion is abruptly reversed. A significant pressure pulse is then formed, and a second cavity develops which will be smaller than the first. Higher pressures and extensive damage may well have already occurred due to projectile entrance, exit, fluid shock, and fluid pressures; nevertheless, the pressures associated with cavity collapse are significant.

Williams (9) has measured the pressures at the tank well due to cavity collapse. These tests were for 0.50 cal AP at approximately 0.84 km/sec fired into three foot cubic tanks. Kistler Model 603 acceleration compensated piezoelectric pressure transducers were mounted flush with but isolated from the tank wall. The loading on the tank wall due to the cavity collapse is shown in Figure 24. These results are for the transducer at the center of the tank side wall. The other transducers, located at the same depth and halfway between the center and the edge, normally saw considerably lower pressures. The t = 0 reference for these pulses is the time of cavity collapse, approximately 26 msec after impact. The pulses are separated by about 1.4 to 1.8 msec.

There are two items to note from the information in Figure 24. First, there was no measured pulse from the cavity collapse when reticulated foam was in the tank. Second, the pressure pulse was about 10 bars measured at the wall. It is difficult to compare this pressure to most recorded drag phase pressures since the latter are normally taken near the trajectory. However, Williams also provides data at the wall for these shots. This information shows pulses of shorter duration and lower amplitude and with shapes similar to the pulse shapes typically measured near the center of the tank as shown in Figure 25. The pulses measured had peak pressures of about 4 bars (also at the wall), and pulse widths of about 0.5 msec; thus both in terms of the peak pressure and in terms of impulse per unit area, the cavity collapse pressures are significant.

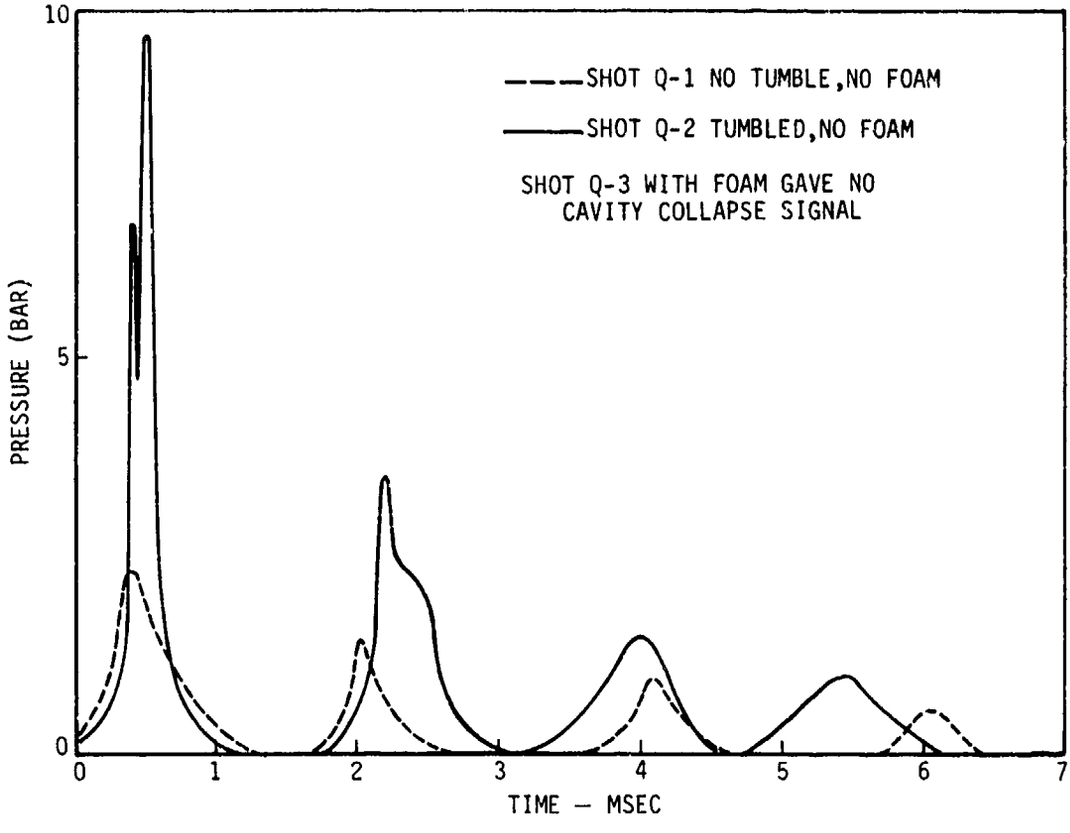

Figure 24. Pressure at Center of Side Wall From Cavity Collapse

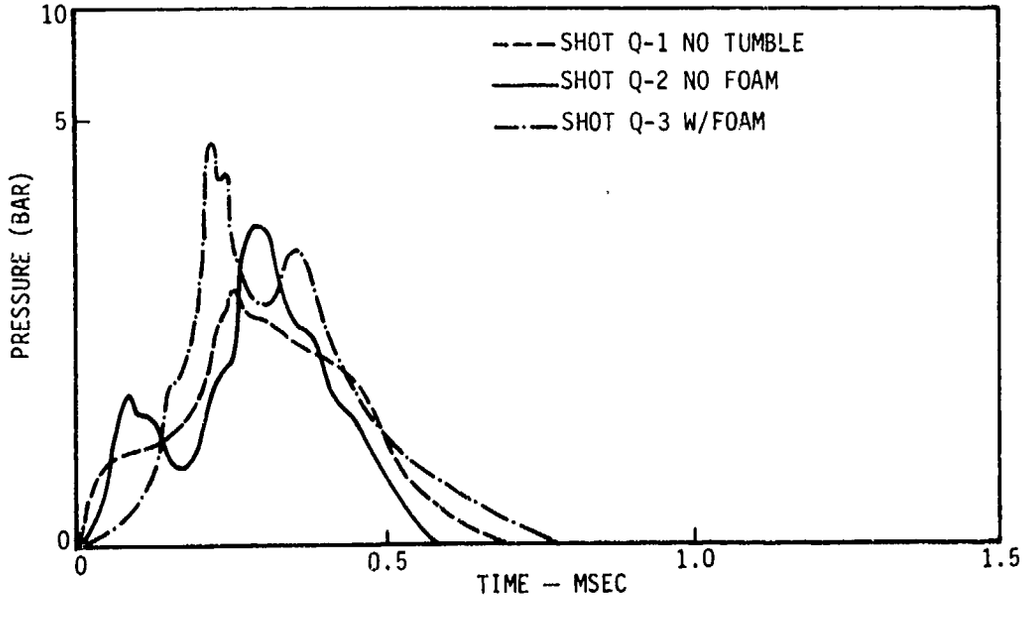

Figure 25. Pressure at Center of Side Wall From Fluid Drag Phase

The analysis of the cavity expansion has been dealt with in some detail and it would be desirable to use these equations for cavity collapse also. However, Lundstrom's model of the cavity is not considered valid for cavity collapse. Though it has not been verified, Yurkovich's model is considered valid for cavity collapse provided care is used in applying the equation. Further, the cavity is observed to become spherical before collapse begins, so that Yurkovich's spherical bubble approach becomes more appropriate here than for cavity formation.

5. DISCUSSION

Two principal relations were discussed in this section. The first was for the transfer of energy from the projectile to the fluid, which required finding the terms in $dE_P = dE_f + dw$. Here, the solution for the term dw presented no difficulty.

The term dE_P, however, was found to depend upon knowledge of both the projectile presented area, $A_P(x)$, and the projectile drag coefficient, $C_D(x)$, where these terms are given as unknown functions of position. The simplification is to fix the presented area at its value at the projectile's maximum radius. Then testing data can be used to infer values to the remaining coefficient of drag function.

A preferred approach would be to observe $A_P(x)$, and then infer from experiment the appropriate values of $C_D(\theta)$, where θ represents the projectile attitude, and so also determines $A_P(\theta)$. The tumbling function, θ, would then vary from test to test. Though more difficult to measure, tumbling functions could then be assumed for analysis to give best, worst, and "average" conditions.

The third term, dE_f, was found by Yurkovich and Lundstrom through very different approaches. Yurkovich integrated the velocity potential for a spherical bubble and made the assumption that the general form of the result would be valid for similar shapes. Lundstrom's solution depends only upon the assumption of an incompressible fluid, and even that assumption is somewhat mitigated by the finite upper limit of integration in Equation 131. Since Lundstrom's result is more than twice as large as Yurkovich's, one of the two should be chosen as preferable. The Lundstrom form is more difficult to obtain, but, on the other hand has been verified by many tests (31) and has the added advantage of being derived from a physically more appealing model.

The second principal relation of this section involves Bernoulli's equation. Once solved, Bernoulli's equation gives the pressure field in the fluid which is used as a basis of predicting tank wall loading and wall rupture due to the fluid drag phase of hydrodynamic ram. In both cases, Bernoulli's equation is solved with recourse to a velocity potential function. Lundstrom's assumption of a line of sources leads to a more complex model for which no results are claimed for cavity collapse but which has been frequently verified for cavity formation (31). Yurkovich's model has not been verified nor compared analytically to Lundstrom's. But, it has the advantage of being simpler, and has the possibility of being used for cavity collapse, especially since the cavity normally becomes spherical before it begins to collapse.

SECTION V

TANK WALL LOADING AND RESPONSE

Two problems need to be discussed in this section. Obviously, the response of the tank wall to the fluid pressures needs to be known, but there are several computer solutions already available which deal with the response of plates and membranes of various shapes to given loadings. What is needed more especially is a model for predicting how the fluid pressures, which are presumed known from the models of the previous section, load the tank walls.

Four approaches to loading or response have been suggested by authors working with hydrodynamic ram. Chou developed an analysis of the shock produced by hypervelocity impact. He uses the Uf yand-Mindlin equations to describe the wall response to fluid shock. Yurkovich did not treat the wall response in detail but instead presented a simplified solution to illustrate the general considerations to be dealt with. Lundstrom and Ball both dealt with wall loading. Lundstrom presents the Kirchoff relation which should correctly predict wall loading but which requires extensive computer time. Ball applies piston theory to the fluid loading of the tank wall. Piston theory is presently the most attractive approach because of its simplicity; none of these solutions have yet been verified.

1. FRONT WALL RESPONSE TO SHOCK

Chou (17, 18) has referenced the analysis of Jahsman (19) and applied those techniques to the observations by Stepka, Morse and Dengler (6) of tank wall fracture due to impact by hypervelocity particles. Chou presents the appropriate form of the Uflyand-Mindlin equations, gives the characteristic equation solution, and applies appropriate boundary conditions for a circular hole in an infinite plate.

Assuming a thin elastic plate with no initial surface tractions and an axisymmetric load, the Uflyand-Mindlin equations can be written in polar coordinates:

$$\frac{\partial M_R}{\partial R} + \frac{(M_R - M_\theta)}{R} - Q_R = \frac{\rho h^3}{12} \frac{\partial^2 \Phi}{\partial t^2} \tag{166}$$

$$\frac{\partial Q_R}{\partial R} + \frac{Q_R}{R} = \rho h \frac{\partial^2 d}{\partial t^2} \tag{167}$$

where

$$M_R = D\left[\frac{\partial \Phi}{\partial R} + \frac{\nu}{R} \Phi\right] \tag{168}$$

$$M_\theta = D\left[\frac{\Phi}{R} + \nu \frac{\partial \Phi}{\partial R}\right] \tag{169}$$

and

$$Q_R = k_2^2 Gh\left[\Phi + \frac{\partial \Phi}{\partial R}\right] \tag{170}$$

Most of the terms in Equations 168 and 169 are represented in Figure 26.

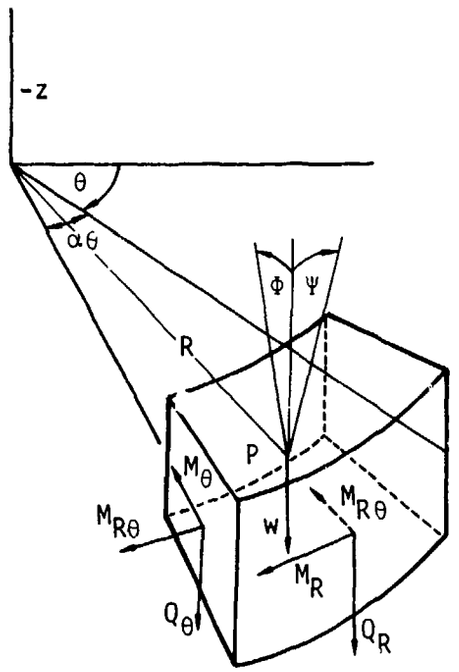

Figure 26. Moments, Shear Stress Resultants, Rotations, and Displacements in a Thin Elastic Plate

The stress moments are radial bending, M_R, tangential bending, M_θ, and twisting, $M_{R\theta}$. The shear stress resultants are transverse, Q_R, and radial, Q_θ; Φ and Ψ are the rotations of the cross section about the tangential and radial axis; w is the transverse displacement of the midplane; and h is the plate thickness. Axisymmetric loading conditions require that $M_{R\theta} = Q_\theta = \frac{\partial}{\partial \theta} = 0$.

The following terms are defined for Equations 168 and 169. The flexural rigidity is given by

$$D = \frac{E h^3}{12(1-\nu^2)} \tag{171}$$

where E is the modulus of elasticity and ν is Poisson's ratio. A shear stress resultant constant, k_2, is introduced to account for warping over the plate cross section. Equations 168 and 169 can be found by integration of Hook's Law of relations.

Chou uses the method of characteristics to solve the Uflyand-Mindlin equations; this method will not be explained here, only the results will be outlined. One reference for the method of characteristics is Karpp (20).

Substitution of Equations 168 and 169 into Equations 166 and 167 yields a system of two hyperbolic second-order equations in Φ and w :

$$\Phi_{RR} - \frac{1}{C_p^2}\Phi_{tt} = \frac{k_2^2 Gh}{D}(\Phi + w_R) + \frac{\Phi}{R^2} - \frac{\Phi_R}{R} \tag{172}$$

$$w_{RR} - \frac{1}{k_2^2 C_2^2} w_{tt} = -\frac{(\Phi + w_R)}{R} - \Phi_R - \frac{F(R,t)}{k_2^2 Gh} \tag{173}$$

where $F(R,t)$ is a known resultant surface traction term, C_p is the plate velocity, and C_2 is the shear wave velocity. C_p and C_2 are defined by

$$C_p^2 = \frac{E}{\rho(1-\nu^2)} \tag{174}$$

$$C_2^2 = \frac{G}{\rho} \tag{175}$$

The four physical characteristics are then given by

$$I^{\pm} : \frac{dR}{dt} = \pm C_p \tag{176}$$

$$II^{\pm} : \frac{dR}{dt} = \pm k_2 C_2 \tag{177}$$

The characteristic equations now follow as

$$I^{\pm} : \mp d\Phi_R + \frac{1}{C_p} d\Phi_t = \mp \left[\frac{k_2^2 Gh}{D} (\Phi + w_R) + \frac{\Phi}{R^2} - \frac{\Phi_R}{R} \right] dR \qquad (178)$$

$$II^{\pm} : dw_R \mp \frac{1}{k_2 C_2} dw_t = -\left[\frac{\Phi + w_R}{R} + \Phi_R + \frac{F(R,t)}{k_2^2 Gh} \right] \qquad (179)$$

where the upper signs refer to I^+ and II^+ and the lower signs to I^- and II^-. Based on continuity, two final equations will be written:

$$d\Phi = \Phi_R dR + \Phi_t dt \qquad (180)$$

$$dw = w_R dR + w_t dt \qquad (181)$$

Equations 178 and 179 now provide six equations in six variables: Φ_R, Φ_t, w_R, w_t, Φ, and w.

To establish initial and boundary conditions, recall that the model is an infinite plate with a circular hole. The radius of the hole is R_o, and the plate is initially at rest with no loads applied. Thus, initial conditions for $R_o \leq R < \infty$ at $t = 0$ are $\Phi_R = \Phi_t = w_R = w_t = 0$. The boundary conditions are $\Phi_R = M_R = 0$ at $R = R_o$.

For additional comments and a discussion of the numerical techniques governing solution of this problem (especially the method of handling the discontinuities in the first derivatives of ϕ and w), the reader is referenced to Chou's works (17, 18).

2. YURKOVICH'S SPRING MASS MODEL

The Yurkovich analysis of the tank wall response (8) is intended to provide insight rather than an accurate model, since a full treatment of the problem is both long and complex. Thus, with admitted simplifications, the problem can be viewed as a pressure loading on a circular section of the tank wall. If the fluid flow and the wall response are all in one direction, the forces can be balanced relatively easily by considering an equivalent spring mass system.

With reference to Figure 27, the force equation can be written,

$$F_f = F_w + F_{\ddot{w}} \tag{182}$$

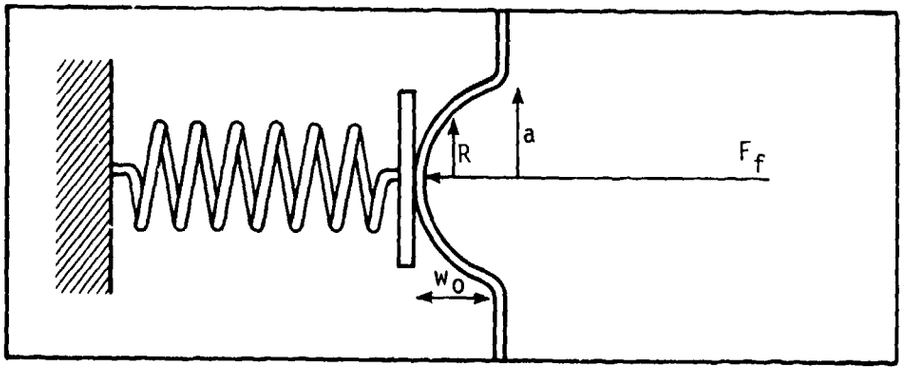

Figure 27. Yurkovich's Wall Response Model

where F_f is the force exerted on the wall by the fluid, and F_w and $F_{\ddot{w}}$ are the forces exerted by the wall; $F_{\ddot{w}}$ is the force due to the kinetic energy of the wall; and F_w is the force on the fluid due to the equivalent spring displacement. Before solving for these forces, Yurkovich assumes the wall is excited to the first mode of plate vibration, and, with reference to Timoshenko (21:452), approximates the wall displacement with

$$w = w_o \left[1 - \left(\frac{R}{a} \right)^2 \right]^2 \tag{183}$$

where w_o is the displacement of the center, a is the radius of the plate portion of the wall, and R is the radial distance.

The force due to the fluid is estimated with an equivalent force, which is considered to act at the center of the plate; the pressure is estimated by

$$P(R,t) = P_{av}(t) \frac{w}{w_o} \tag{184}$$

where $P_{av}(t)$ is the average pressure due to the shock. Then the force on the wall by the fluid is

$$F_f = \int_0^{2\pi} \int_0^a P_{av}(t) \frac{w}{w_o} R dR d\theta = \frac{\pi a^2}{3} P_{av} \tag{185}$$

where Equation 188 was used for the wall displacements.

The force on the system due to a wall displacement of amount w is given by $F_w = k_e w$. The equivalent spring constant k_e , is evaluated by considering the potential energy of a compressed spring, and equating this to the potential energy of a circular wall segment due to bending strain (20:448). The potential energy of the compressed spring is then

$$V = \frac{k_e w^2}{2} = \pi D_P \int_0^a \left\{ \left(w_{rr} + \frac{w_r}{r} \right)^2 - 2(1-\nu) w_{rr} \frac{w_r}{r} \right\} r\,dr \quad (186)$$

where D_P is the flexural rigidity of the plate. To evaluate the integral, Equation 183 is used again for the wall displacement; after taking the necessary derivatives, expanding, and integrating, the potential energy becomes

$$V = \frac{k_e w^2}{2} = \pi D_P \left(\frac{w_o}{a} \right)^2 \frac{32}{3} \quad (187)$$

Thus, for $w = w_o$,

$$k_e = \frac{\pi D_P}{3} \left(\frac{8}{a} \right)^2 \quad (188)$$

and

$$F_w = \frac{\pi D_P}{3} \left(\frac{8}{a} \right)^2 w \quad (189)$$

The force due to the kinetic energy of the wall can be written in terms of an equivalent mass of the plate, $F_{\ddot{w}} = m_e \ddot{w}$ concentrated at the center. The equivalent mass can be found by evaluating the expression for the kinetic energy of the plate

$$K = \frac{m_e \dot{w}^2}{2} = \frac{1}{2} \int_0^{2\pi} \int_0^a \rho h \dot{w}^2 R dR d\theta \tag{190}$$

where ρ, h, and w are the wall density, thickness, and displacement respectively. The wall displacement is again given by Equation 183 so that integration of Equation 190 then gives

$$m_e = 2\pi a^2 \left(\frac{\rho h}{10}\right) \tag{191}$$

and

$$F_{\ddot{w}} = \frac{2\pi \rho h a^2}{10} \ddot{w} \tag{192}$$

Expressions for all the terms of the force equation have now been written: $F(t)$, k_e, and m_e. Writing out the force equation (Equation 182) and rearranging terms gives

$$\ddot{w} + \omega_n^2 w = \frac{P_{av}(t)}{6\left(\frac{\rho h}{10}\right)} \tag{193}$$

where

$$\omega_n^2 = \frac{k_e}{m_e} = \frac{32\, D_p}{3a^4\left(\frac{\rho_h}{10}\right)} \tag{194}$$

is defined to be the natural frequency of the system.

A refinement to Equation 194 is possible. By considering all the fluid within the shock surface to not only exert a force on the wall, but to be accelerated to the same velocities as the wall, an inertial correction can be made to m_e. The mass of the fluid within the hemispherical shock surface is $\frac{2\pi}{3}\rho_f a^3$ giving

$$m_e' = m_e + \frac{2\pi}{3}\rho_f a^2 = 2\pi a^3\left[\frac{\rho_w h}{10} + \frac{\rho_f a}{3}\right] \tag{195}$$

where ρ_w is now the density of tank wall and ρ_f is the fluid density.

Note that the plate radius, a, must coincide with the shock radius, r_s, since more distant portions of the tank wall are unaffected by the shock pressures.

The adjusted force equation now becomes

$$\ddot{w} + (\omega_n')^2 w = \frac{P_{av}(t)}{6\left[\frac{\rho_w h}{10} + \frac{\rho_f a}{3}\right]} \tag{196}$$

and the corresponding natural frequency is

$$(\omega_n')^2 = \frac{32\, D_p}{3a^4\left[\frac{\rho_w h}{10} + \frac{\rho_f a}{3}\right]} \tag{197}$$

Calculations for the wall velocities and displacements require numerical integration of Equation 196. The necessary difference equations are derived by Yurkovich (8:41).

3. WALL LOADING PREDICTED BY THE KIRCHOFF RELATION

Neither Yurkovich's nor Lundstrom's methods of calculating the pressures in the fuel tank account for the pressures due to reflections from the tank walls. These pressures can be significant and should be accounted for before considering wall response, thus Lundstrom presents the Kirchoff relation for calculating the pressures at the tank wall. The pressures at each point within the fluid as well as at the tank wall are given by

$$P(\vec{r}, t) = P_i(\vec{r}, t) + \frac{1}{4\pi}\int_s \frac{1}{r}\left[\frac{\partial_p(\vec{r}', \tau)}{\partial n}\right] dS + \frac{1}{4\pi}\int_s \left[\frac{P(\vec{r}', r)}{r^2} + \frac{1}{rc}\frac{\partial_p(\vec{r}', \tau)}{\partial t}\right]\frac{dr}{dn}\, dS \tag{198}$$

where $\vec{r}$ is a vector from an arbitrary origin to some point where the pressure is to be calculated, $\vec{r}'$ is measured from the same origin to successive points along the tank wall from which reflected disturbances could emanate, and then the source and observation point are separated by $r = |\vec{r} - \vec{r}'|$. Retarded time is given by τ, and n is the outward normal to the tank surface. Equation 197 is valid only for pressure fields which satisfy the wave equation, and only for points of the fluid which are enclosed by surfaces which are concave inward (i.e., no part of the surrounding surface can be bent toward the point). Thus, tank walls with saddle points and reflections from the cavity surface cannot be treated with Equation 198.

To apply Equation 198, $\frac{\partial P}{\partial n}$ must be written in another form. Bernoulli's equation, Equation 28, is somewhat simplified for no external forces and for small velocities (i.e., for the point $\vec{r}$ not near the cavity surface or the bullet):

$$P = -\rho \frac{\partial \phi}{\partial t} \tag{199}$$

The partial derivative of Equation 199 with respect to the outer normal gives

$$\frac{\partial P}{\partial n} = -\rho \frac{\partial}{\partial t} \left(\frac{\partial \phi}{\partial n} \right) \tag{200}$$

Since $\frac{\partial \phi}{\partial n}$ is just the component of ϕ in the n direction, $\vec{u} = \nabla \phi$ leads to $\vec{u} \cdot \hat{n} = u_n = \frac{\partial \phi}{\partial n}$ and thus

$$\frac{\partial P}{\partial n} = - \rho \frac{\partial u_n}{\partial t} \tag{201}$$

Finally, for points which coincide with the wall surface, all the pressure components are doubled, and Lundstrom concludes

$$P(\vec{r}, t) = 2P_i(\vec{r}, t) - \frac{\rho}{2\pi} \int_s \frac{1}{r} \left[\frac{\partial u_n(\vec{r}', \tau)}{\partial t} \right] dS + \frac{1}{2\pi} \int_s \left[\frac{P(\vec{r}', \tau)}{r^2} + \frac{1}{rc} \frac{\partial P(\vec{r}', \tau)}{\partial t} \right] \frac{dr}{dn} dS \tag{202}$$

Lundstrom anticipates that a numerical solution of Equation 202 will be accurate, but large computer storage and long running times have discouraged its use.

4. BALL'S APPLICATION OF PISTON THEORY

A final method of solving the problem of waves reflected from tank walls is the use of piston theory as advanced by Ball (23). The assumption is made that the elements of the wall can be treated as elements of area A and mass m attached to springs of spring constant k as in Figure 28. Then the total force AP(t) acting on the wall due to the fluid

pressures is just that which contributes to wall acceleration $m\ddot{w}$, and that which contributes to the displacement of the spring kw. Thus, the statement of the idealized one-dimensional model is given by

$$m\ddot{w} + kw = AP(t) \tag{203}$$

Additionally, the incident pressure is modeled by a step pressure pulse beginning at time zero, as also shown in Figure 28. The pressure at the wall is the sum of the incident step pressure and the reflected pressure, $P(t) = P_i + P_r(t)$, where the reflected pressure depends on the

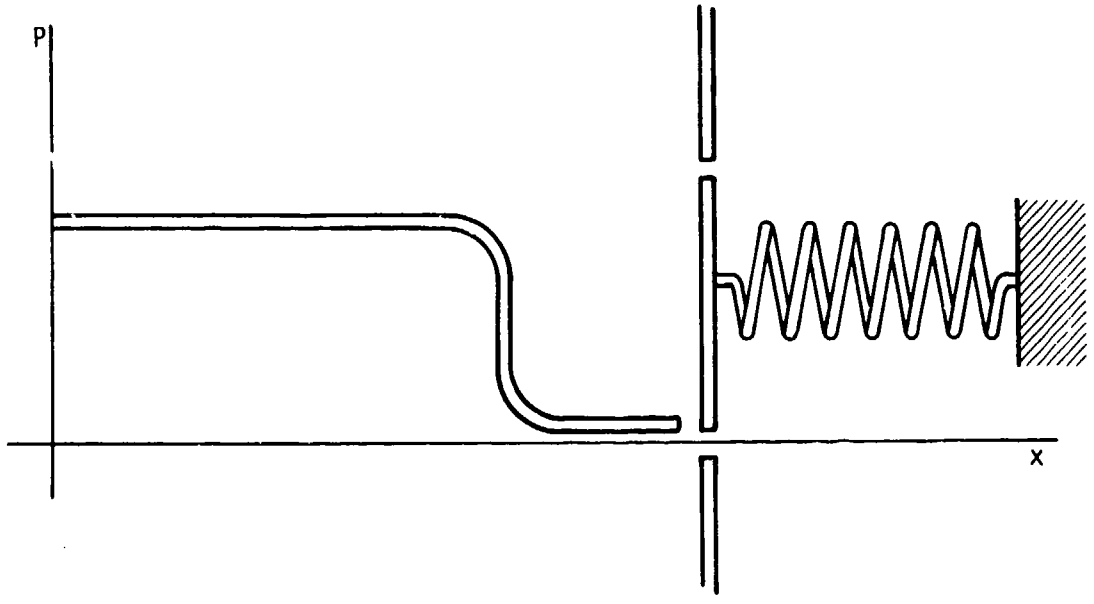

Figure 28. Ball Wall Response Model

wall motion and can be negative. The incident pressure is constant, and the reflected pressure is approximated from the simplified form of Bernoulli's equation, $P(t)=P_i+P_r(t)$, where the subscript r refers to the reflected wave. The pressure function is

$$P(t) = P_i - \rho\dot{\phi}_r(t) \tag{204}$$

The basic pressure equation for piston theory is just Equation 204 with the term $\dot{\phi}_r(t)$ rewritten in terms of the fluid and wall velocities. To find this form for $\dot{\phi}_r$, recall that ϕ satisfies the wave equation, Equation 25, repeated here for convenience:

$$c^2 \nabla^2 \phi = \ddot{\phi} \tag{205}$$

The solution of the wave equation in exponential form is given by

$$\phi = \phi_i + \phi_r = \alpha e^{i\lambda(x - ct)} + \beta e^{i\lambda(x + ct)} \tag{206}$$

where α and β are arbitrary constants, and λ is a scalar constant for the wave. It follows from differentiation of Equation 206 that

$$u_i = \frac{\partial \phi_i}{\partial u} = -\frac{1}{c}\dot{\phi}_i \tag{207}$$

and

$$u_r = \frac{\partial \phi_r}{\partial x} = \frac{1}{c} \dot{\phi}_r \tag{208}$$

The incident and reflected pressures can now be written from the simplified form of Bernoulli's equation and Equations 207 and 208:

$$P_i = \rho c u_i \tag{209}$$

and

$$P_r = -\rho c u_r \tag{210}$$

Finally, neglecting cavitation, the wall velocity must equal the fluid velocity at the wall

$$\dot{w} = u = u_i + u_r \tag{211}$$

By combining Equations 207 and 208 with the above condition, the pressure function can be put in the form

$$P(t) = P_i + \rho c \left(u_i - \dot{w} \right) \tag{212}$$

The pressure function can be written in the final form by consideration of Equations 208 and 209 as

$$P(t) = 2P_i - \rho c \dot{w} \tag{213}$$

The force equation can now be solved. Using this last form of the pressure in Equation 203 gives

$$\ddot{w} + 2\zeta \dot{w} + \omega^2 w = \gamma \tag{214}$$

where the following terms were defined:

$$\zeta = \frac{\zeta c A}{2m} \tag{215}$$

$$\omega^2 = \frac{k}{m} \tag{216}$$

$$\gamma = \frac{2AP_i}{m} \tag{217}$$

The solution of Equation 214 is obtained in Appendix D as

$$w = \frac{\gamma}{\omega^2}\left[1 + \frac{1}{2\zeta^*}\left(\alpha^- w_1 - \alpha^+ w_2\right)\right] \tag{218}$$

where the following terms are defined

$$\zeta^* = \sqrt{\zeta^2 - \omega^2} \tag{219}$$

$$\alpha^+ = -\zeta + \zeta^* \tag{220}$$

$$\alpha^- = -\zeta - \zeta^* \tag{221}$$

$$w_1 = e^{\alpha^+ t} \tag{222}$$

$$w_2 = e^{\alpha^- t} \tag{223}$$

It follows that

$$\dot{w} = \frac{\gamma}{2\zeta^*} (w_1 - w_2) \tag{224}$$

and thus

$$P(1) = 2P_i \left[1 - \frac{\zeta}{\zeta^*} (w_1 - w_2) \right] \tag{225}$$

The only variable in Equation 225 is time, and most of the parameters are known; the spring constant is a parameter which must be estimated. Rather than approximate the spring constant itself, Ball estimates

the frequency of the wall (k/m) from the lowest natural frequency of a square plate (21:441) with width a and thickness h given by

$$\omega_{n\ell} = \frac{2\pi^2 h}{a^2}\sqrt{\frac{E}{12(1-\nu^2)\rho}} \tag{226}$$

where E is Young's modulus and ν is Poisson's ratio. The incident pressure P_i is also an unknown constant, but rather than stipulate values it is more convenient to consider the ratio $\frac{P(t)}{2P_i}$.

Equation 225 is plotted in Figure 29 for an aluminum wall 2.5 mm thick for ω = 100, 200, 500, and 1000. The problem divides naturally into two parts, for early times (less than 10^{-4} sec) and for later times (greater than 10^{-4} sec).

After approximating the parameters to be encountered in hydraulic ram problems, two forms of the solution will be found: the first form will be valid for early times (less than 10^{-4} sec), the second form will be valid for later times (greater than 10^{-4} sec).

For this problem, a typical value of ζ is computed to be 7.7×10^4 sec^{-1} (This number is based on densities of 785 kg/m^3 for JP-4, 2770 kg/m^3 for aluminum, and a sound velocity of 1360 m/sec in the fuel.) From Equation 226, the lowest natural frequencies of two half-inch plates, 10 and 20 inches square, are found to be 600 and 150 rad/sec, respectively. Thus, the natural frequencies for this problem can be assumed to be less than 1000 rad/sec and ζ^* can be expanded as

$$\sqrt{\zeta^2-\omega^2} \cong \zeta - \frac{\omega^2}{2\zeta} - \frac{\omega^4}{\gamma\zeta^3} - \cdots \tag{227}$$

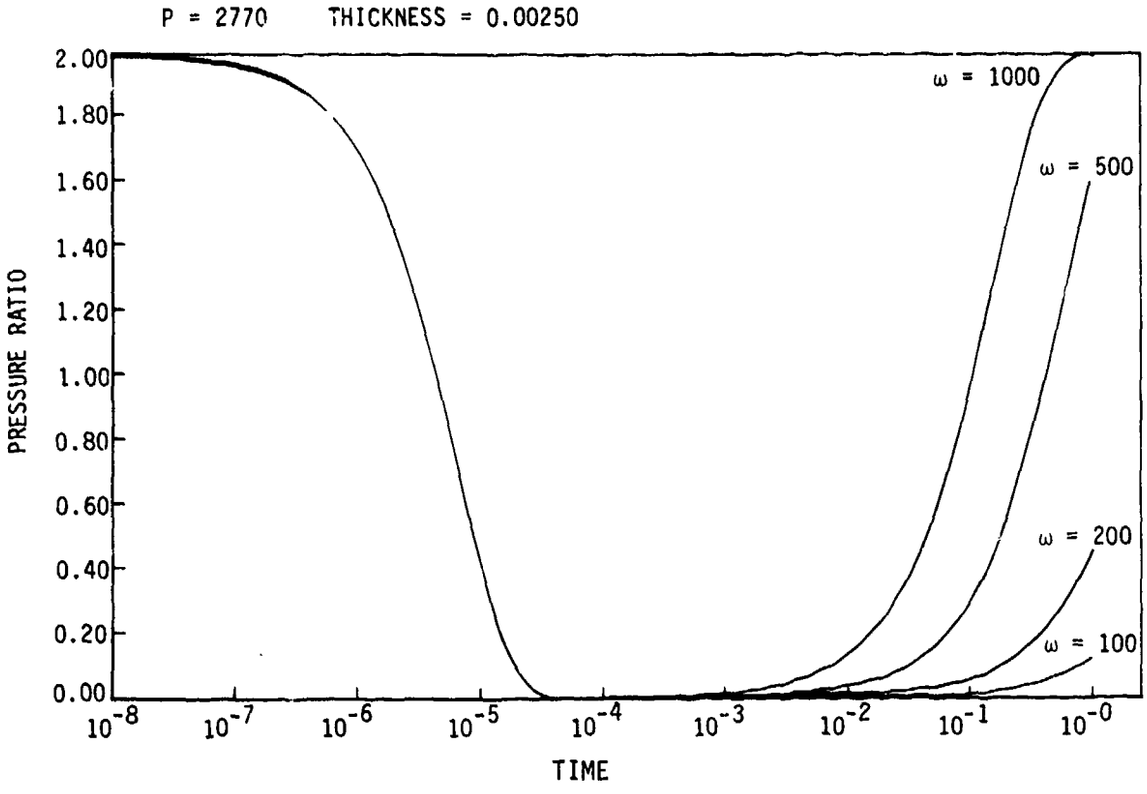

Figure 29. Piston Theory Prediction for Pressure Ratio, $P(t)/P_i$, at the Tank Wall

This expansion allows Equation 218 and Equations 224 and 225 to be rewritten as:

$$w = \frac{\gamma}{\omega^2}\left[1-\left(\frac{\omega^2}{4\zeta^2}+1\right)e^{-\frac{\omega^2}{2\zeta}t}+\frac{\omega^2}{4\zeta^2}e^{\left(-2\zeta+\frac{\omega^2}{2\zeta}\right)t}\right] \qquad (228)$$

$$\dot{w} = \frac{\gamma}{2\zeta}\left[e^{-\frac{\omega^2}{2\zeta}t}-e^{\left(-2\zeta+\frac{\omega^2}{2\zeta}\right)t}\right] \qquad (229)$$

$$\frac{P(t)}{2P_i} = 1-e^{-\frac{\omega^2}{2\zeta}t}+e^{\left(-2\zeta+\frac{\omega^2}{2\zeta}t\right)} \qquad (230)$$

For the case where $w^2/2\zeta$ is less than 100 sec^{-1}, two time regimes become apparent in Equation 230 and lead to two approximations:

For $0 < t < 10^{-4}$,

$$\frac{P(t)}{2P_i} \cong e^{-2\zeta t} \tag{231}$$

and for $10^{-4} < t$,

$$\frac{P(t)}{2P_i} \cong 1 - e^{-\frac{\omega^2}{2\zeta} t} \tag{232}$$

These equations represent inertial and elastic effects, respectively. For $w^2/2\zeta = 100$, the effects are separated by about 1 msec.

Since the elastic response is noted to occur relatively late in the process, Ball next questions the possibility of treating the fluid pressure pulse on the wall as an impulsive load. For an impulsive load, the incident pressure of infinite duration is replaced by an incident pressure pulse which acts for time t_p. For t greater than t_p, the term P_i in Equation 217 becomes zero; thus, the solution must satisfy two equations: For $0 < t \leq t_p$,

$$\ddot{w} + 2\zeta \dot{w} + \omega^2 w = \gamma \tag{233}$$

and for $t_p < t$,

$$\ddot{w} + 2\zeta \dot{w} + \omega^2 w = 0 \tag{234}$$

Assuming a solution of the form $w = e^{\alpha t}$, and using the same notation as before,

$$w = c_1 e^{\alpha^+ t} + c_2 e^{\alpha^- t} \tag{235}$$

and

$$\dot{w} = c_1 \alpha^+ e^{\alpha^+ t} + c_2 \alpha^- e^{\alpha^- t} \tag{236}$$

Since the functions $w(t)$ and $\dot{w}(t)$ are known at $t = t_p$ from the previous solution, the constants c_1 and c_2 can be evaluated by a simultaneous solution of Equations 235 and 236:

$$c_1 = \left[w(t_p) \left(\frac{-\alpha^-}{2\zeta^*} \right) + \dot{w}(t_p) \frac{1}{2\zeta^*} \right] e^{-\alpha^+ t_p} \tag{237}$$

and

$$C_2 = \left[w(t_p)\left(\frac{\alpha^+}{2\zeta^*}\right) - \dot{w}(t_p)\frac{1}{2\zeta^*}\right] e^{-\alpha^- t_p} \tag{238}$$

Then, for $\zeta >> \omega$, the following assumptions are justified: $\zeta^* \cong \zeta$, $\alpha^+ \cong -\frac{w^2}{2\zeta}$, and $\alpha^- \cong 2\zeta + \frac{w^2}{2\zeta}$. With these substitutions, approximate values of the constants c_1 and c_2 can be used to write the solution of Equation 235, as follows:

$$\begin{aligned} w(t) \cong & \left[w(t_p)\left(1 + \frac{\omega^2}{4\zeta^2}\right) + \dot{w}(t_p)\frac{1}{2\zeta}\right] e^{-\frac{\omega^2}{2\zeta}(t - t_p)} \\ & - \left[w(t_p)\left(\frac{\omega}{2\zeta}\right)^2 + \dot{w}(t_p)\frac{1}{2\zeta}\right] e^{\left(-2\zeta + \frac{\omega^2}{2\zeta}\right)(t - t_p)} \end{aligned} \tag{239}$$

Finally, to describe an impulsive load, the finite pressure pulse is taken to be large enough and of short enough duration that the wall can be considered to have remained stationary ($w(t_p) = 0$) while receiving an initial velocity ($\dot{w}(t_p) = \gamma t_p$). It can be seen from Equation 217 that γ is a measure of the acceleration of the wall from the incident

pressure. Substitution of these values for w and $\dot{w}$ into Equation 239 gives the wall displacement due to impulsive loading.

$$w(t)_{imp} = \frac{\gamma t_p}{2\zeta}\left[e^{-\frac{\omega^2}{2\zeta}(t-t_p)} - e^{\left(-2\zeta+\frac{\omega^2}{2\zeta}\right)(t-t_p)}\right] \qquad (240)$$

To determine the accuracy of the impulse load assumption, the values of $w(t_p)$ and $\dot{w}(t_p)$ are obtained from Equations 228 and 229 and substituted into Equation 239. After making these substitutions and simplifying the results for the conditions that 1) $\frac{\omega^2}{2\zeta} \cong 0$ and 2) t_p is small enough to approximate $e^{-\frac{\omega^2}{2\zeta}t_p}$ with $1-\frac{\omega^2}{2\zeta}t_p$, the first two terms of the expansion, then

$$w(t)\Big|_{t\geq t_p} \cong \frac{\gamma t_p}{2\zeta}\left[e^{-\frac{\omega^2}{2\zeta}(t-t_p)} + \right.$$

$$\left. \frac{\omega^2}{4\zeta^2} e^{-2\zeta t_p} e^{\left(-2\zeta+\frac{\omega^2}{2\zeta}\right)(t-t_p)}\right] \qquad (241)$$

The first term is a long time response, and the second term is a short time response. Comparison of Equation 241 to 240 shows that the impulse assumption correctly predicts the long time response, but not the short time response.

5. DISCUSSION

Learning the response of the tank wall is one of the most important end products of hydrodynamic ram studies. It is also the most difficult, especially when realistic fuel tank geometries are of interest. Chou's approach, using the method of characteristics, seems particularly appropriate for the shock effects. This is because the shocks are very localized, and tank geometries become less important the farther the observer moves from the impact point.

All of the other analyses were concerned with the loading of the wall to fluid pressures. The complexities of the problem become apparent in reviewing these analyses. The wall is loaded not only by the pressure field created by the slowing projectile, but also by reflected pressure from other surfaces as well as the wall's own motion. Once the loading on the wall is known, this information can be analyzed by several available wall response computer programs to estimate damage. The Kirchoff relation can be used to compute the wall loading once the pressure field is known, but it is a lengthy process and, so, of questionable practical value. Piston theory effectively isolates the variables (Equation 228) so that with only the incident pressure field known, the total pressure at the wall can be calculated, and wall response can be computed.

There is an added necessity for isolating the variables as piston theory does. In measuring pressures due to fluid drag on the projectile, the pressure field at the wall-fluid boundary is rather difficult

to obtain. On the other hand, the pressures in an infinite fluid (one where the tank walls are sufficiently distant that there are no reflections) are measured routinely and with comparative ease.

The flow of information necessary to obtain damage estimates is indicated in a very general manner in the following figure.

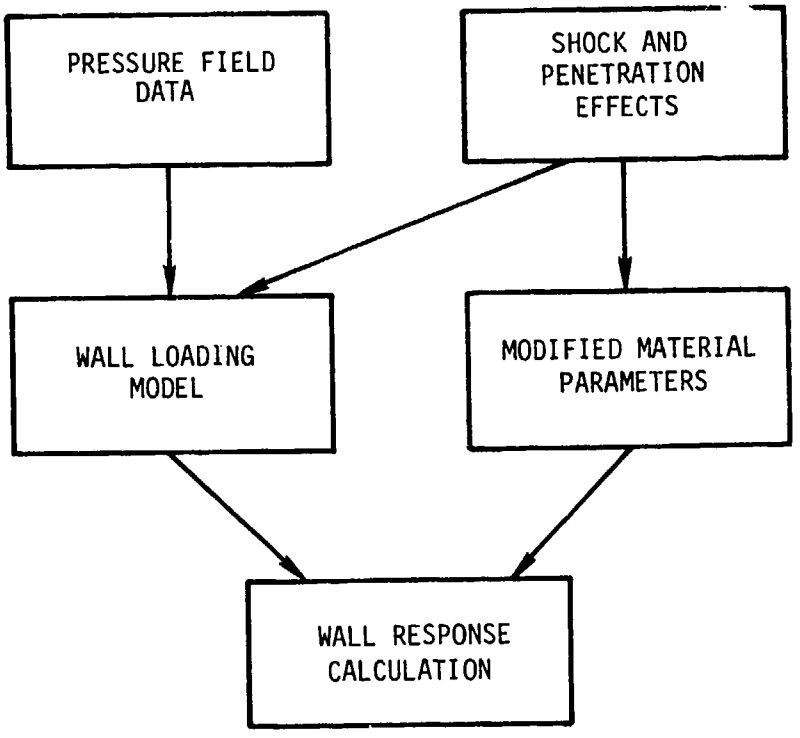

Figure 30. Information Flow for Predicting Wall Response Due to Hydrodynamic Ram

SECTION VI

DAMAGE REDUCTION

The final goal for hydrodynamic ram studies is to develop ways to eliminate the extensive fracture that occurs immediately after impact by a projectile. If the damage could be contained to a mere hole in the entrance and exit walls, that level of damage would be considered acceptable and the fuel loss would be minimal. Four methods to reduce hydrodynamic ram damage have been tested, but only one method, foam-backed walls, has shown much promise. Additionally, there are three analysis techniques that can be applied to the latter.

1. DAMAGE REDUCTION TECHNIQUES

Two reports treat damage reduction methods in detail; the first, by Stepka and Morse (25), deals with ways to minimize damage to spacecraft fuel tanks through fuel pressure attenuation. Bristow and Lundberg (26) consider the specific problem of bullets impacting aircraft fuel tanks. Damage reduction is also discussed in several other reports and has been the subject of, or included in, several testing programs.

In most damage reduction techniques, the goal is to absorb the fluid energy before it can damage the tank walls - reasoning that to minimize damage, the shock or high pressure pulse must be spread out over time or space or both. The suggested methods include adding substances to the fuel to retard the propagation of the wave, and adding shock absorbing material to the inside of the tank wall.

An entirely different approach was taken by Bristow and Lundberg (26). They tested a viscoelastic additive to the fuel whose viscosity increases with increasing strain rate. The high pressure regions generated by the projectile were expected to generate a highly viscous region and thus increase the drag on the projectile.

To test this concept, 0.50-cal projectiles were fired into a tank containing a mixture of fuel and up to 1% viscoelastic additive. Unfortunately, there was no measurable change in the hydrodynamic ram parameters; projectile characteristics, fluid drag, and pressure pulses remained the same. Thus, the addition of a viscoelastic substance to the fluid in this manner has not affected the hydrodynamic ram damage mechanism.

As an addition to this testing program, Bristow and Lundberg added ordinary whiffle balls to the fuel to see if they had any retarding effect on the pressure pulse. But again, there was no measurable change in the hydrodynamic ram characteristics.

A second ram attenuation technique is to absorb the fluid energy before it impacts the tank wall by the addition of a gas to the fuel. Williams (9) recommended that nitrogen be bubbled through the fuel. Clark (27) later investigated the attenuation properties of air entrapped in water by foam and found significant pressure reduction; in addition he noted that the ram attenuation properties of freon should be superior to air. There are two advantages to using the gas: (1) the bubbles are not needed until the aircraft is near the target,

so that the generators need not be turned on for most of the mission and need not even be provided for all the tanks, (2) inerting of the ullage is an advantageous byproduct; both freon and nitrogen are inert and, further, nitrogen will scrub the oxygen from the fuel. Williams has recommended that the volume of the gas be about 6% N, which is difficult to attain with available generators.

The most promising method to reduce the fracture at the entrance and exit walls is to back the tank wall panels with a foam which isolates the fluid from the wall. Stepka and Morse (25) studied this technique for application to spacecraft fuel tanks, and more recently this same concept was tested for use in aircraft fuel tanks (28).

A typical foam-backed panel is just an ordinary tank wall backed with an easily compressible material such as polyurethane foam. Typical configurations for test purposes are illustrated in Figure 31. The plastic sheet between the foam and the fluid allows the easily compressible material to isolate the tank wall to some extent from the fluid shock pulses. Several materials besides the polyurethane foam have been tested, including air, rigid foams, and honeycomb materials.

Stepka and Morse conducted several tests using different hypervelocity projectiles against several target configurations. Appropriate parts of those tests have been extracted and reproduced in

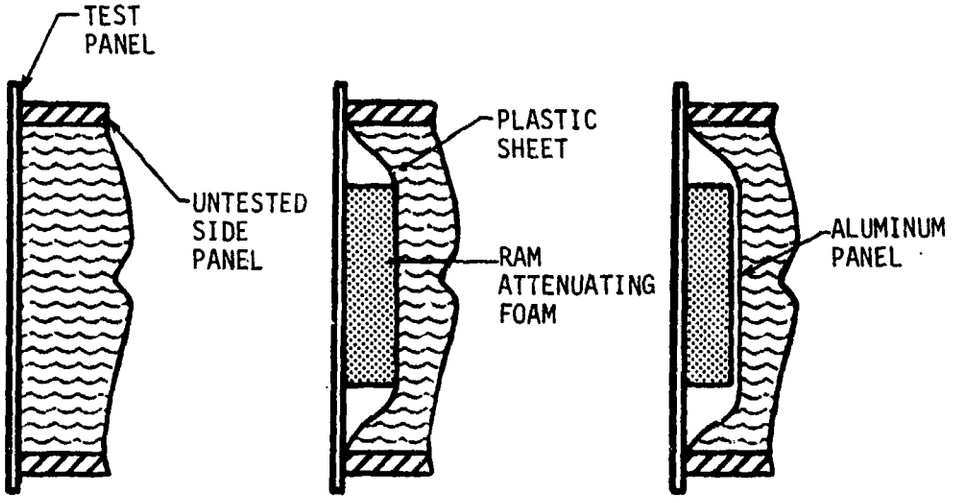

Figure 31. Test Configurations for Ram Attenuating Foams

Table I. These results indicate that both foam and honeycomb materials provide significant protection of the fuel tank wall from hypervelocity impact. This moderate success implies that some method of isolating the fuel from the tank wall can at least reduce the degree of fracturing, even for ordnance impact into fuel tanks.

Dynamic Science (28) conducted tests of the same attenuation concept using 14.5 mm API-T against a representative integral fuel tank. Information was obtained from two vertical panels and from the bottom panel for a test configuration similar to B of Figure 31, except that the panels were reinforced with Z-stiffeners. Both flexible and rigid foams were tested. A cursory examination of the damage data from this program, summarized in Table II, indicates that a shock absorbing material can significantly reduce the damage to the front wall, but that

TABLE I

FRACTURE AND PUNCTURE DATA FOR SOME RAM ATTENUATING FOAMS FROM HYPERVELOCITY IMPACT

A1 - basic	B1 - air	C1 - 3/4 in. open or closed cell polyurethane foam
A2 - double wall	B2 - fibrous matting	
	B3 - foam rubber	D2 - 1 in. honeycomb
	B4 - 1/2 in. open cell polyurethane foam	
	B5 - 3/8 or 3/4 in. closed cell polyurethane foam	
	B6 - 1 in. honeycomb	

Projectile: Nylon cylinder (5.56 mm length and diameter)

configuration	velocity (km/sec)	fracture (f) or puncture (p)
A1	4.95, 6.01, 6.43, 6.46	f, f, f, f
A2	5.48, 5.73	f, f
B1	5.94	f
B2	5.88, 6.14	f
B3	6.28	p
B4	5.63, 5.69, 5.82, 6.09	p, f, p, p with small cracks and/or deformation
B5 (3/8)	6.00, 6.09	f, f
B5 (3/4)	5.63, 5.78, 5.87, 5.97	p, p, p, p
B6	5.87, 5.94	p, p
C1	5.94, 5.97	p, p
C2	5.48, 5.82, 5.94	p, p, f

TABLE II

DAMAGE SUMMARY FOR A TANK IMPACTED BY 14.5 API-T

Projectile: Soviet 14.5 mm API-T, velocity range 997 to 1050 m/sec

Tank Dimensions. 3 ft x 3 ft with either a 1 ft or 2 ft shotline

Test Panels: 18 in. x 18 in. with 4 Z-stiffeners, each stiffener had 18 rivets

1 ft shotline			2 ft shotline			
impact vel. (km/sec)	panel damage[1] (rivets remaining)[2] entrance	exit	impact vel. (km/sec)	panel damage[1] (rivets remaining)[2] entrance	exit	bottom[3]
		A baseline				
1030	mod(26)*	des(13)*	1043	sev(27)*	sev(15)*	(67)*
		B1 1.5 in. flexible foam				
1024	min(15)*	des(0)*	1034	min(17)*	sev(8)*	(34)*
1027	min(19)*	des(0)*	-	min(14)*	sev(16)*	(8)*
1029	min(30)*	des(8)*	-	sev(19)	sev(19)*	(10)*
		B2 1.5 in. rigid foam over 1.5 in flexible foam				
1017	min(37)	sev(12)*	-	min(28)*	sev(17)*	(10)(2)
997	min(40)	sev(6)*	1028	min(19)*	ext(20)*	(23)(1)
1026	min(13)*	sev(13)*	-	min(18)*	ext(22)*	(23)
		B3 3 in. flexible foam				
1050	min(31)*	sev(13)*	1043	min(23)*	mod(56)	(10)*
1041	min(17)	des(10)*	-	min(18)*	mod(10)	(21)*
1038	min(25)(2)	sev(11)*	1041	min(21)*	mod(20)*	(19)
		B4 3 in. rigid foam				
1023	mod(40)	sev(14)*	1026	min(32)*	ext(45)	(40)
1024	min(30)	des(6)*	1023	min(23)*	sev(21)*	(70)
1026	min(55)*	sev(20)*	-	min(29)*	mod(20)*	(71)

1 min = minor damage - projectile silhouette
mod = moderate damage - cracks
ext = extensive damage - large cracks, some rupture, 80% of panel gone
sev = severe damage - large ruptured area
des = destroyed panel

2 * = all rivets failed
(N) = N is the number of rivets that remained in the panel

this same material may have no marked effect on protecting the rear wall. It must be added that, most frequently, combat inflicted damage is from an impact into the bottom of the tank, and that a flexible foam then will already be compressed to some extent due to the weight of the fuel, thus reducing its ability to absorb shocks.

2. DAMAGE REDUCTION ANALYSIS

There are three analyses of compressible foams available. Stepka and Morse (25) used an analysis based on shock Hugoniot curves to approximate the maximum pressures at the interfaces of the different materials, but that analysis does not account for the thickness of the materials. Torvik (29) has suggested an analysis based on the "snowplow" effect which will approximate the reduction of the pressure as the pulse traverses a distance of foam. Williams (9) gives a calculation for the minimum thickness of foam based on the time required for the rarefaction wave to overtake the shock front.

a. Shock Hugoniot Analysis. A minimum amount of information about shock Hugoniots is presented here to aid in using this analysis method. For further information the reader is referred to the literature, especially Duvall (30) and Cole (3).

For this shock analysis, the effects of the projectile and the hole it creates are ignored. The shock pulse is assumed to be created in the fluid through a nearly instantaneous deposition of energy by the projectile. This analysis considers only the maximum pressures impacting

at the fluid-foam boundary as described by a one-dimensional model. Boundary conditions determine the state of the shock which can exist at the boundary, and hence the shock which can initially be transmitted through the foam. The shock can be described similarly at the foam-tank wall boundary.

The set of states that can exist at the material interfaces is described by shock Hugoniot curves. These curves represent the locus of all states of a material that can be reached from given initial conditions. In a fluid, the Hugoniot is a plot of the pressures against particle velocities; in a metal, the pressure is replaced by the stress normal to the shock front. The information necessary to generate the Hugoniot must be obtained from experiment, but at the same time this data allows the development of an equation of state from which the Hugoniot can later be extracted.

When a shock wave reaches a boundary, part of it is transmitted, and part is reflected. The transmitted wave will also be a shock, but the reflected wave may not be. The reflected wave may be a compressive wave or a rarefaction wave depending on whether its pressure is higher or lower than the incident wave. If it has a higher pressure, it is compressive, and may be a shock. The Hugoniot curve in Figure 32 may then be reflected about the vertical axis and its intersection with the $P = 0$ axis adjusted to describe the states available to the reflected wave, **I** . If the reflected wave is a rarefaction wave, the reflection

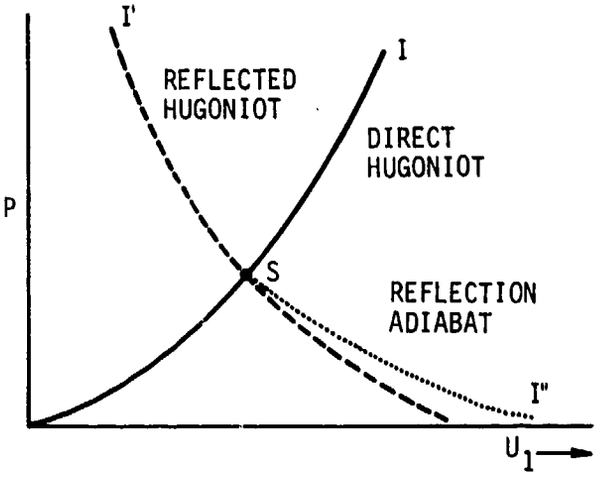

Figure 32. Direct Hugoniot, Reflected Hugoniot, and Reflection Adiabat

adiabat must be used but, in practice, this curve is nearly identical to the continuation of the reflected Hugoniot, and so the reflected Hugoniot is used exclusively.

The intersection of the reflected Hugoniot with the particle velocity axis is the particle velocity U_P. For the shock wave transmitted to the fluid from the projectile, U_P is taken to be the velocity of the projectile immediately after it has penetrated the tank wall. For thin walls, the velocity may be taken as the impact velocity. After locating the intersection point on the particle velocity axis, the reflected and direct Hugoniots will intersect at some state **S**, which describes the only values of fluid pressure and fluid particle velocity the curves can

share. This is illustrated in Figure 33. The Hugoniots of additional materials can then be added, and a final estimate of the expected maximum pressures can be made.

Figure 34 illustrates how the maximum expected pressures at the fuel tank wall are determined graphically for layers of different materials.

b. "Snowplow" Analysis. Following the works of Hermann (31) and Salvadori, et al (32), Torvik (29) has described the application of "snowplow" model to the attenuation of shock waves in porous materials. This model predicts the decay of the peak pressure with the square of the distance the shock wave has penetrated.

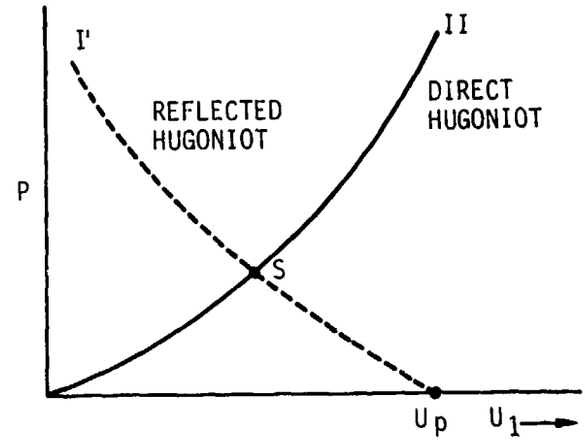

Figure 33. Identification of Boundary and Initial Conditions Using the Direct and Reflected Hugoniot

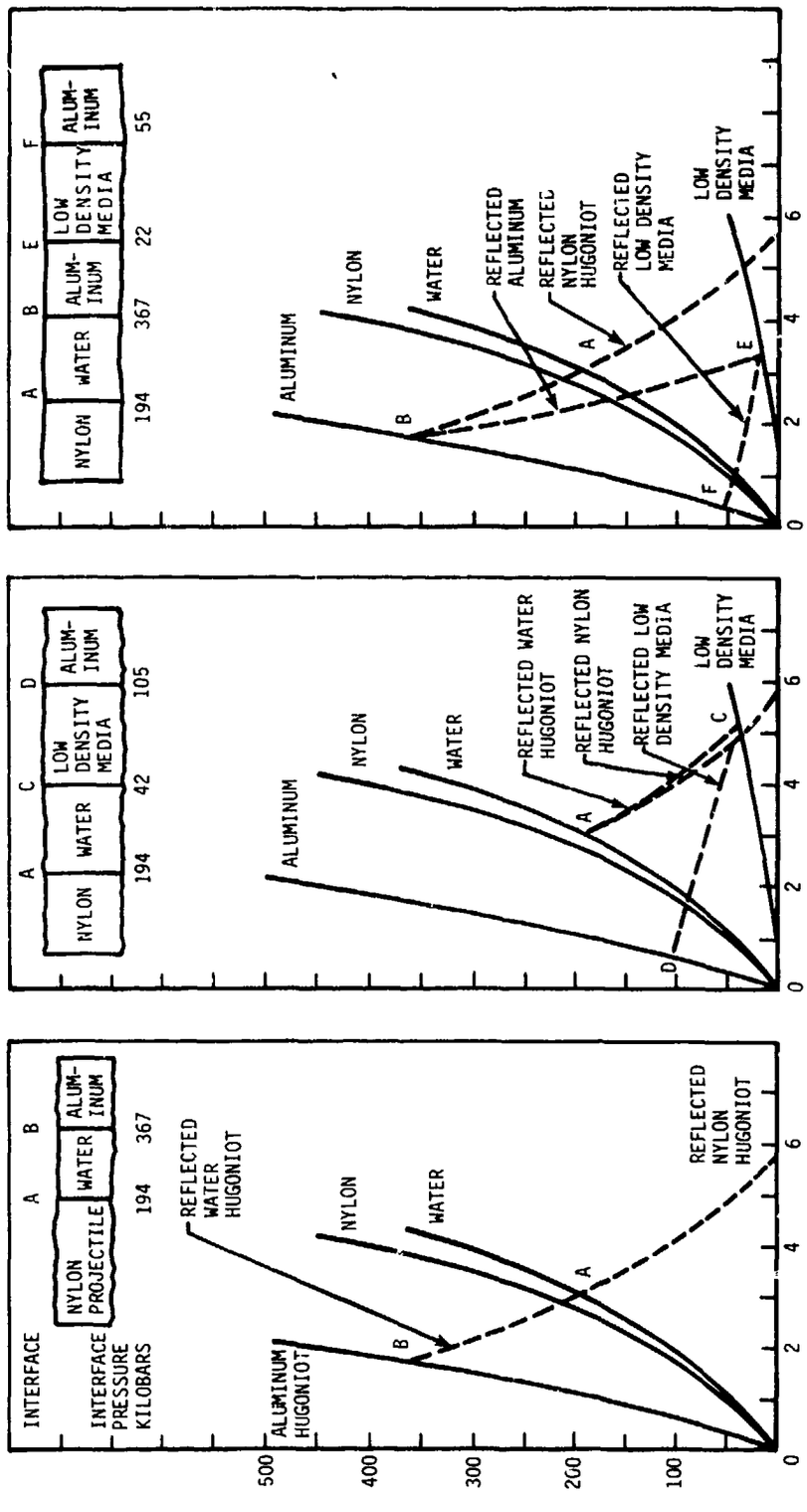

a. TEST CONFIGURATION A

b. TEST CONFIGURATION B

c. TEST CONFIGURATION C

(EXAMPLE OF A NYLON PROJECTILE IMPACTING A WATER-FILLED TANK AT 5.8 KM/SEC) (25:27)

Figure 34. Example for the Calculation of Maximum Interface Pressures

Torvik considers a porous material (foam) in one dimension as it is being subjected to a shock wave, as illustrated in Figure 35. The foam has been approximated as a "locking solid," i.e., any applied pressure compresses the foam its maximum amount. Thus, before the shock front, the foam has a density of ρ_0, and immediately behind the shock front, the foam has a density of ρ_f. The model further requires constant momentum in the material behind the shock front. Thus, as the mass of the foam is increased with the passing shock front, the particle velocities must decrease accordingly. At the same time, the particle velocities are required to be uniform so that ρ_f is constant throughout the compressed region.

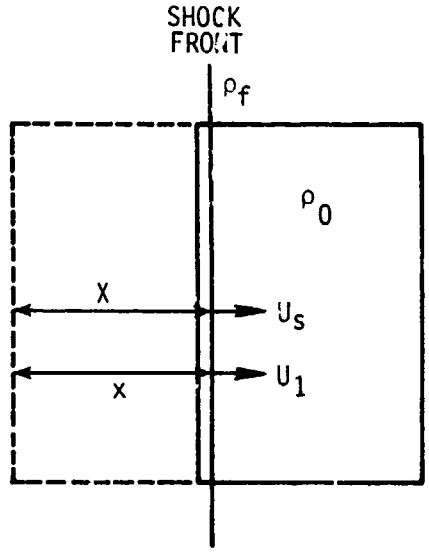

Figure 35. "Snowplow" Diagram

The following terms can be defined with reference to Figure 35: u_1 is the particle velocity just behind the shock front; then, with the assumption of a locking solid, u_1, the particle velocity for all the material behind the shock front, is just u_1. The shock moves with velocity, U_s, and has traversed a distance X into the foam. An arbitrary particle of the compressed foam is located at x.

The pressure is to be evaluated ultimately from an integration of the conservation of momentum (Equation 2) written in two dimensions:

$$\frac{\partial P}{\partial x} = -\rho_o \frac{\partial u}{\partial t} \tag{242}$$

The term $\frac{\partial U}{\partial t}$ is just $\frac{\partial U_1}{\partial X} \frac{\partial X}{\partial t}$ since the locking solid assumption requires that all the particle velocities be the same, and $\frac{\partial X}{\partial t}$ is the velocity of the shock front, U_s. To evaluate $\frac{\partial U_1}{\partial X}$, U_1 is determined from the impulse per unit area I_o. Using ξ as a dummy variable for integration, a slice of the foam has mass per unit area $\rho_o d\xi$. Thus,

$$I_o = u_1(X) \int_0^X \rho_o d\xi \tag{243}$$

is integrated easily to give

$$I_o = U_1(X) X \rho_o \tag{244}$$

The desired partial derivative is then given by

$$\frac{\partial u_1}{\partial X} = - \frac{I_0}{\rho_0 X^2} \tag{245}$$

The pressure follows from

$$dP = \frac{I_0}{X^2} U_s \, dx \tag{246}$$

Finally, the conservation of mass across the shock front (Equation 12) can be rearranged to give

$$\bar{u}_1 = \frac{\rho_f - \rho_0}{\rho_f} \tag{247}$$

where $\bar{u}_1$ was defined earlier (Equation 31) as

$$\bar{u}_1 = \frac{u_1}{U_s} \tag{248}$$

Taking $\bar{u}_1$ as constant for the locking material, and using Equation 242 for u_1 allows the integration of Equation 246 resulting in

$$P = \frac{I_0^2}{\bar{u}_1 \rho_0} \cdot \frac{x}{X^3} \tag{249}$$

The assumption of the locking solid leads to the prediction of a triangular shock pulse shape shown in Figure 36, with a maximum amplitude determined by the distance the shock has traveled in the foam.

c. Annihilation Calculation. Another method of analysis can be applied to the foam. Williams (9:16) observed that after the shock wave has progressed through the foam a short distance, a rarefaction wave is formed behind the shock. The rarefaction wave has a higher velocity than the shock wave and so overtakes it; since the particles behind a strong rarefaction wave have very low densities, the shock can be annihilated.

The shock is assumed to be a pulse of duration, t_p. During this time the shock progresses the distance $U_s t_p$, while the free surface travels only $u t_p$. The rarefaction wave is then formed, and will catch the shock wave in the time t_c. The rarefaction wave travels with velocity C_r, the release velocity. The relationship between these distances is shown in Figure 37. Conservation of mass across the shock (Equation 12) is used to write the particle velocity, u, in terms of the shock velocity

$$u = u_s \left(1 - \rho_o/\rho\right) \tag{250}$$

Using the distances shown in Figure 31 the following relationship can be made:

$$U_s \left(t_p + t_c\right) = U_s \left(1 - \rho_o/\rho\right) + C_r t_c \tag{251}$$

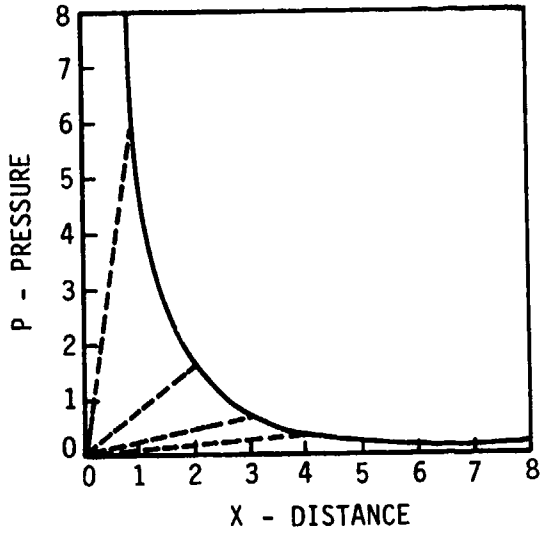

Figure 36. Pressure vs Distance for a Locking Solid (From Torvik)

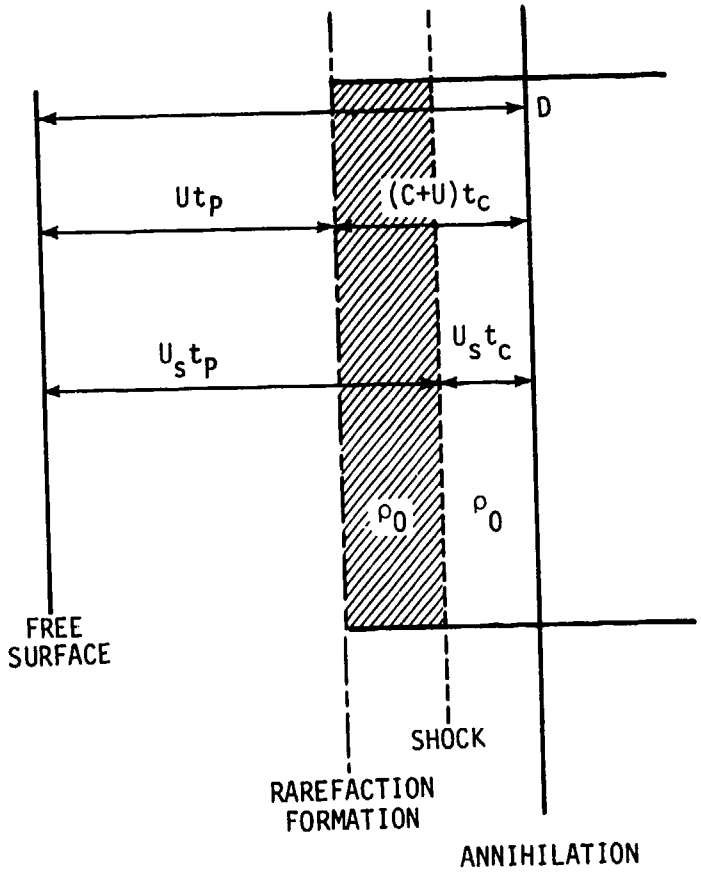

Figure 37. "Annihilation" Diagram

which leads to

$$t_c = t_p \frac{U_s \rho_o}{C_r \rho} \tag{252}$$

Thus, the distance required for annihilation of the shock is

$$D = U_s (t_p + t_c) = U_s t_p \left(1 + \frac{U_s \rho_o}{C_r \rho}\right) \tag{253}$$

The numbers necessary for this calculation can be taken from the Equation of State information in Figure 38. The Rayleigh line is the compression path for a particle exposed to a shock wave traveling with constant velocity. The Rayleigh line is given by

$$\left(\frac{\partial P}{\partial v}\right)_{U_s} = - \frac{U_s}{V_o} \tag{254}$$

which can be obtained from the jump conditions given in Equations 12 and 13. The release path is known from experiment and has been added to the diagram. Thus, using the variables from this diagram and assuming a shock pulse time of 8 μsec, annihilation is anticipated at 8.52 μsec after impact, and 3.07 mm into the foam. The 8 μsec time pulse corresponds to an intermediate value between normal and tumbled entry calculations for a 0.50 cal projectile.

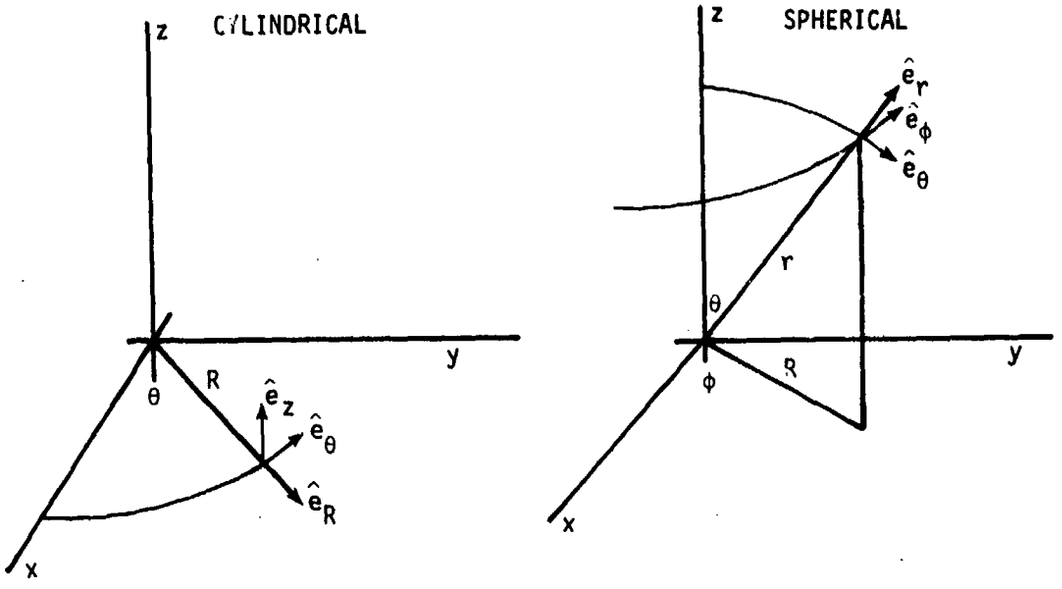

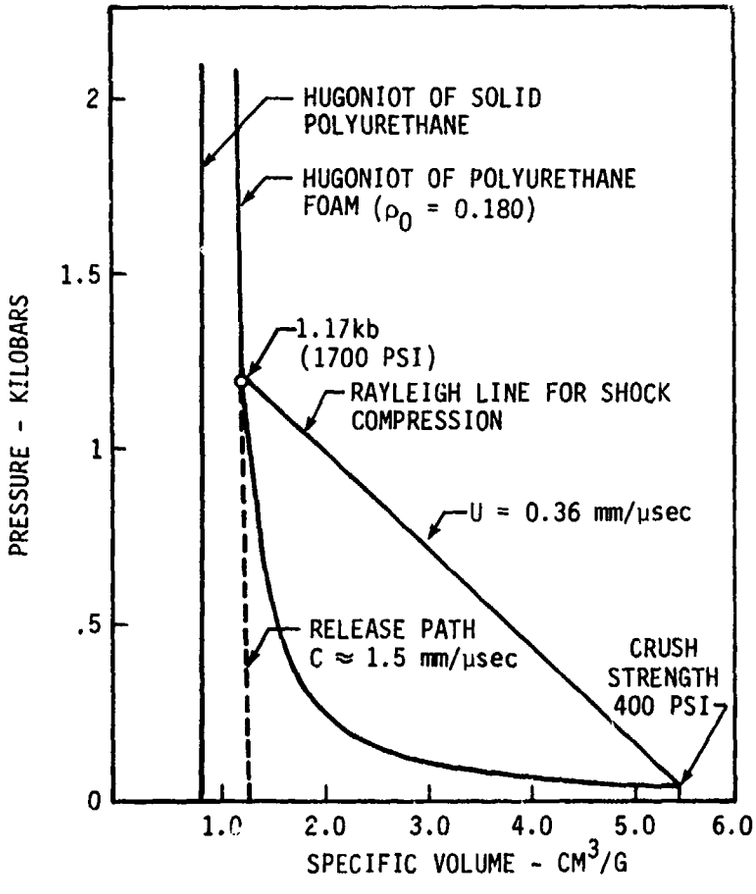

Figure 38. Hugoniot Equation of State of Polyurethane Foam (ρ_0 = 0.186 g/cm^3)

3. DISCUSSION

It was noted in this section that Williams' description of shock annihilation predicts the total elimination of the shock within only 0.3 cm of foam. Torvik's snowplow model also can be used to estimate the distance required for a stipulated amount of pressure reduction, and a comparison of the two predictions is useful. A rough number value for the snowplow prediction can be given by using Equation 249 with $x = \mathbf{I}$ (the maximum pressure plane). The same variables as in the Williams' calculation are used: ρ_0 = 0.186 g/cm^3, ρ_f = 0.833 g/cm^3, t_p = 8 μsec, and an initial pressure of 400 bar (5800 psi) - approximately the peak measured pressure 1/2 inch from the impact point of a 0.50 cal projectile. Thus 2.66 cm are required to reduce the pulse to 10 bars, and 8.42 cm are required to reduce the pulse to only 1 bar.

The snowplow model may accurately predict the pressure reduction due to the impulsively formed shock, but it does not predict any change in the impulse delivered to the wall for typical fuel tank ram problems. Consider the following simplified example. Let the 400 bar, 8 μsec impulse above be reduced to one bar with about 9 cm of foam. If the impulse remains unchanged, then the one bar pulse is spread out to 0.32×10^{-2} sec. But from the section on wall loading, the natural frequency of the wall was found to be of the order of one cycle per 10^{-2} sec. Thus the wall still sees the load as nearly impulsive. Since the wall sees both loads as nearly identical impulses, the wall response is not much affected by the reduced pressure.

Tests to date of up to 3 inches of foam have shown only moderate damage reduction, and that at the front wall where the shock would also be expected to predominate. This could indicate that the shock is predominant in the early reaction, and that the foam has some moderating effect on the shock. This test, though, does certainly indicate the importance of testing foams and foam configurations for their responses to shocks and pressures separately.

Nitrogen is currently being tested as a method to inert the ullage. Nitrogen gas bubbles in the fuel would not only scrub the oxygen but would also provide ram attenuation. Studies of this method must also be recommended.

Finally, a remark about self-sealing materials is appropriate. Although primarily intended to seal the hole after the projectile has passed through, these materials also exhibit ram attenuation properties. Self-sealing materials, when combined with other attenuation materials, may be particularly desirable. The preceding analyses should be applicable after appropriate modification.

SECTION VII

CONCLUSIONS

The ultimate objective of hydrodynamic ram studies is to eliminate the extensive fracture and rupture that follows the impact of a fuel tank by an ordnance projectile. Although this goal may eventually be shown to be unreachable, it is certainly possible to reduce damage to a minimum. To do this, it is necessary that each phase of the phenomenon be observed in detail and fully analyzed. An understanding of the phenomenon will permit the accurate evaluation of ram attenuating mechanisms and may result in suggestions for others. More importantly, this understanding of the ram event will allow the analysis of fuel tanks and fuel tank systems while they are still in the planning stages.

Thus far, analysis and testing of liquid-filled containers have shown that hydrodynamic ram is a very complex phenomenon, and have tried to simplify its study by separating it into its major events. This simplification will prove most useful if fracture can be associated primarily with only one of these major events. It remains now to be demonstrated when and how fracture occurs so that it can be determined which phase predominates in causing rupture under given conditions.

Some aspects of hydrodynamic ram were treated rather fully. Yurkovich gave an analysis of the shock phase and the drag phase, and

an approximate approach to the wall response. The shock phase work has been verified only against data from hypervelocity studies and its applicability to ordnance projectiles, while reasonable as a limiting case, has not been verified.

Lundstrom has described the drag phase of the event in considerable detail and developed a solution of Bernoulli's equation to describe the pressure field.

Chow has used the method of characteristics to describe tank wall response to shocks, but his work has not been verified for bullets. Ball has recommended piston theory for studying the wall response to both fluid shocks and pressures.

The next logical step in the hydrodynamic ram studies is to verify existing models and their assumptions. Shock fronts at the impact point and pressure pulses in the fluid have both been measured routinely. This information has permitted the calculation of wall loading, which is necessary to predict wall response. But because the pressure loading at the wall has been difficult to measure, the wall loading models have not been verified. However, Ytterbium gages can be used to get pressure measurements at the wall-fluid interface, though with some difficulty. In addition, wall response itself has not been measured except at isolated points with strain gages; yet wall response, including fracture, can be measured over areas larger than 2 sq ft and at time intervals of approximately 10μ sec using moiré fringes and high speed photography.

To a large extent, this lack of data exists because it is very difficult to obtain. Ytterbium gages have been used to get pressure measurements at the wall fluid interface, but only with much difficulty. A moiré fringe technique to measure wall motion has been suggested recently, but the system is critically dependent upon finding an adequate light source.

Although many pieces of information, such as strain and strain rates within the tank walls, may be essential to predicting the response of the tank to bullet impact, they cannot be measured directly. This information must be properly inferred from verified analytical models or from computer codes whose accuracy is known. Thus it is expected that the abundance of detail available from two-dimensional wave propagation codes will make those codes invaluable for understanding the damage mechanisms, failure criteria, and attenuation possibilities associated with hydrodynamic ram.

The study and prediction of wall response is of fundamental importance. Once the loading is determined, several codes can be used to predict deformation and failure. STAGS and BR-1 have both been modified to account for hydrodynamic ram loading. But accurate loading predictions, particularly at the exit and entrance regions, are not available from observation or current models. Only the general Lagrangian or Eulerian codes mentioned above are able to predict this type of loading.

The following tasks and study areas are recommended.

1. Collection of wall fracture data to determine the extent of wall fracture as a function of time. This data should be obtained for several projectiles, velocities and masses, and for various degrees of tumble at entry. This data needs to be obtained for both entrance and exit walls; similar data needs to be obtained for side walls.

2. A model needs to be developed for exit wall impact.

3. The existing fluid shock model must be verified for ordnance projectiles.

As a final comment, the explication of available computer programs in study areas of hydrodynamic ram has been beyond the intent of this report. Yet, the use of these codes is essential; nearly all of the preceding analysis has been programmed to facilitate obtaining numerical results. Additionally, most of the work is so complex that it can only be approached with the aid of the computer.

APPENDIX A

GRADIENT, DIVERGENCE, CURL, AND LaPLACIAN EQUATIONS IN CYLINDRICAL AND SPHERICAL COORDINATES

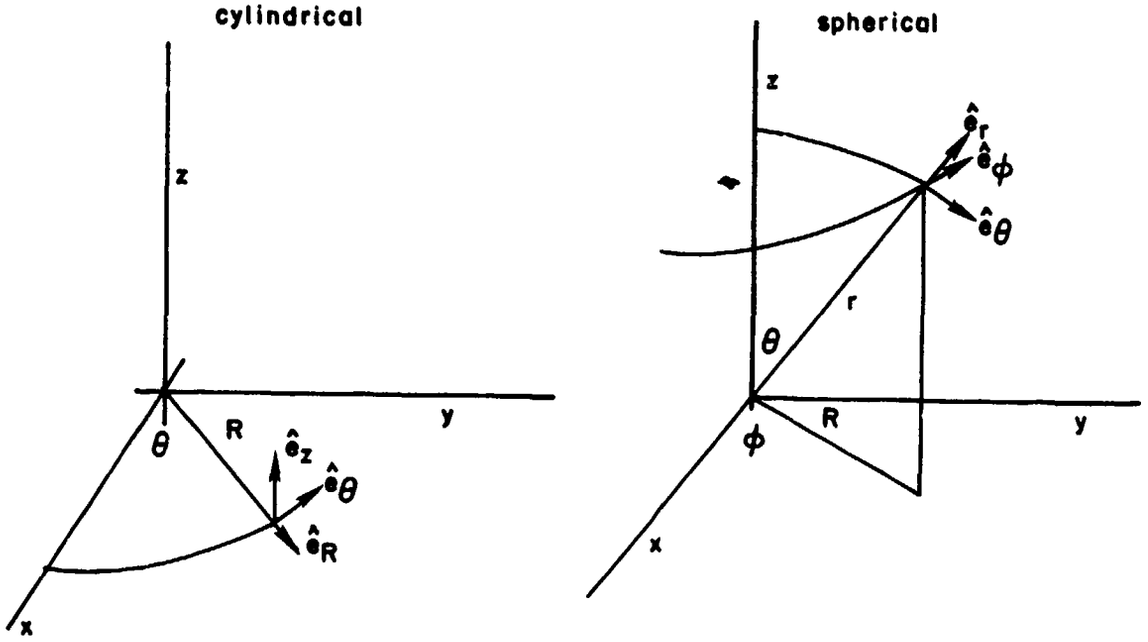

	cylindrical	spherical
∇	$\hat{e}_R \frac{\partial}{\partial_R} + \hat{e}_\theta \frac{1}{r} \frac{\partial}{\partial\theta} + \hat{e}_z \frac{\partial}{\partial z}$	$\hat{e}_r \frac{\partial}{\partial r} + \hat{e}_\theta \frac{1}{r} \frac{\partial}{\partial\theta} + \hat{e}_\phi \frac{1}{r\sin\theta} \frac{\partial}{\partial\phi}$
$\nabla\cdot$	$\frac{1}{R} \frac{\partial}{\partial_R} R + \frac{1}{R} \frac{\partial}{\partial\theta} + \frac{\partial}{\partial z}$	$\frac{1}{r^2} \frac{\partial}{\partial r} r^2 + \frac{1}{r\sin\theta} \frac{\partial}{\partial\theta} \sin\theta + \frac{1}{r\sin\theta} \frac{\partial}{\partial\phi}$
$\nabla\times$	$\hat{e}_R \left(\frac{1}{R} \frac{\partial}{\partial\theta} - \frac{\partial}{\partial z}\right)$	$\hat{e}_r \frac{1}{r\sin\theta} \left(\frac{\partial}{\partial\theta}\sin\theta - \frac{\partial}{\partial\phi}\right)$
	$+ \hat{e}_\theta \left(\frac{\partial}{\partial z} - \frac{\partial}{\partial R}\right)$	$+ \hat{e}_\theta \frac{1}{r\sin\theta} \left(\frac{\partial}{\partial\phi} - \sin\theta \frac{\partial}{\partial r} r\right)$
	$+ \hat{e}_z \left(\frac{1}{R} \frac{\partial}{\partial_R} R - \frac{1}{R} \frac{\partial}{\partial\theta}\right)$	$+ \hat{e}_\phi \frac{1}{r} \left(\frac{\partial}{\partial_r} r - \frac{\partial}{\partial\theta}\right)$
∇^2	$\frac{1}{R} \frac{\partial}{\partial R} \left(R \frac{\partial}{\partial R}\right) + \frac{1}{R^2} \frac{\partial^2}{\partial\theta^2} + \frac{\partial^2}{\partial z^2}$	$\frac{1}{r^2} \frac{\partial}{\partial r} \left(r^2 \frac{\partial}{\partial r}\right) + \frac{1}{r^2\sin\theta} \frac{\partial}{\partial\theta}\left(\sin\theta \frac{\partial}{\partial\theta}\right)$
		$+ \frac{1}{r^2\sin^2\theta} \frac{\partial^2}{\partial\phi^2}$

APPENDIX B

EXAMPLES SHOWING THAT THE SCALAR POTENTIAL SATISFIES THE WAVE EQUATION

To show that the scalar potential ϕ satisfies the wave equation, Equation 1 is rewritten as:

$$\nabla \cdot \vec{u} = - \frac{1}{\rho} \frac{d\rho}{dt} \tag{B1}$$

It is necessary to first rewrite the differential $\frac{d\rho}{dt}$. Density is a function of both pressure and entropy, but entropy can be assumed constant: this assumption is verified numerically by Cole (3:sec. 2.6). Using the definition of sound velocity $c^2 = \left(\frac{dP}{d\rho}\right)_s$ and assuming constant entropy, the derivative $\frac{dP}{dt} = \frac{dP}{d\rho} \frac{d\rho}{dt}$ leads to

$$\frac{d\rho}{dt} = \frac{1}{c^2} \frac{dP}{dt} = \frac{\rho}{c^2} \frac{di}{dt} \tag{B2}$$

The assumption of constant entropy also allows (from $di = T\,dS + \tau\,dP$)

$$\nabla \rho = \rho \nabla i \tag{B3}$$

and thus the conservation of momentum equation (Equation 2) becomes

$$\frac{d\vec{u}}{dt} = - \nabla i \tag{B4}$$

When written out and simplified, this last equation is

$$\frac{\partial \vec{u}}{\partial t} = -\nabla I + \vec{u} \times (\nabla \times \vec{U}) \tag{B5}$$

where $\nabla i = \nabla I - (\vec{u} \cdot \nabla)\vec{u} - \vec{u} \times (\nabla \times \vec{u})$ follows from the definition of kinetic enthalpy: $I = i - i_0 + \frac{\vec{u} \cdot \vec{u}}{2}$. The assumption of irrotational motion then eliminates the last term on the right and gives $\frac{\partial}{\partial t} \nabla \phi = -\nabla I$ which leads to the conclusion that

$$I = -\frac{\partial \phi}{\partial t} \tag{B6}$$

Now the expression for $\nabla \cdot \vec{u}$ can be expanded to give

$$\nabla \cdot \vec{u} = -\frac{1}{c^2} \left(\frac{\partial i}{\partial t} + \vec{u} \cdot \nabla i \right) \tag{B7}$$

where the two terms in parenthesis are to be rewritten. From the kinetic enthalpy:

$$\begin{aligned} \frac{\partial i}{\partial t} &= \frac{\partial I}{\partial t} - \frac{1}{2} \frac{\partial}{\partial t} (\vec{u} \cdot \vec{u}) \\ &= \frac{\partial I}{\partial t} - \frac{1}{2} \frac{d}{dt} (\vec{u} \cdot \vec{u}) + \frac{1}{2} (\vec{u} \cdot \nabla)(\vec{u} \cdot \vec{u}) \end{aligned} \tag{B8}$$

and using $\nabla i = -\frac{du}{dt}$

$$\vec{u} \cdot \nabla i = -\vec{u} \cdot \frac{d\vec{u}}{dt} = -\frac{1}{2}\frac{d}{dt}(\vec{u} \cdot \vec{u})$$
$$= -\frac{1}{2}\frac{\partial}{\partial i}(\vec{u} \cdot \vec{u}) - \frac{1}{2}(\vec{u} \cdot \nabla)(\vec{u} \cdot \vec{u}) \quad \text{(B9)}$$

Substitution of these last forms for $\frac{\partial i}{\partial t}$ and $\vec{u} \cdot \nabla i$ into Equation B7 gives the desired result:

$$\nabla \cdot \vec{u} = -\frac{1}{c^2}\left[\frac{\partial I}{\partial t} - \frac{\partial}{\partial t}(\vec{u} \cdot \vec{u}) - \frac{1}{2}(\vec{u} \cdot \nabla)(\vec{u} \cdot \vec{u})\right] \quad \text{(B10)}$$

APPENDIX C

DERIVATION OF THE CONSERVATION EQUATIONS IN NONDIMENSIONAL FORM

Derivation of the Conservation equations in nondimensional form.

1. CONTINUITY EQUATION

The continuity equation is given by Equation 6 as

$$\frac{\partial \rho}{\partial t} + \rho \frac{\partial u}{\partial r} + u \frac{\partial \rho}{\partial r} + 2 \frac{\rho u}{r} = 0 \qquad \text{(C1)}$$

Using the substitutions

$$\rho = \rho_o \bar{\rho} \left(\bar{r}, M_s \right), \qquad u = U_s \bar{u} \left(\bar{r}, M_s \right), \qquad \text{and} \quad r = r_s \bar{r} \qquad \text{(C2)}$$

leads to

$$\rho_o \left(\frac{\partial \bar{\rho}}{\partial \bar{r}} \frac{\partial \bar{r}}{\partial t} + \frac{\partial \bar{\rho}}{\partial M_s} \frac{\partial M_s}{\partial t} \right) + \rho_o U_s \bar{\rho} \left(\frac{\partial \bar{u}}{\partial \bar{r}} \frac{\partial \bar{r}}{\partial r} + \frac{\partial \bar{u}}{\partial M_s} \frac{\partial M_s}{\partial r} \right)$$

$$+ \rho_o U_s \bar{u} \left(\frac{\partial \bar{\rho}}{\partial \bar{r}} \frac{\partial \bar{r}}{\partial r} + \frac{\partial \bar{\zeta}}{\partial M_s} \frac{\partial M_s}{\partial r} \right) + \frac{2 \rho_o U_s \bar{\rho} \bar{u}}{r_s \bar{r}} = 0 \qquad \text{(C3)}$$

Using $t = \frac{r_s}{u_s} = \frac{r_s}{C_o M_s}$, the above terms are evaluated as

$$\frac{\partial \bar{r}}{\partial t} = - \frac{r}{U_s t^2} = - \frac{\bar{r} U_s}{r_s^2}$$

$$\frac{\partial \bar{r}}{\partial r} = \frac{1}{r_s}$$

$$\frac{\partial M_s}{\partial t} = \frac{a_s}{C_o} \qquad \text{(C4)}$$

$$\frac{\partial M_s}{\partial r} = 0$$

Proper rearrangement gives the desired result:

$$(\bar{u} - \bar{r}) \frac{\partial \bar{\rho}}{\partial \bar{r}} + \bar{\rho} \frac{\partial \bar{u}}{\partial \bar{r}} + 2 \frac{\bar{\rho}\, \bar{u}}{\bar{r}} = - \beta M_s \frac{\partial \bar{\rho}}{\partial M_s} \qquad \text{(C5)}$$

where

$$\beta = \frac{r_s\, a_s}{U_s^2} = \frac{r_s\, \dot{U}_s}{U_s^2} \qquad \text{(C6)}$$

2. CONSERVATION OF MOMENTUM

The conservation of momentum is given by Equation 7

$$\frac{\partial u}{\partial t} + u \frac{\partial u}{\partial r} + \frac{1}{\rho} \frac{\partial P}{\partial r} = 0 \qquad (C7)$$

Using the substitutions in Equation C6 and

$$P = \rho_0 U_s^2 \bar{P} \qquad (C8)$$

leads to

$$U_s \left(\frac{\partial \bar{u}}{\partial \bar{r}} \frac{\partial \bar{r}}{\partial t} + \frac{\partial \bar{u}}{\partial M_s} \frac{\partial M_s}{\partial t} \right) + \bar{u} \frac{\partial U_s}{\partial t}$$

$$+ U_s \bar{u} \left[U_s \left(\frac{\partial \bar{u}}{\partial \bar{r}} \frac{\partial \bar{r}}{\partial r} + \frac{\partial \bar{u}}{\partial M_s} \frac{\partial M_s}{\partial r} \right) + \bar{u} \frac{\partial U_s}{\partial r} \right] \qquad (C9)$$

$$+ \frac{1}{\rho_0 \bar{\rho}} \left[\rho_0 \left(2 U_s \bar{P} \frac{\partial U_s}{\partial r} + U_s^2 \left\{ \frac{\partial \bar{P}}{\partial \bar{r}} \frac{\partial \bar{r}}{\partial r} + \frac{\partial \bar{P}}{\partial M_s} \frac{\partial M_s}{\partial r} \right\} \right) \right] = 0$$

Since $U_s = U_s(t)$, and $\frac{\partial U_s}{\partial r} = 0$, Equation C9 reduces to

$$(\bar{u} - \bar{r}) \frac{\partial \bar{u}}{\partial \bar{r}} + \beta \bar{u} + \frac{1}{\rho} \frac{\partial \bar{P}}{\partial \bar{r}} = -\beta M_s \frac{\partial \bar{u}}{\partial M_s} \qquad (C10)$$

3. CONSERVATION OF ENERGY

Conservation of energy is given by Equation 8 as

$$\frac{\partial e}{\partial t} + u\frac{\partial e}{\partial r} - \frac{P}{\rho^2}\left(\frac{\partial \rho}{\partial t} + u\frac{\partial \rho}{\partial r}\right) = 0 \qquad (C11)$$

In addition to the identities given in Equations C2 and C8,

$$e = U_s^2 \bar{e} \qquad (C12)$$

Following the same procedures as before, these substitutions lead to

$$U_s^2\left(\frac{\partial \bar{e}}{\partial \bar{r}}\frac{\partial \bar{r}}{\partial t} + \frac{\partial \bar{e}}{\partial M_s}\frac{\partial M_s}{\partial t}\right) + 2U_s\bar{e}\frac{\partial U_s}{\partial t}$$

$$+ U_s\bar{u}\left[U_s^2\left(\frac{\partial e}{\partial \bar{r}}\frac{\partial \bar{r}}{\partial r} + \frac{\partial \bar{e}}{\partial M_s}\frac{\partial M_s}{\partial r}\right) + 2U_s\bar{e}\frac{\partial U_s}{\partial r}\right]$$

$$+ \frac{\rho_o U_s^2 \bar{P}}{\bar{\rho}^2 \rho}\left[\rho_o\left(\frac{\partial \bar{\rho}}{\partial \bar{r}}\frac{\partial \bar{r}}{\partial t} + \frac{\partial \rho}{\partial M_s}\frac{\partial M_s}{\partial t}\right) + U_s\rho_o\bar{u}\left(\frac{\partial \bar{\rho}}{\partial \bar{r}}\frac{\partial \bar{r}}{\partial r} + \frac{\partial \bar{\rho}}{\partial M_s}\frac{\partial M}{\partial r}\right)\right] = 0 \qquad (C13)$$

Substituting and simplying gives the desired result:

$$(\bar{u} - \bar{r})\left[\frac{\partial \bar{e}}{\partial \bar{r}} - \frac{\bar{P}}{\bar{\rho}^2}\frac{\partial \bar{\rho}}{\partial \bar{r}}\right] + 2\bar{e}\beta = -\beta M_s\left[\frac{\partial \bar{e}}{\partial M_s} - \frac{\bar{P}}{\bar{\rho}^2}\frac{\partial \bar{\rho}}{\partial M_s}\right] \qquad (C14)$$

APPENDIX D

THE SOLUTION OF THE FORCE EQUATION

The solution of the force equation

$$\ddot{w} + 2\zeta \dot{w} + \omega^2 w = \gamma \tag{D1}$$

is a little lengthy, but straightforward. It is a second order linear differential equation that can be handled by the method of variation of parameters, as in Ross (24). Assuming a solution of the homogeneous part of the form $w = e^{\alpha t}$ yields a complementary solution

$$w_c = c_1 e^{\alpha^+ t} + c_2 e^{\alpha^- t} \tag{D2}$$

where

$$\alpha^+ = -\zeta + \zeta^* \tag{D3}$$

$$\alpha^- = -\zeta - \zeta^* \tag{D4}$$

$$\zeta^* = \sqrt{\zeta^2 - \omega^2} \tag{D5}$$

Then, by the variation of the parameters method, the following equation remains to be solved:

$$w = c_1 w_1 + c_1 w_2 + \nu_1 w_1 + \nu_2 w_2 \tag{D6}$$

where

$$w_1 = e^{\alpha^+ t} \tag{D7}$$

$$w_2 = e^{\alpha^- t} \tag{D8}$$

The parameters V_1 , and V_2 are to be determined from

$$\nu_1 = -\int \frac{\gamma w_2}{W} dt \tag{D9}$$

and

$$\nu_2 = \int \frac{\gamma w_1}{W} dt \tag{D10}$$

where

$$W = \begin{vmatrix} w_1 & w_2 \\ \dot{w}_1 & \dot{w}_2 \end{vmatrix} = 2 w_1 w_2 \zeta^* \tag{D11}$$

The solution of the particular equation now yields

$$\nu_1 w_1 + \nu_2 w_2 = \frac{\gamma}{\omega^2} \tag{D12}$$

The constants c_1 and c_2 of the complete solution are determined from the initial conditions, $w = \dot{w} = 0$ at $t = 0$. Thus,

$$c_1 = \frac{\gamma \alpha^-}{2\omega^2 \zeta^*} \tag{D13}$$

and

$$c_2 = -\frac{\gamma \alpha^+}{2\omega^2 \zeta^*} \tag{D14}$$

Making these substitutions in Equation D6 gives the solution of the force equation

$$w = \frac{\gamma}{\omega^2}\left[1 + \frac{1}{2\zeta^*}(\alpha^- w_1 - \alpha^+ w_2)\right] \tag{D15}$$

One differentiation of Equation D15 gives

$$\dot{w} = \frac{\gamma}{2\zeta^*}(w_1 - w_2) \tag{D16}$$

and a second differentiation gives

$$\ddot{w} = \frac{\gamma}{2\zeta^*}(\alpha^+ w_1 - \alpha^- w_2) \tag{D17}$$

Using the easily derived relations that

$$\alpha^+ + \alpha^- = 2\zeta \tag{D18}$$

and

$$\alpha^+ \alpha^- = \omega^2 \tag{D19}$$

the solution of the force equation can be easily verified by substitution.

APPENDIX E

CONSTANTS, PARAMETERS, AND CONVERSION FACTORS

1. CONVERSION FACTORS

density	1 kg/m^3	= 3.6127292×10^{-5} lbm/in^3
		= 6.2427961×10^{-2} lbm/ft^3
energy	1 joule	= 0.737562 ft lb
length	1 meter	= 39.370039 in
		= 3.2808399 ft
mass	1 kg	= 2.2046226 lbm
	1 grain	= 6.479891×10^{-5} kg
		= 1.4285714×10^{-4} lbm
pressure	1 bar	= 10^5 N/m^2
		= 14.503774 lb/in^2
velocity	1 km/sec	= 1 m/msec = 1 mm/μsec
		= 39.370079 in/msec

2. CONSTANTS

E = modulus of elasticity in tension, Young's modulus

G = modulus of rigidity, modulus of elasticity in shear

ν = Poisson's ratio

ρ = density

	E (kbar)	G (kbar)	$\rho(kg/m^3)$	C* (m/s)	ν
2024 aluminum sheet	724	276	2770	5112	.33
7075 aluminum sheet	710	269	2800	5034	.33
JP-4			785		
JP-5			816	1361	
water			1000	1495	

* for aluminum, C is derived from $C = \sqrt{\frac{E}{\rho}}$

3. CONSTANTS FOR SOME TYPICAL PROJECTILES

Caliber - Description (bullet length in mm)	Projectile Length (mm)	Diameter (mm)	Mass (grams)	Muzzle Velocity (km/sec)
7.62 - M1943, Type PS (39)	26.97	7.87	7.97 - 8.035	0.707 - 0.732
7.62 (54)	29.97	7.89	9.59 - 9.655	0.8696
30 cal AP (M2) (63)	35.51	7.82	10.74	0.8382 - 0.8534
12.7 API (108)	63.5	12.97	48.84	0.8382 - 0.8687
50 cal AP (M2) (99)	58.67	12.97	45.55	0.8543
14.5 Heavy API (113.8)	50.55	14.9	64.22	0.9997
23 API (150.5)	106.5	22.56	187.8	0.8839 - 0.9144

APPENDIX F

A WORKING BIBLIOGRAPHY FOR HYDRODYNAMIC RAM*

Hydrodynamic Ram

Bach, J. H. Fuel Tank Mechanisms Induced by High Explosive Incendiary Projectile Threats. Hawthorne, California: Northrop Corp, Feb 1974.

Bond, Thomas. Response of Fuel Cells of the UH-1D Helicopter to Hydraulic Ram Forces. BRL MR 2289. Aberdeen Proving Ground, Maryland: Ballistic Research Laboratories, AMXBR-XM-SE, Apr 1973.

Bristow, Robert J., and Douglas L. Henry. Investigation of Ballistic-Tolerant Fuel Tanks. Boeing Report D 180-17504-1 USAAMRDL TR 73-68, Seattle, Washington: The Boeing Co., Aug 1973.

Chou, Pei Chi, Richard Schaller, and James Hcburg. Analytical Study of the Fracture of Liquid-Filled Tanks Impacted by Hypervelocity Particles. Drexel Rpt. No. 160-9. NASA CR-72169. Philadelphia, Pennsylvania: Drexel Institute of Technology, Mar. 1967.

Ferguson, C. W. Hypervelocity Impact Effects of Liquid Hydrogen Tanks, Final Report. MNASA CR 54852. 1965. N 66 22267.

Fuhs, A.E., R. E. Ball, and H. L. Power. FY73 Hydraulic Ram Studies. Monterey, California: Naval Postgraduate School, Feb. 1974.

Gonsalves, J. Fuel System Hydraulic Ram Testing. Philadelphia, Pennsylvania: The Boeing Co., May 1973. (Report prepared under contract: DAAJ01 73 C 0007(P40)

Jex, David William. Hypervelocity Impact Tests on a Proposed Lunar Tug Fuel Tank Configuration. Alabama: Marshall Space Flight Center, Apr 1971. NASA TM X-64597. N71 26040.

Lundstrom, Eric A. Fluid Dynamic Analysis of Hydraulic Ram. NWC TP China Lake, California: Naval Weapons Center, July 1971. AD 889 485.

Lundstrom, Eric A. and E. W. Stull. Fluid Dynamic Analysis of Hydraulic Ram II (Results of Experiments). Naval Weapons Center, California: Joint Technical Coordinating Group/Aircraft Survivability, 1973.

Lundstrom, E. A. and W. K. Fund. Fluid Dynamic Analysis of Hydraulic Ram III (Result of Analysis). JTCG/AS -74-T015. China Lake, California" Naval Weapons Center, October 1974.

Morse, C. Robert and Francis S. Stepka. Effect of Projectile Size and Material on Impact Fracture of Walls of Liquid-Filled Tanks. NASA TN D 3627. Sept 1966. N66 37155.

*This list is intended to be complete with respect to the items which treat hydrodynamic ram. Only selected items dealing with fluid shocks, wall responses, projectile penetration of plates, etc. have been included.

Bjork, R. L. and A. E. Olshaker. A Proposed Scaling Law for Hypervelocity Between Projectile and a Target of Dissimilar Material. AD 339. RM 2926 PR. Santa Monica, California: Rand Corp, May 1965.

Bouma, D. D. and W. C. Burkitt. Multivariable Analysis of the Mechanics of Penetration of High Speed Particles. NASA CR 664. N67 16664.

Byrnside, N. C., P. J. Torvik, and H. F. Swift. "Impact Crater Formation at Intermediate Velocities." Journal of Basic Engineering. Jun 1972, pp. 394-400.

Chou, Pei Chi. "Perforation of Plates by High Speed Projectiles." Developments in Mechanics. Vol I. Edited by J. E. Lay and L. E. Melvin. New York: Plenum Press, 1961.

Chou, Pei Chi, et al. A Parametric Study of the Hypervelocity Perforation of Viscoplastic Plates. DIT 125-3. Drexel Institute of Technology, Jan 1963. Unclassified report. AD 406296.

Ezra, A. A. et al. Effect of Material Properties on the Penetration of Target Projectiles. AIAA Preprint 63-194. A-63-18452.

Fields, Thomas E. The Effect of Projectile Shape on the Ballistic Perforation of Thin Metal Plates. AD 693-151. AFML-TR-69-202, July 1969.

Fuchs, O. P. "Impact Phenomena." AIAA Journal. Vol. 1. Sept 1963. pp. 2124 -2126.

Hermann, Walter and Arfan H. Jones. Survey of Hypervelocity Impact Information. ASRL Report No. 99-1, Sept 1961, plus addendum Oct 1961 MIT Aeroelastic and Structures Research Lab.

Kinslow, Ron, editor. High Velocity Impact Phenomena. New York: Academic Press Inc., 1970.

Sedgwick, R. T. Theoretical Investigation of Metallic Performance by Kinetic Energy Projectiles. AFATL-TR-69-54. Eglin AFB, Florida: AFATL, AF Sys Command, Apr 69.

Sedgwick, R. T. and L. J. Hageman. Numerical, Analytical, and Experimental Investigation of Penetration by Kinetic Energy Projectiles. AFATL-TR-72-48. Eglin AFB, Florida: AF Armament Lab., Mar 72.

Nix, W. L. Hydraulic Ram Effect of Small Arms Fire on Aircraft Fuel Tanks. ERR FW 1091. Forth Worth, Texas: General Dynamics, Dec 1970. AD 889 735L.

Power, H. L. FY 74 Experimental Hydraulic Ram Studies. Monterey, California: Naval Post Graduate School, August 1974.

Stepka, Francis S. Projectile-Impact-Induced Fracture of Liquid-Filled Filament-Reinforced Plastic or Aluminum Tanks. NASA TN D 3456. Washington, D. C.: National Aeronautics and Space Administration, Jun 1966. N66 27059.

Stepka, Francis S., C. R. Morse, and R. P. Dengler. Investigation of Characteristics of Pressure Waves Generated in Water Filled Tanks Impacted by High-Velocity Projectiles. NASA TN D 3143. Washington D. C.: National Aeronautics and Space Administration, Dec 1965. N66 13291.

Stepka, Francis S., and C. Robert Morse. Preliminary Investigation of Catastrophic Fracture of Liquid-Filled Tanks Impacted by High-Velocity Particles. NASA TN 1537. Washington: National Aeronautics and Space Administration, May 1963.

Williams, Roger F. Shock Effects in Fuel Cells. SRI Rpt. Accession No. L-23995. Menlo Park, California: Stanford Research Inst., Oct 1969.

Willis, R. L. Projectile-Hydraulic Ram Dynamics Investigation, Final Report. St. Louis: McDonnell Aircraft Co., August 1969. Report 604-331.

Yurkovich, R. Hydraulic Ram: A Fuel Tank Vulnerability Study. MDC G 964. St. Louis, Missouri: McDonnell Aircraft Corp., Sept 1969.

Penetration

Awerbuch, J. and S. R. Bodner. Experimental Investigation of Normal Perforation of Projectiles in Metallic Plates. MED Report No. 41. Haifa, Israel: Israel Institute of Technology, June 1973.

Awerbuch, Jonathan. A Mechanics Approach to Projectile Penetration. MED Report No. 28. Haifa, Israel: Israel Inst. of Technology, May 1970.

Beynet, P. and R. Plunkett. "Plate Impact and Plastic Deformation by Projectiles." Experimental Mechanics. V. 2, N. 2. Feb 1971. pp 64-70.

Thompson, Louis J. and William R. Bryant. "Projectile Penetration Theory." Presentation: Conference on Rapid Penetration of Terrestial Materials: Feb 1-3, 1972, at Texam A&M. AD 746 140.

Thomson, Robert G. and E. T. Kruszewski. Effect of Target Material Yield Strength on Hypervelocity Perforation and Ballistic Limit. Paper presented at the 7th Hypervelocity Impact Symposium, Tampa, Florida. Nov 1964. N66 33369. Also in Proceedings, Seventh Hypervelocity Impact Symposium, Vol V Experiments. Orlando, Florida: Martin Co., 1965.

Walsh, J. M. et al. Summary Report on the Theory of Hypervelocity Impact. San Diego, Calif: John Jay Hopkins Laboratory for Pure and Applied Science, Mar 1964. AD 436 251.

Walsh, J. M. et al. "Shock-Wave Compression of Twenty-Seven Metals, Equation of State of Metals," Physics Review. Vol 108. 15 Oct 57. pp 196-216.

Wingrove, A. L. "Forces for Projectile Penetration of Aluminum." Journal of Physics D. British Journal of Applied Physics. Vol 5, No. 7. 1972. p. 1294.

Fluid Response

Akinsete, V. A. "Initial Phases of the Collapse of an Empty Cavity in a Liquid." International Journal of Engineering Science. Vol 12, No. 10. Oct 1974. pp 837-851.

Bristow, R. J. and J. F. Lundberg. Projectile Penetration Through Rheoptic Fuels. AFAPL TR 68-151. Seattle, Washington: Boeing Co., Nov 1968. AD 745 801.

Bristow, R. J. Impact into Fluids. Seattle, Washington: The Boeing Co., Mar 1967. FADS 40.

Cardea, G. C. and P. J. Torvik. "Cavity Growth and Collapse Phase of Hydraulic Ram." Journal of Aircraft. Vol 11, No 4. Apr 1974. pp 252-254.

Cardea, George C. The Cavitation Phase of Hydraulic Ram Described by Equations Derived for UnderWater Explosions. AFIT Thesis, GAW/MC/74-3. Wright-Patterson AFB, Ohio: Air Force Institute of Technology, Dec 1973.

Cheng, R. Y. K., and T. J. W. Leland. Numerical Solution for Low-Velocity Penetration of Rigid Body into Still Water. International Conference on Numerical Methods in Fluid Dynamics, Southampton, England: 26-28 Sept 73. A74-11431.

Chou, Pei Chi, Harbans S. Sidhu, and Robert R. Karpp. Analysis of Peak Pressure Generated in Water by High Velocity Impact. Philadelphia, Penn; Drexel Institute of Tech. Apr 1963. DIT Report No. 160-1. X 63 13839.

Easter, John R. Fluid Response to Plate Impact. Thesis. Wright-Patterson Air Force Base, Ohio: Air Force Institute of Technology, Jun 1972. AD 748 340.

Fischer, R. F. A Theoretical Investigation of Shock Waves in Water and Water-Polyurethene Mixtures. AFIT Thesis. Dayton, Ohio: Air Force Institute of Technology, Wright-Patterson AFB, Jun 1971. AD 741 456.

Gerlach, C. R. Investigation of Water Impact of Blunt Rigid Bodies - Real Fluid Effects. San Antonio, Texas: Southwest Research Inst. Dec 29, 1967. AD 663-893.

Holm, Clifford Milton. Hydraulic Ram Pressure Measurements. Thesis. Monterey, California: Naval Postgraduate School. Dec 1974.

Heyda, James F. "Shock Front Variation in Time for High Speed Impact into Water." Proceedings of the Sixth Symp on Hypervelocity Impact. Vol II, Part 1. Conference held in Cleveland, Ohio, 30 Apr - 2 May, 1963. AD 423063.

Hoerner, Sighard F. Fluid Dynamic Drag - Practical Information on Aerodynamic Drag and Hydrodynamic Resistance. Second Edition. Midland Park: published by author, 1965.

Latter, Richard. "Similarity Solution for a Spherical Shock Wave." Journal of Applied Physics. Vol 26. Aug 1955. pp 954-960.

McMillen, J. Howard. "Shoc Wave Pressures in Water Produced by Impact of Small Spheres." Physical Review. Vol 68. Nov 1945. pp 198-209.

Myers, M. K. and H. H. Bleich. Transient Excitation of a Liquid Half-by a Decelerating Load and the Associated Transonic Effects. TR No. 44. New York: Columbia University, Apr 1969. Prepared under contract to Office of Naval Research . Contract Nonr-266(86).

Walsh, J. M. and M. H. Rice. "Dynamic Compression of Liquids from Measurements on Strong Shock Waves." J. Chem. Phys. Vol 26. Apr 1957. pp 815-823.

Welsh, Robert L. Collapsing Spherical Shock Waves in Water. AS 66-12. University of California, Berkeley, Sep 1966. AD 800 314.

Winters, David W. Dynamic Response of Water to Ballistic Impact. Wright-Patterson AFB, Ohio: Air Force Institute of Technology, June 1970. GAW/MC/70-7.

Wall Response

Aitken-Cade, Philip B. Iso-Damage Curves for Plates Under Blast Loading. GAW/MC/74-1. Wright-Patterson AFB, Ohio: Air Force Institute of Tech., Mar 1974.

Bach, G. C. and J. H. Lee. "Shock Propagation in Solid Media." presented at the 5th Aerospace Sciences Meeting of the AIAA, Jan 23-26, 1967. Paper No. 67-141. New York, N. Y.: AIAA, Jan 1967. A67-18290.

Ball, Robert E. Prediction of the Response of the Exit Wall of the NWC 50 Cubic Feet Tank to Hydraulic Ram. NPS-57Bp74031. Monterey, Calif.: Naval Post Graduate School, Mar 1974.

Ball, R. E., H. L. Power, and A. E. Fuhs. "Fuel Tank Response to Hydraulic Ram During the Shock Phase." Journal of Aircraft. Vol 10. Sept 1973. pp 571-527.

Bedrosian, Bedros and Frank L. DiMaggio. "Acoustic Approximations in Fluid-Shell Interactions." J. of the Eng. Mechs. Div., Proc. of the Am. Soc. of Civ. Engs., EM. Vol 3. Jun 1972. pp 731-742.

Bitzberger, John Charles. Two Dimensional Analysis of Fluid-Structure Interaction by Method of Finite Differences - Hydraulic Ram, the Fuel Tank Problem. Thesis. Monterey, Calif.: Naval Post Graduate School, Jun 74.

Chou, Pei Chi, and Alan K. Hopkins, editors. Dynamic Response of Materials to Intense Impulsive Loading. Wright-Patterson AFB, Ohio: Air Force Materials Laboratory (Alan Hopkins), Aug 1972.

Chou, Pei Chi, and Richard W. Moritmer. A Unified Approach to One-Dimensional Elastic Waves by the Method of Characteristics. Lewis Research Center, NASA, Apr 1966. N66 38719.

Chou, Pei Chi, and Herbert A. Koenig. Flexural Waves in Elastic Circular Plates by the Method of Characteristics. DIT Rpt No. 160-6. Philadelphia, Penn.: Drexel Institute of Tech., Aug 1965.

Duvall, George E. "Some Properties and Applications of Shock Wave." Response of Metals to High Velocity Deformation. Edited by Shewmon and Zackay. New York: Interscience Publishers, 1961.

Fung, W. K. Analysis of Hydraulic Ram - Structural Response I (Results of Experiment). JTCG/AS-74-t-020(1). China Lake, Calif.: Naval Weapons Center, Dec 1974.

Germain, Paul, and E. H. Lee. "Plane Waves in Elastic-Plastic Solids." International Symposium on Foundations of Plasticity. Warsaw, Poland, Aug 30-Sept 2, 1972. Leiden, Netherlands: Noordhoff International Publishing, 1973. pp 257-270. A74-13992.

Klosner, Jerome M. "Inadequacies of Piston Theory in Fluid-Shell Interactions." Journal of the Engineering Mechanics Division, Proceedings of the American Society of Civil Engineers. EM. Vol 2. Apr 1970. pp 143-159.

Kolsky, H. Some Recent Experimental Investigations in Stress-Wave Propagation and Fracture. Tech Report 19. Brown University, Jun 1971.

Page, Bruce Dean. Fuel Cell Entry Wall Response to Hydraulic Ram. Thesis. Monterey, Calif.: Naval Post Graduate School, Mar 1975.

Riney, T. D., J. F. Heyda, and E. Heer. Impact, Shock Focussing, and Stress Propagation in Thin Plates. AFATL-TR-66-71. Eglin AFB, Florida: AFATL, AF Sys Command, Jul 1966.

Riney, T. D., J. F. Heyda, and C. H. Mok. Theory of Impact, Stress Propagation and Dynamic Fracture. AFATL-TR-67. Air Force Systems Command. Eglin AFB, Florida. Apr 1967.

Sewall, Robert G. S., and Gilbert Ford Kinney. Response of Structures to Blast: A New Criterion. NWC TP 4422. AD 839152. China Lake, Calif.: Naval Weapons Center, Jun 1968.

Ram Attenuation

Breuninger, John R. Jr. An Experimental Study of Attenuation of Shock Shock Waves in Aircraft Fuel Tanks. AFIT Thesis; GA/MC/73-3. Wright-Patterson AFB, Ohio: Air Force Institute of Technology, June 1973.

Bristow, Robert J. "Design of Hydraulic Ram Resistant Structure." Proceedings of the Army Symposium on Solid Mechanics, 1972. AMMRC MS 73-2. AD 423063.

Clark, J. W. Experimental Study of Attenuation of Shock Waves in Three Mixtures. AFIT Thesis. Wright-patterson AFB, Ohio: Air Force Institute of Technology, Jun 1972. AD 748-350.

Dewitt, Richard J., and Patrick H. Zabel. Test of Hydraulic Ram Buffering Materials. Dynamic Science Report 1560-74-43. Phoenix, Arizona: Dynamic Science Div, Ultrasystems, Inc., 30 May 1974.

Fowles, G. R. "Attenuation of the Shock Wave Produced by a Flying Plate." Journal of Applied Physics. Vol 31, No 4. Apr 1960. pp 655-662.

Ostroumov, G. A., and V. M. Kryachko. "Experimental Investigation of Compression Waves in Polyurethane Foam." Polymer Mechanics. Vol 6, No 1. Dec 1972. pp 146-149.

Salvadori, Mario G., Richard Skalak, and Paul Weidlinger. "Waves and Shocks in Locking and Dissipative Media." J. of the Proceed. of the Am. Soc. of Civ. Eng., Engineering Mechanics Div. April 1960. pp 77-105.

Sarpkaya, Turgut. "Prop gation of Surges in Highly Deformable Systems." Developments in Mechanics. Vol I. Edited by J. E. Lay and L. E. Malvern. New York: Plenum Press, 1961.

Stepka, F. S., and C. R. Morse. Methods for Reduction of Fractured Damage of Projectile-Impacted Liquid-Filled Tanks. NASA TM X-1224. Washington, D. C.: National Aeronautics and Space Administration, Mar 1966.

Torvik, Peter J., and James W. Clark. "The Reduction of Impact Induced Pressures in Fuel Tanks." The Shock and Vibration Bulletin, Part 2. Vol 43. June 1973. pp 203-208.

Torvik, Peter J. "A Note on the Attenuation of Planar, One-Dimensional Shock Waves in Porous Materials." Mar 1972. Unpublished Report.

Torvik, P. J., and R. F. Prater. "A Simple Model for the Shock Wave Induced by High Speed Impact." Journal of Spacecraft and Rockets. Vol 9, No 1. Jan 1972. pp 13-18. AD 708-134.

Torvik, Peter J. A Simple Theory for Shock Prop gation in Homogeneous Mixtures. AFIT TR 70-3. WPAFB, Ohio: Air Force Institute of Technology, May 1970.

Torvik, Peter J. On the Attenuation of Diverging Shock Waves in a Porous Material. AFIT TR 71-4. Wright-Patterson AFB, Ohio: Air Force Institute of Technology, School of Engineering, Nov 1971.

Other/General

Bach, G. C., and J. H. Lee. "An Analytical Solution for Blast Waves." AIAA Journal. Vol 8. Feb 1970. pp 271-275.

Birkhoff, Garrett. Hydrodynamics, A Study of Logic, Fact, and Similitude. Princeton, New Jersey: Princeton University Press, 1960.

Birkhoff, Garrett, and E. H. Zarantonello. Jets, Wakes and Cavities. New York: Academic Press, 1957.

Bjork, R. L., M. H. Wagner and H. A. Lang. Radiation Damage Study - Phase II (RADSII) Final Report, Volume VI -- Shock Propagation in Heterogeneous Materials, Book Two of Two Books. SAMSO TR 67-121. Norton Air Force Base, California: Space and Missiled System Organization, Sept 1967.

Clodfelter, R. G., and E. E. Ott. Preliminary Investigation of Fuel Tank Ullage Reactions During Horizontal Gunfire. AFAPL TR 72 55. Nov 72. AD 755 361.

Cole, Robert, Hugh. Underwater Explosions. Princeton, New Jersey: Princeton University Press, 1948.

Courant, Richard and Kurt Otto Friedrichs. Supersonic Flow and Shock Waves. New York: Interscience, 1967.

Fromme, Joseph A. A Practical Model of Three-Dimensional Viscoelasto-plasticity. KN-69-500(RO). Colorado Springs, Colorado: Kaman Nuclear, 12 Nov 69.

Heitz, Roger M. and Victor B. Manire. Self-Sealing Systems for Integral Fuel Tanks. AFML TR 68 183 PT 1. Hawthorne, California: Northrop Corp., July 1968. AD 844 819.

Heitz, Roger M. Self-Sealing Systems for Integral Fuel Tanks, Part 2. AFML TR 183 PT 2. Hawthorne, California: Northrop Corp., June 1969. AD 862 140.

Heitz, Roger M. and Rolf W. Neubert. Self-Sealing Systems for Integral Fuel Tanks, Part 3. AFML TR 68 183 PT 3. Hawthorne, California: Northrop Corp., December 1970. AD 878 230.

Hermann, W. "Constitutive Eq. for the Dynamic Compaction of Ductile Porous Materials." Journal of Applied Physics. Vo. 40, No 6. May 1969. pp 2490-2499.

Herrmann, W., Emmett A. Witmer, John H. Percy, and Arfon H. Jones. Stress Wave Propagation and Spallation in Uniaxial Strain. ASD-TR-62-399. Wright-Patterson Air Force Base, Ohio: Directorate of Aeromechanics, Sept 1962.

Jacobson, M. J.,and J. R. Yamane. The Structural Response of an Empty Metallic Tank to an Internal Blast. NOR 74-317. Los Angeles, California: The Northrop Co., Dec 1974. Proprietary.

Jahsman, W. E. "Propagation of Abrupt Circular Wave Fronts in Elastic Sheets and Plates." Proceedings of the Third U. S. National Congress of Applied Mechanics. New York: The American Society of Mechanical Engineers, 1958.

Chou, P. C. and A. K. Hopkins, editors. Dynamic Response of Materials to Intense Impulsive Loading. Wright-Patterson AFB, Ohio: Air Force Materials Laboratory, Aug 1972.

Keough, Douglas D. Development of a High-Sensitivity Piezoresistive Shock Transducer for the Low Kilobar Range. Mar 25, 1970. DASA 2508. AD 709438.

Keough, Douglas D. Procedure for Fabrication and Operation of Manganin Shock Pressure Gages. AFWL-TR-68-57. Kirtland Air Force Base, New Mexico: Air Force Weapons Lab, Aug 1968. AD 839983.

Kohn, B. J. Compilation of Hugoniot Equations of State. AFWL-TR-69-38. Kirtland Air Force Base, New Mexico: Air Force Weapons Laboratory, Apr 1969. AD 852 300.

Leech, John W., T. H. Piam, E. A. Witmer, and W. Herrmann. Dynamic Response of Shells to Externally-Applied Dynamic Loads. ASD-TR-62-610. Wright-Patterson Air Force Base, Ohio: Aeronautical Systems Division, Nov 1962.

Linde, Ronald K., and Richard C. Crewdson. "Shock Waves in Solids." Scientific American. Vol 220. May 1969. pp 83-91.

Meiselman, Jay, and G. Thomas Burch, Jr. ad John G. Avery. "Techniques for Predicting the Structural Vulnerability of Combat Aircraft to Ballistic Impact." Seattle, Washington: AIAA 3rd Aircraft Design and Operations Meeting, July 1971. AIAA Paper No. 71-777.

Moon, F. C., and C. C. Mow. Wave Propogation in a Composite Material Containing Dispersed Rigid Spherical Inclusions. RM-6139-PR. Santa Monica, California: Rand, Dec 1970.

Porzel, F. B. Height of Burst for Atomic Bombs, 1954; Part I, the Free Air Curve. Los Alamos Scientific Lab Report. Report No. LA 1664. May 1954.

Rice, M. H., and J. M. Walsh. "Equation of State of Water to 250 Kilobars." The Journal of Chemical Physics. Vol 26, No 4. Apr 1957. pp 824-830.

Rice, M. H., R. G. McQueen and J. M. Walsh. "Compression of Solids by Strong Shock Waves." Solid State Physics. Vol 6. Edited by Seitz and Turnbull. New York: Academic Press, 1958.

Shaw, R. P. An Integral Equation Formulation of Acoustic Fluid-Elastic Shell Dynamic Interaction Problems. Report No. 61. Buffalo, New York: State University of New York at Buffalo, Sept 1971.

Shaw, Richard Paul. An Integral Equation Formulation of Dynamic Acoustic Fluid - Elastic Solid Interaction Problems. Buffalo, New York: State University of New York at Buffalo, May 1971. Report No. 60. Prepared under contract for Office of Naval Research.

Soderberg, Staffan. Numerical Solution of the Generation of a Hydrodynamic Shock Caused by a Moving Piston. Stockholm, Sweden: Research Institute for National Defense, Apr 1968. FOA Reports. Vol 2, No 2. AD 842-024.

Taylor, G. I. "The Formation of a Blast Wave by a Very Intense Explosion, I, Theoretical Discussion." Proceedings of the Royal Society (London), Series A. Vol 201. 1950. pp 159-174.

VonNeumann and R. D. Richtmyer. "A Method for the Numerical Calculation of Hydrodynamic Shocks." Journal of Applied Physics. Vol 21. Mar 1950. pp 232-237.

Williams, R. F. Pressure Transducer for Measuring Shock Profiles, Phase X: Measurement of Low-Pressure Shock Wave Profiles. Menlo Park, California: Stanford Research Institute, May 31, 1965. DASA 1653. AD 468715.

Williams, Roger F. Examination of Possible Modifications to the Ytterbium Shock Wave Transducer. SRI Report, prepared for contract N66001-70-c-0572. Menlo Park, California: Stanford Research Institute, 15 May 1970.

Winchester, H. F. et al. Fuel Tank Vulnerability Reduction. MDC J-0044. Long Beach, California: McDonnell Douglas Corporation, Apr 1970. AD870435.

Wooten, D. C. and M. Cowperthwaite. Investigation of Low-Velocity Detonation Phenomena in Liquid Propellants, Fuels, and Explosives. Menlo Park, California: Stanford Research Institute, Apr 1971. AD 723 677.

REFERENCES

1. Stepka, Francis S., and C. Robert Morse. Preliminary Investigation of Catastrophic Fracture of Liquid-Filled Tanks Impacted by High-Velocity Particles. NASA TN 1537. Washington: National Aeronautics and Space Administration, May 1963.

2. Lundstrom, Eric A., and E. W. Stull. Fluid Dynamic Analysis of Hydraulic Ram II (Results of Experiments). Naval Weapons Center, California: Joint Technical Coordinating Group/Aircraft Survivability, 1973.

3. Cole, Robert, Hugh. Underwater Explosions. Princeton, New Jersey: Princeton University Press, 1948.

4. Courant, Richard, and Kurt Otto Friedrichs. Supersonic Flow and Shock Waves. New York: Interscience, 1967.

5. Bach, G. C., and J. H. Lee. Shock Propagation in Solid Media presented at 5th Aerospace Sciences Meeting of the AIAA Jan 23-26, 1967. Paper No. 67-141. New York, N.Y.: AIAA, Jan 1967.

6. Stepka, Francis S., C. R. Morse, and R. P. Dengler. Investigation of Characteristics of Pressure Waves Generated in Water-Filled Tanks Impacted by High-Velocity Projectiles. NASA TN D3143. Washington D.C.: National Aeronautics and Space Administration, Dec 1965. N66 13291.

7. McMillen, J. Howard. "Shock Wave Pressures in Water Produced by Impact of Small Spheres." Physical Review, 68: 198-209 (Nov 1945).

8. Yurkovich, R. Hydraulic Ram: A Fuel Tank Vulnerability Study. MDC G 964. St. Louis, Missouri: McDonnell Aircraft Corp., Sep 1969.

9. Williams, Roger F. Shock Effects in Fuel Cells. SRI Rpt. Accession No. L-23995. Menlo Park, California: Standard Research Inst., Oct 1969.

10. Heyda, James F. Shock Front Variation in Time for High Speed Impact Into Water. Valley Forge, Penn: Space Science Lab, Missile and Space Division General Electric Company, May 1963.

11. Porzel, F. B. Height of Burst for Atomic Bombs, 1954; Part I, the Free Air Curve. Los Alamos Scientific Lab Report, Rpt No. LA 1664 (May 1954).

12. Cardea, G. C., and P. J. Torvik. "Cavity Growth and Collapse Phase of Hydraulic Ram." Journal of Aircraft, Vol II, No. 4: 252-254 (Apr 1974).

13. Lundstrom, Eric A. Fluid Dynamic Analysis of Hydraulic Ram. NWC TP 5227. China Lake, Calif: Naval Weapons Center, July 1971. AD 889 485.

14. Lamb, Sir. Horace. Hydrodynamics. New York: Dover Publications, 1945.

15. Birkhoff, Garrett, and E. H. Zarantonello. Jets, Wakes and Cavities. New York: Academic Press, 1957.

16. Wylie, C. R., Jr. Advanced Engineering Mathematics (3rd ed). New York: McGraw-Hill Book Co., 1966.

17. Chou, Pei Chi, Richard Schaller, and James Hoburg. Analytical Study of the Fracture of Liquid-Filled Tanks Impacted by Hypervelocity Particles. Drexel Rpt No. 160-9. NASA CR-72169. Phila. Penn: Drexel Inst. of Tech., Mar 1967.

18. Chou, Pei Chi and Herbert A. Koenig. Flexural Waves in Elastic Circular Plates by the Method of Characteristics. DIT Rpt No. 160-6. Phila. Penn: Drexel Institute of Tech., Aug 1965.

19. Jahsman, W. E. "Propagation of Abrupt Circular Wave Fronts in Elastic Sheets and Plates." in Proceedings of the Third US National Congress of Applied Mechanics. New York: The American Society of Mechanical Engineers, 1958.

20. Karpp, R., and P. C. Chou. "The Method of Characteristics," in Dynamic Response of Materials to Intense Impulsive Loading. edited by P. C. Chou and A. K. Hopkins. Wright-Patterson Air Force Base, Ohio: Air Force Materials Laboratory, Aug 1972.

21. Timoshenko, S., in Collaboration with Young, D. H. Vibration Problems in Engineering (3rd edition). New York: D. Van Nostrand Co., Ltd. Jan 1955.

22. Tikhonov, A. N., and A. A. Samarskii. Equations of Mathematical Physics. New York: The MacMillan Co., 1963.

23. Fuhs, A. E., R. E. Ball, and H. L. Power. FY 73 Hydraulic Ram Studies. Monterey, Calif: Naval Postgraduate School, Feb 1974.

24. Ross, Shepley L. Differential Equations. New York: Blaisdell Publishing Company, 1965.

25. Stepka, F. S., and C. R. Morse. Methods for Reduction of Fracture Damage of Projectile-Impacted Liquid-Filled Tanks. NASA TM X-1224. Washington, D.C.: National Aeronautics and Space Administration, Mar 1966.

26. Bristow, R. J., and J. F. Lundberg. Projectile Penetration Through Rheoptic Fuels. AFAPL TR 68-151. Seattle, Washington: Boeing Co., Nov 1968. AD 745 801.

27. Clark

28. Dewitt, Richard J., and Patrick H. Zabel. Tests of Hydraulic Ram Buffering Materials. Dynamic Science Report 1560-74-43. Phoenix, Ariz: Dynamics Science Div, Ultrasystems, Inc., 30 May 74.

29. Torvik, Peter J. A Note on the Attenuation of Planar, One-Dimensional Shock Wave in Porous Materials. Unpublished note.

30. Duvall, George E. "Some Properties and Applications of Shock Waves" in Response of Metals to High Velocity Deformation. edited by Shewmon and Zackay. New York: Interscience Publishers, 1961.

31. Hermann, W. "Constitutive Equation for the Dynamic Compaction of Ductile Porous Materials." Journal of Applied Physics, v.40, n.6: 2490-2499 (May 1969).

32. Salvadori, Mario G., Richard Skalak, and Paul Weidlinger. "Waves and Shocks in Locking and Dissipative Media." J. of the Engineering Mechanics Division, Proc. of the Am. Soc. of Civil Engs, EM 2: 77-105 (Apr 1960).